

**An Electrophysiological Cardiac Model with  
Applications to Ischemia Detection and Infarction  
Localization**

**by**

**Mohamed A. Mneimneh, B.S., M.S.**

**A Dissertation submitted to the Faculty of the Graduate School,  
Marquette University, in Partial Fulfillment of the Requirements for the  
Degree of Doctor of Philosophy  
Milwaukee, Wisconsin  
August, 2008**

---

## Acknowledgement

First the author wishes to thank GOD for giving him the patience and determination to complete this work. The author would like to proclaim his appreciation for his advisor Prof. Richard J. Povinelli for his supervision, guidance, and assistance for making this work possible.

Additionally, the author would like to thank his committee members Prof. Edwin E. Yaz, Prof. Michael T. Johnson, Prof. George F. Corliss, and Prof. Kristina M. Ropella for their valuable help that made this work achievable.

The author would like to thank his lab mate Kevin Indrebo for his help throughout this work.

Special recognition for the National Science Foundation through their contract with Marquette University in addition to the Electrical and Computer Engineering Department for their financial support.

The author would like to present his deepest appreciation for his mother for her continual support. The author would like to thank his father Prof. Ali Mneimneh for his financial support and continual help during all these years. The author would also like to thank his Brother, Saad, and Sister, Ola, Sister in law, Hanan, and brother in law, Dr. M. Bouji.

Finally, the author would like with great appreciation to thank his fiancé for her help, moral support, patience and understanding.

## **Abstract**

A novel electrophysiological cardiac model is introduced in this dissertation. The cardiac model considers six key regions that characterize the cardiac electrical activity allowing a sufficiently fast solution to forward and inverse problems. The major drawback of current cardiac modeling methods is computational complexity because they model more than 100,000 regions of the heart. This complexity does not allow current techniques to be used in sufficiently fast diagnostics. In contrast to previous models, the ECM is used as a basis for two sufficiently fast clinical diagnostic applications. The first is the detection of an ischemic heart. The second is the localization of myocardial infarction. A brief overview of the cardiac activity and its relation to the modeling method is presented. Additionally, a historical review of the related fields is discussed. The electrophysiological cardiac modeling method, including the cardiac model, forward and inverse problems solutions, and the diagnostic applications are described in detail.

# I. Table of Contents

Acknowledgement .....	ii
Abstract .....	iii
I. Table of Contents .....	iv
II. List of Figures .....	vi
III. List of Tables .....	viii
Chapter 1 Introduction.....	1
1.1 Problem Statement .....	4
1.2 Main Contributions .....	7
1.3 Dissertation Outline .....	8
Chapter 2 The Heart and Coronary Artery Disease.....	9
2.1 Cardiac Mechanical System.....	9
2.1.1 Heart Chambers and Valves.....	10
2.1.2 Cardiac Mechanical Activity and Blood Flow.....	12
2.2 Conduction System .....	13
2.2.1 Cardiac Cell Electrophysiology .....	13
2.2.2 Cardiac Conduction Sequence .....	15
2.3 Electric Activity Measurement .....	18
2.3.1 Wave Identification.....	20
2.3.2 Intervals and Segments .....	21
2.4 Cardiac Activity Summary .....	22
2.5 Coronary Artery Disease.....	23
2.5.1 Coronary Circulation .....	23
2.5.2 Myocardial Ischemia, Injury, and Infarction .....	24
2.5.3 Coronary Artery Disease ECG Effects .....	25
2.6 Summary of Chapter .....	30
Chapter 3 Background of the Problem .....	31
3.1 Cardiac Modeling.....	31
3.1.1 Geometric Modeling .....	32
3.1.2 Cell Modeling .....	33
3.1.3 Tissue Modeling.....	36
3.1.4 Forward Problem .....	37
3.1.5 Inverse Problem .....	38
3.2 Diagnoses of Myocardial Ischemia, Injury, and Infarct .....	40
3.2.1 Cardiac Catheterization.....	40
3.2.2 Echocardiogram .....	42
3.2.3 Magnetic Resonance Imaging.....	43
3.2.4 Electrocardiograms .....	44
Chapter 4 Datasets .....	50
4.1 PTB Dataset .....	50
4.2 Long Term ST Dataset.....	51
4.3 A General Gaussian Signal Model.....	53
4.4 Summary .....	55
Chapter 5 Cardiac Modeling.....	56

5.1	Electrophysiological Cardiac Model.....	57
5.1.1	Cardiac Region Electrical Activity Model.....	60
5.2	Forward Problem Solution.....	65
5.2.1	ECG Generation.....	65
5.3	Discussion.....	77
Chapter 6	Inverse Problem Solution (through optimization) .....	79
6.1	Inverse Problem Solution.....	80
6.2	Inverse Problem Setup (Optimization Problem).....	82
6.3	Initial Condition.....	88
6.4	Nonlinear Constrained Optimization .....	91
6.5	Discussion.....	92
Chapter 7	Ischemia Detection and Infarction Localization .....	93
7.1	Methods.....	93
7.1.1	Ischemia Detection.....	94
7.1.2	Infarction Localization.....	102
7.2	Discussion.....	105
Chapter 8	Results of Modeling Problem Solution.....	107
8.1	Actual Electrocardiogram Experiment .....	107
8.1.1	Healthy ECG.....	108
8.1.2	Ischemic ECG .....	115
8.1.3	Infarcted ECG .....	121
8.2	Results Analysis.....	127
8.3	Simulated Electrocardiogram Experiment.....	132
8.4	Multilead Electrocardiogram Generation .....	135
8.5	Summary and Discussion.....	139
Chapter 9	Diagnostic Methods Results .....	141
9.1	Ten-Fold Cross Validation.....	141
9.2	Ischemic Diagnostic Experiment .....	142
9.2.1	Ten-Fold Cross Validation Experiment.....	143
9.2.2	Summary and Discussion for the Ischemia Detection Experiment .....	145
9.3	Infarction Localization Experiment .....	145
9.3.1	Summary and Discussion for the Infarction Localization Experiment...	149
9.4	Summary and Discussion.....	149
Chapter 10	Conclusion .....	151
10.1	Future Recommendations .....	152
Appendix A	Luo-Rudy Model.....	154
Appendix B	RPS/GMM Approach toward Myocardial Infarction Localization .....	156
B.1.	RPS/GMM approach.....	156
B.2.	Reconstructed Phase Space.....	157
B.3.	Gaussian Mixture Model.....	157
References	.....	159

## II. List of Figures

Figure 1-1: Sketch of the proposed heart model.....	2
Figure 1-2: The cardiac modeling problem.....	5
Figure 2-1: A detailed sketch of the heart [9].....	11
Figure 2-2: A cardiac cell action potential.....	14
Figure 2-3: Conduction system of the heart [12].....	16
Figure 2-4 Electric Activity (activation sequence) of the heart cells generating an ECG signal [14].....	17
Figure 2-5: Electrocardiographic view of the heart.....	19
Figure 2-6: A sample annotated ECG signal at Lead I.....	20
Figure 2-7: How myocardial infarction occurs [16].....	25
Figure 2-8: Left ventricular chamber areas.....	27
Figure 3-1: The Seldinger approach catheterization method [20].....	41
Figure 3-2: A sample echocardiogram [21].....	43
Figure 3-3: Cardiac MRI image [22].....	44
Figure 4-1: Example of ST deviation calculation.....	52
Figure 4-2: Definition of ST event.....	53
Figure 5-1: Sketch of the human body and the heart model.....	58
Figure 5-2: A ECG signal at Lead I.....	59
Figure 5-3: Conduction activity of the heart.....	61
Figure 5-4: Model for cardiac region electrical activity.....	62
Figure 5-5: Comparison between the diffsig model and Luo-Rudy model.....	63
Figure 5-6: Error between the Luo-Rudy and diffsig cell activity.....	64
Figure 5-7: P wave modeled as the difference between two sigmoids.....	69
Figure 5-8 PR interval generation using the differential sigmoid model.....	70
Figure 5-9: Q wave generation.....	72
Figure 5-10: R wave and T wave generation.....	72
Figure 5-11: S wave and T wave generation.....	73
Figure 5-12: ST segment generation.....	74
Figure 6-1: Block diagram of inverse problem solution.....	81
Figure 6-2: Actual ECG signal at lead II.....	89
Figure 6-3: Initial condition signal.....	90
Figure 6-4: Initial condition signal compared to the signal to be fitted.....	90
Figure 7-1: Block diagram of the ischemia detection method.....	94
Figure 7-2: Preprocessing representation of the ECG signals.....	95
Figure 7-3: Block diagram of the beat diagnostic method.....	97
Figure 7-4: Demonstration of the PCA process.....	99
Figure 7-5: Block diagram of the infarction localization method.....	103
Figure 8-1: Actual healthy beat at lead II.....	109
Figure 8-2: Cardiac region activity, inverse problem solution.....	109
Figure 8-3: ECM-generated ECG, forward problem solution.....	111
Figure 8-4: A comparison between an actual ECG and ECM-generated ECG.....	111
Figure 8-5: The error between the actual and ECM-generated ECG.....	111
Figure 8-6: Percentage error between the actual and ECM-generated ECG.....	112

---

Figure 8-7: Gaussian fit between error distribution and normal distribution. ....	113
Figure 8-8: Cross-correlation of the residual error. ....	114
Figure 8-9: Comparison between cross-correlation of the residual and white Gaussian noise. ....	114
Figure 8-10: Actual ischemic ECG. ....	116
Figure 8-11: Inverse problem solution for an ischemic ECG. ....	116
Figure 8-12: ECM-generated ischemic beat, forward problem solution. ....	117
Figure 8-13: Comparison between ECM-generated and actual ECG. ....	118
Figure 8-14: Actual error between ECM-generated and actual ECG. ....	118
Figure 8-15: Percentage error between the ECM-generated and actual ECG. ....	119
Figure 8-16: Gaussian fit between error distribution and normal distribution. ....	120
Figure 8-17: Cross-correlation of the residual error. ....	120
Figure 8-18: Comparison between cross-correlation of the residual and white noise. ....	121
Figure 8-19: Actual infarcted ECG. ....	122
Figure 8-20: Inverse problem solution for an infarcted ECG. ....	122
Figure 8-21: ECM-generated infarcted beat, forward problem solution. ....	123
Figure 8-22: Comparison between ECM-generated and actual ECG. ....	124
Figure 8-23: Actual error between ECM-generated and actual ECG. ....	124
Figure 8-24: Percentage error between ECM-generated and actual ECG. ....	125
Figure 8-25: Gaussian fit between error distribution and normal distribution. ....	126
Figure 8-26: Cross-correlation of the residual error. ....	126
Figure 8-27: Comparison between cross-correlation of the residual and white noise. ....	127
Figure 8-28: Perturbed sequence of ECG features signal measured at lead II. ....	128
Figure 8-29: Zero padded ECG signal measured at lead II. ....	129
Figure 8-30: Comparison between ECG-generated and actual ECG. ....	129
Figure 8-31: Error between ECG-generated and actual ECG. ....	130
Figure 8-32: Comparison between ECM-generated and actual ECG. ....	131
Figure 8-33: Error between Actual and ECM-generated ECG. ....	131
Figure 8-34: The simulated signal used in this experiment. ....	133
Figure 8-35: T wave end variation. ....	134
Figure 8-36: Comparison between actual ECG and ECM-ECG at lead I. ....	136
Figure 8-37: Error between actual and ECM-ECG at lead I. ....	136
Figure 8-38: Comparison between actual ECG and ECM-ECG at lead II. ....	137
Figure 8-39: Error between actual and ECM-ECG at lead II. ....	137
Figure 8-40: Comparison between actual ECG and ECM-ECG at lead III. ....	138
Figure 8-41: Error between actual and ECM-ECG at lead III. ....	138
Figure B-1: Block diagram describing the GMM/KLT approach. ....	157

### III. List of Tables

Table 2.1: Sequence of mechanical and electrical events during a single cardiac cycle [15].....	23
Table 2.2: Progressive phases of acute myocardial infarction [11].....	28
Table 2.3: ECG changes seen in acute myocardial infarction [11].....	30
Table 4.1: Parameters of the GGSM used to simulate an ECG.....	55
Table 7.1: ECG changes seen in acute myocardial infarction [45].....	105
Table 8.1: Error comparison between original and obtained T wave end. ....	135
Table 8.2: Percentage error of the comparison of the multilead ECM and actual ECGs	139
Table 9.1: Confusion matrix for the diagnostic method using ECM without PCA.....	143
Table 9.2: Confusion matrix for the diagnostic method using PCA.....	143
Table 9.3: Confusion matrix for the diagnostic method using ECM with PCA.....	143
Table 9.4: Comparison between the ECM-PCA/C4.5 approach and Stamkapoulos method applied to the LT-ST database. ....	144
Table 9.5: The available infarction locations with the respective number of records. ...	146
Table 9.6: Confusion matrix of the ECM-Localizer method.....	147
Table 9.7: Confusion matrix of the PCA-Localizer method.....	147
Table 9.8: Confusion matrix of the ECM/PCA-Localizer method.....	148
Table 9.9: Application of the diagnostic methods for the 13 classes.....	148
Table 9.10: Comparison between the ECM-PCA/C4.5 and RPS/GMM method. ....	149

## Chapter 1 Introduction

This dissertation presents a novel approach for modeling the heart that addresses both the cardiac electrophysiology at the body surface (forward problem) and the electrical activity in key cardiac regions (inverse problem). This model is the basis for two clinical diagnostic methods. The first allows for sufficiently fast localization of myocardial infarction. The second provides a mechanism for identifying an ischemic heart. These diagnostic methods use the forward and inverse problem solutions and machine learning approaches to diagnose automatically, noninvasively, and accurately these two serious heart conditions. Moreover, the diagnostic methods have high true positive and negative accuracies suitable to be used in clinical expert systems. The accuracies for the ischemia detection and infarction localization methods are 91% and 68.57%, respectively. These results outperform existing automatic approaches. The highest published accuracy for automatic ischemia detection is 87.83% [1], while the highest published accuracy for automatic infarction localization methods is 58.74% [2]. Furthermore, the average run time for the diagnostic methods is 10 seconds.

The importance of the two diagnostic methods can be seen in the potential impact on early screening of myocardial ischemia and on quickly identifying the location of myocardial infarction. As noted by the World Health Organization, ischemic heart disease is the leading cause of death in the world with almost 7.2 million fatalities per year [3]. The diagnostic method can be used in the early screening of myocardial ischemia. Early screening of myocardial ischemia is proven to help prevent heart attacks [4].

Moreover, according to the American Heart Association, myocardial infarction is the leading cause of death in the United States with approximately 3,000 people having a heart attack per day [5]. The rapid and noninvasive localization of myocardial infarction may help physicians quickly treat the blockage with the appropriate drugs or procedures at the indicated heart region [4].

These diagnostic methods are based on the modeling approach, which is illustrated at a high level by Figure 1-1. The electrophysiological cardiac model (ECM) divides the heart into six important electrical regions: sinoatrial (SA) node, atrioventricular (AV) node, bundle branches (Bb), Purkinje fibers (Pf), right ventricle (RV), and left ventricle (LV). Individual models are used to represent the electrical activation and conduction of each region. The interaction between regions is also modeled, as well as the net behavior of the whole cardiac model at the body surface. A sketch of the heart model is shown in Figure 1-1. The left part sketches the heart and the modeled regions. The right side of Figure 1-1 shows examples of the model-generated electrical activity at each of the regions.

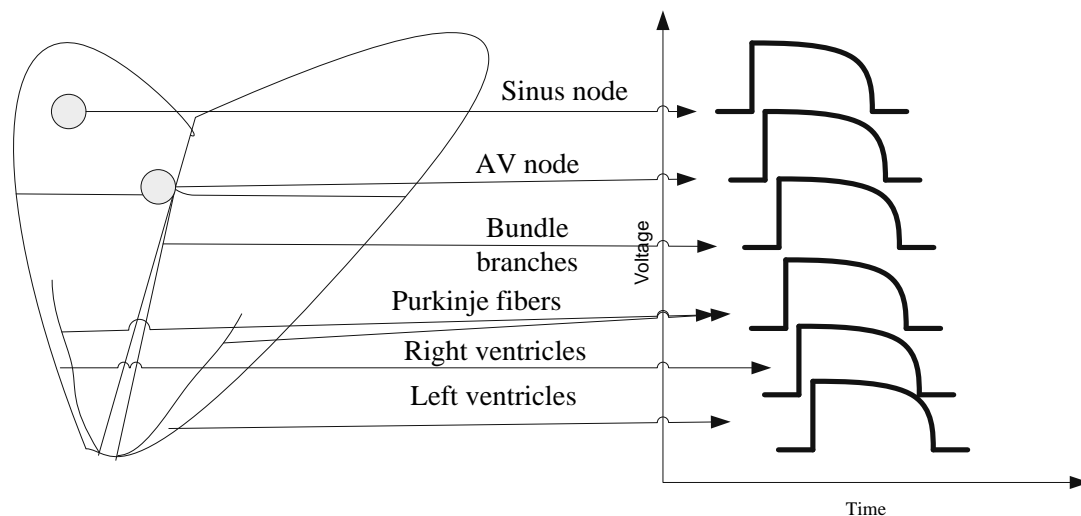


Figure 1-1: Sketch of the proposed heart model.

---

In contrast to the ECM, most cardiac modeling methods focus on simulating the chemical dynamics of the cardiac cells using nonlinear coupled differential equations. To set up the forward and inverse problems, these methods simultaneously model more than 100,000 cells or attempt to solve Maxwell's equations using numerical methods such as finite element and finite difference techniques. Such methods require a geometrical representation of the heart and body torso for each individual. The advantages of these models are their ability to represent the ion concentrations of the cardiac cells. However, the disadvantages of these methods are their complexity and dependency on the cardiac and body geometry, which make them inadequate for developing sufficiently fast diagnostic methods. For example, in [6, 7], these models did not generate accurate electrocardiograms (ECGs) due to the dependency of the solution on the geometric models of the heart and torso and the conductivity of the tissue, which are generally unknown and vary with each individual.

In comparison with the finite element modeling methods, the ECM models six electrically important regions of the heart and thereby yields a far less complex model. The advantage of the presented approach is that it provides a direct solution independent of geometrical modeling for the forward and inverse problems. Furthermore, it is able to model the time and the pace of activation and conduction of the modeled cardiac regions. The time and the pace of activation and conduction of the cardiac regions play important roles in clinical diagnostics, such as myocardial infarction localization and myocardial ischemia detection. Additionally, the presented model has the ability to generate accurate ECGs. The disadvantage of the ECM is the inability to capture the chemical dynamics and the ionic concentrations in the cardiac cells.

## ***1.1 Problem Statement***

The major drawback of the current modeling methods is that they cannot be used in sufficiently fast diagnosis due to their complexity and the dependency on the geometry of the heart and body torso. As a result, these methods cannot be used in building patient independent diagnostic methods [6, 7]. Therefore, this work focuses on building a patient-independent cardiac model that can provide a sufficiently fast forward and inverse problems solutions.

The problem addressed in this work is the modeling of the cardiac electrical system. The cardiac modeling problem is divided into two sub-problems. The first is to model the action potentials of the cardiac regions. The second is to define the interaction between the cardiac electrical subsystems and their measured output at the body surface. Figure 1-2 provides a graphical illustration of the cardiac modeling problem. The upper part of the figure shows the heart represented as several unknown electrical systems, which represent the action potential of the main cardiac regions. The lower part of the figure shows the ECG measured at the body surface. The relationship between the action potentials and the measured ECG are defined as the forward and inverse problems. The forward problem is the generation of the ECG from the cardiac action potential. The inverse problem is the estimation of the cardiac electrical activity from measured ECGs.

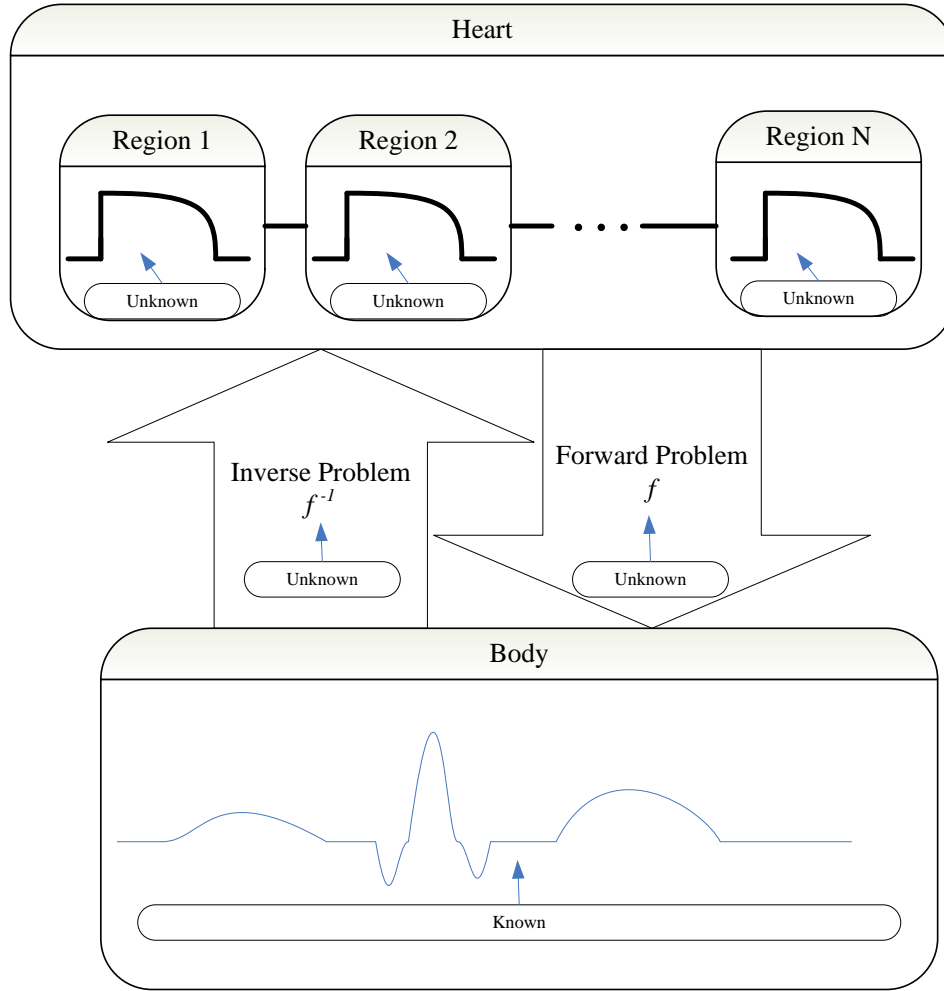


Figure 1-2: The cardiac modeling problem.

To further clarify the cardiac modeling problem, a mathematical representation of the problem is formulated. Consider the hypothesis that the heart can be represented by a vector of  $N$  electrical regions

$$Heart = \begin{bmatrix} region_1 \\ region_2 \\ \vdots \\ region_N \end{bmatrix}. \quad (1.1)$$

In this case, the cardiac modeling sub-problem is to determine the function  $\phi$  that represents the action potentials at the cardiac regions  $\phi(region_1)$ ,  $\phi(region_2)$ ,

...,  $\phi(\text{region}_n)$ . The aim of the second sub-problem is to determine the functions  $f$  and  $f^{-1}$  described in equations (1.2) and (1.3), respectively:

$$f \begin{bmatrix} \phi(\text{region}_1) \\ \phi(\text{region}_2) \\ \vdots \\ \phi(\text{region}_n) \end{bmatrix} = ECG, \quad (1.2)$$

$$\begin{bmatrix} \phi(\text{region}_1) \\ \phi(\text{region}_2) \\ \vdots \\ \phi(\text{region}_n) \end{bmatrix} = f^{-1}(ECG). \quad (1.3)$$

Equation (1.2) describes the forward problem as the function,  $f$ , that generates the ECG from the electrical activity at the cardiac regions ( $\text{region}_1, \text{region}_2, \dots, \text{region}_n$ ).

Equation (1.3) represents the inverse problem as the function  $f^{-1}$  that estimates the cardiac electrical activity from measured ECGs.

One of the difficulties of the cardiac modeling problem is that as stated in (1.2) and (1.3), the solution is not uniquely defined. This is seen in (1.2) and (1.3) as the number of unknown parameters is greater than that of known parameters. This work addresses this difficulty by considering a finite number of regions, constraining the activity of each region to the cardiac electrophysiology, and using least squares optimization.

As clinical applications to the presented model, this work presents two automatic diagnostic methods based on the presented ECM. The first is the detection of myocardial ischemia. The second is the localization of myocardial infarction.

For the myocardial ischemia detection method, the problem is to build an accurate classification approach that determines whether a heart is ischemic. This provides an early noninvasive screening tool for the detection of myocardial ischemia.

Myocardial infarction is known to affect the cardiac electrical activity at the infarcted region. Therefore, the problem is to develop an accurate multiclass classification approach to determine whether a certain heart region is infarcted. This provides a method for quickly localizing the infarcted region, enabling physicians to administer treatment to that specific region.

## ***1.2 Main Contributions***

This dissertation introduces, develops, and elaborates a cardiac model that sets the basis for two automatic, noninvasive methods for clinical diagnostics. The main contributions of this dissertation include:

1. Development of a cardiac electrophysiological model that can be used to solve the forward and inverse problems. This model provides a simple method for estimating the cardiac electrical activity from measured electrocardiograms.
2. Development of a direct solution for generating electrocardiograms and solving the forward problem. This solution is used as a basis for solving the inverse problem.
3. Development of an inverse problem solution using nonlinear constrained optimization. The applied constraints are based on the cardiac electrophysiology.
4. Development of classification methods that use the presented cardiac model and machine learning methods for the detection of myocardial ischemia and localization of myocardial infarction.

### ***1.3 Dissertation Outline***

The remainder of the dissertation is divided into ten chapters. Chapter 2 presents the heart anatomy, cardiac mechanical and conduction systems, and background regarding ischemic disease. Chapter 3 reviews the previous methods used in solving the forward and inverse problem. Chapter 3 also reviews previous methods used in signal denoising, detection of myocardial ischemia, and identification of myocardial infarction.

Chapter 4 presents the real patient datasets as well as the simulated signals used in this work along with the preprocessing applied to each of the sets. Chapter 5 presents the mathematical formulation for the ECM for single electrocardiograms. Chapter 6 presents the optimization methods used for fitting the signal generated from the model to that of real ECG signals. Chapter 7 describes the theory of the method used for the detection of myocardial ischemia and identification of myocardial infarction.

Chapter 8 presents results of the ECM generating accurate electrocardiograms. Chapter 9 presents the results of the classification method presented in chapter 7 in application to myocardial ischemia detection and myocardial infarction localization. Chapter 10 discusses the obtained results and presents a conclusion and suggestions for future work.

## **Chapter 2      The Heart and Coronary Artery Disease**

As presented in the Chapter 1, this work proposes an electrophysiological cardiac model that can be used in sufficiently fast clinical diagnostics. Since this work addresses the cardiac modeling problem, this chapter, the first of two background chapters, describes the generation and conduction of the cardiac electrical activity and the measurement at the body surface. Moreover, this chapter provides the necessary background for understanding the cardiac mechanical system, i.e. anatomy, mechanical activity, and blood flow.

Additionally, since the main clinical applications of this work are the identification of myocardial ischemia and the localization of myocardial infarction, this chapter presents a functional overview of myocardial ischemia and infarction.

This chapter is divided into five main sections. The first section describes the cardiac mechanical system by presenting the heart chambers and valves and their role in the circulatory system. The second section explains the cardiac conduction system and how the cardiac cells generate and conduct the electrical activity. The third portrays how electrocardiograms are measured at the body surface followed by a summary of the cardiac electrical and mechanical systems. Finally, an overview of the causes of myocardial ischemia, injury, and infarction and their effect on electrocardiograms is presented.

### ***2.1 Cardiac Mechanical System***

The heart is the core of the circulatory system, pumping blood to the cells of the body. The cardiac mechanical system is controlled by an electrical system that allows the

---

heart to function properly. The heart consists of mechanical pumps that activates sequentially. This sequential pumping is controlled by the cardiac electrical system. If a problem occurs in the electrical system of the heart, it can cause disruption in the pump's behavior, thus leading to disastrous effects on the body. Therefore, understanding the cardiac mechanical system helps in understanding the behavior of the electrical system.

The heart is a muscular organ approximately 12 cm by 9 cm that weight 300-400 grams [8] and protected by an incasing layer of fat. The purpose of the heart is to supply oxygenated blood to the body's cells. The heart is a complex pump consisting of several chambers, valves, arteries, and veins. The role of the heart valves and chambers in the cardiac mechanical activity and blood flow are described in the next section.

### **2.1.1 Heart Chambers and Valves**

This section describes the inner chambers and valves of the heart. The valves and chambers play an important role in the circulatory system, thus a brief overview of their activity is presented. The heart is divided into right and left halves, separated by an inner wall called the septum. The upper chambers are the left and right atrium, and the lower chambers are the left and right ventricles as seen in Figure 2-1.

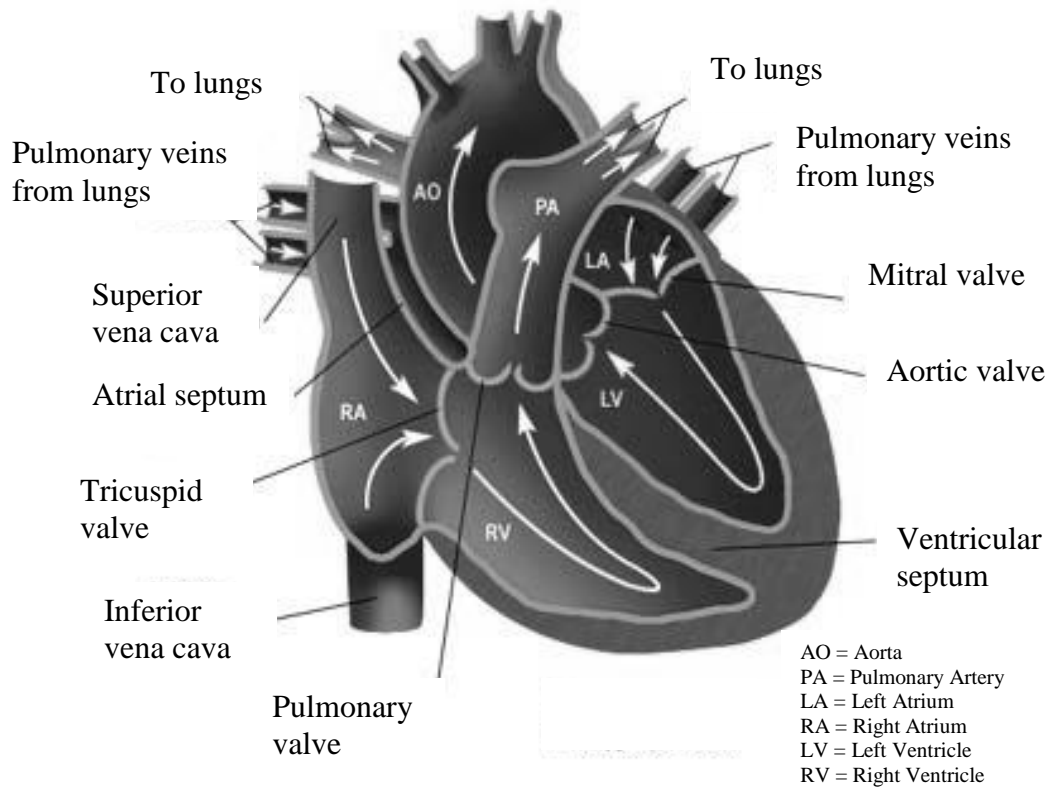


Figure 2-1: A detailed sketch of the heart [9].<sup>1</sup>

The purpose of the atria is to receive blood as it comes to the heart. The right atrium receives oxygen-depleted blood from the body and the left atrium receives oxygen-rich blood from the lungs. The ventricles are larger than the atria because they pump the blood throughout the body. The right ventricle pumps the oxygen-devoid blood to the lungs to absorb oxygen and release carbon dioxide. The left ventricle pumps the oxygen-rich blood to the body's organs.

As seen in Figure 2-1, the heart contains four valves that open and close, controlling the flow of blood from the atria to the ventricles and from the ventricles into the two large arteries (pulmonary artery and aorta) connected to the heart. The valves

<sup>1</sup> Copyright ©2007 Medicallook.com. All rights reserved.

open to allow blood to flow through to the next chamber or to one of the arteries, and then they shut to keep blood from flowing backward [8]. The tricuspid valve is located at the right side of the heart between the atrium and the ventricle. The pulmonary valve is located between the right ventricle and the entrance to the pulmonary artery, which carries blood to the lungs. The mitral valve is located between the left atrium and the left ventricle. The aortic valve is located between the left ventricle and the entrance to the aorta, the artery that carries blood to the body.

### **2.1.2 Cardiac Mechanical Activity and Blood Flow**

Now that the heart chambers and valves have been described, the mechanical activity of the heart and its purpose in the circulatory system can be explained. The purpose of the heart is to pump blood into the body. The circulating venous, oxygen rich, blood enters the right atrium through the inferior and superior vena cava as shown in Figure 2-1. The venous blood also enters the right atrium through the coronary sinus. The blood goes through the tricuspid valve into the right ventricle. The blood crosses the pulmonic valve into the pulmonary arteries, where it is transported into the lungs. The carbon dioxide is replaced with oxygen in the lung alveoli. The saturation of oxygen in the blood on the right side of the heart is on average 75% before and 95% after leaving the lungs.

The oxygenated blood returns from the lungs to the left atrium through the pulmonary veins. The blood passes through the mitral valve to the left ventricle. The left ventricles eject the blood across the aortic valve into the aorta and to the body. As mentioned previously, the forward movement of the blood is ensured by the valves, which prevent the blood from coming back.

## ***2.2 Conduction System***

Now that the mechanical system has been described, this section presents the conduction system that initiates the circulatory system. The focus of studying the cardiac conduction system dates back to 1903, when Einthoven used a dipole model to represent different ECG features. The aim of his study and this dissertation is to understand the myocardial excitation sequence and the tissue conductivity in order to use it in clinical diagnosis of diseases. Since the heart resides inside the human body, from a clinical perspective, the body surface is considered as the interface to the heart. Therefore, it is clinically important to understand the basis of electrical arrhythmias from a cellular and tissue level. So as to understand how electrical activity at the cellular level results in the electrical signals observed at the body's surface.

Section 2.2.1 describes the cardiac cellular electrophysiology and the equations governing conduction. Additionally, section 2.2.2 describes the sequence of activations of the cardiac cells, which will be used in the forward and inverse problem solutions.

### **2.2.1 Cardiac Cell Electrophysiology**

The cardiac cell electrical activity is generated by a chemical and electrical force at the cell membrane. The cardiac cells have a protection mechanism that activates when perturbed by a small potential difference. This protective mechanism elicits a passive response at the cell membrane. If a sufficiently large stimulus occurs, the transmembrane potential rises above the threshold potential, which causes an active response known as the action potential [10]. After such an impulse, the transmembrane is able to move back to its resting state. Figure 2-2 presents an example of an action potential of the cardiac muscle cell.

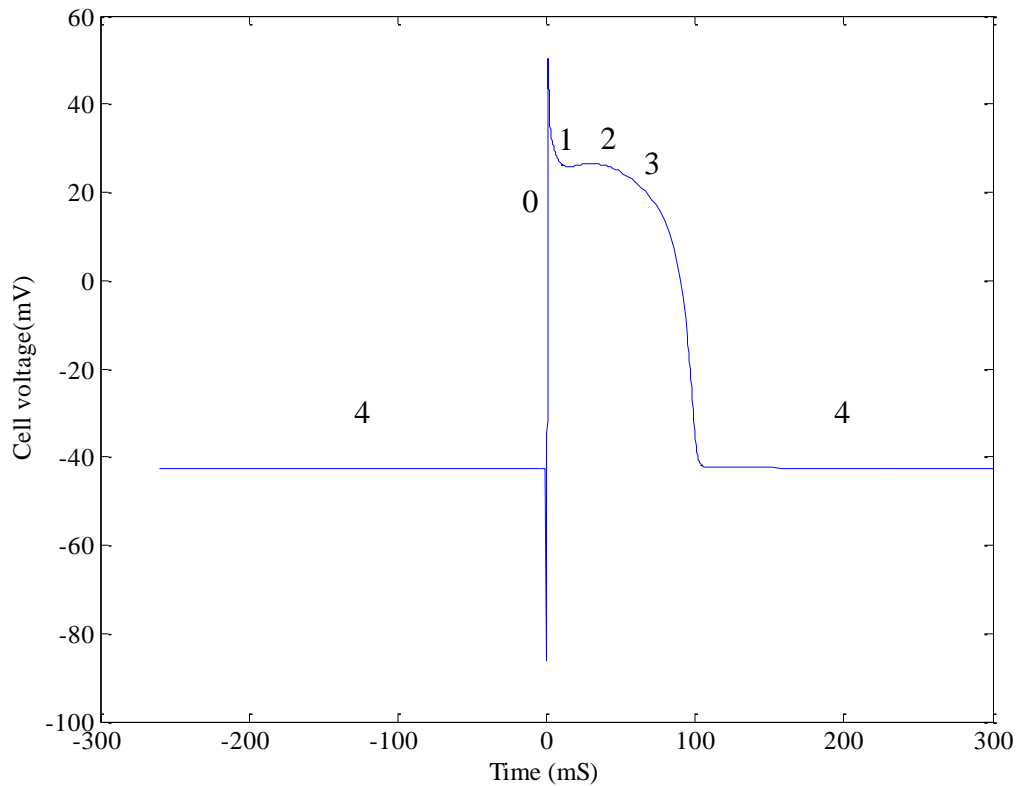


Figure 2-2: A cardiac cell action potential.

The cardiac cell activity is divided into 4 phases as shown in Figure 2-2. These phases are described in the following section.

### 2.2.1.1 Cardiac Cell Phases

The main stages of the cell membrane are described as polarized, depolarized, repolarized, and hyperpolarized. The cell is called polarized when the cell membrane is at rest. Depolarization is the increase in the action potential toward zero [10].

Repolarization is the process where the cell recovers, and its potential returns to a negative stage. The cell is called hyperpolarized when the membrane potential falls below the resting potential.

The action potential shown in Figure 2-2 is labeled with 0-4, indicating the five phases that the cell membrane ions undergo. Phase 0, the upstroke in the action potential is caused by a supra-threshold stimulus due to the rapid influx of sodium ions creating the sodium current [10]. Phase 1, the rapid decrease in the action potential, is due to the outward potassium current, which is known to vary in the different regions of the heart. Phase 2, characterized by the existence and length of the flat segment in the action potential, is due to the inward calcium current. Along with the calcium current, the potassium based current tends to bring the action potential to its resting potential. In phase 3, the calcium current opposes the potassium current that returns the action potential to its resting phase known as phase 4.

Moreover, some cells in the heart that are self-exciting [10], i.e., they produce an action potential at regular intervals in the absence of external stimuli. These cells are found in the SA node, AV node, and Purkinje fibers.

### **2.2.2 Cardiac Conduction Sequence**

Now that the electrical activity of each cell has been described, this section presents the conduction mechanism of the heart tissue, i.e., the sequence in which the cardiac cells activate. The cardiac conduction system is designed to maximize the efficiency of each contraction. The conduction system contains specialized cells that initiate and conduct the cardiac electrical activity. The specialized cells are the Sinoatrial (SA) node, Atrioventricular (AV) node, bundle of His, bundle branches, and Purkinje fibers defined as [11]:

*Sinoatrial (SA) node:* The SA node consists of a cluster of cells in the upper wall of the right atrium. The SA node acts as the heart's natural pacemaker. It fires regularly so that

the heart beats. The average firing rate of the SA node is 60 to 100 impulses per minute in adults. The electrical impulse from the SA node triggers a sequence of electrical events in the heart to control the orderly sequence of muscle contractions that pump the blood out of the heart.

*Atrioventricular (AV) node:* The AV node is one of the major elements in the cardiac conduction system. The AV node has a rate of 40 to 60 impulses per minute. The AV node helps regulate the conduction of electrical impulse from the atria to the ventricles.

*Bundle of His, bundle branches, and Purkinje fibers:* The bundle of His is a collection of heart muscle cells specialized for electrical conduction that transmit the electrical impulses from the AV node (located between the atria and the ventricles) to the point of the apex of the fascicular branches. The bundle of His separates into the bundle branches and Purkinje fibers, which conduct the electric activity through the ventricles.

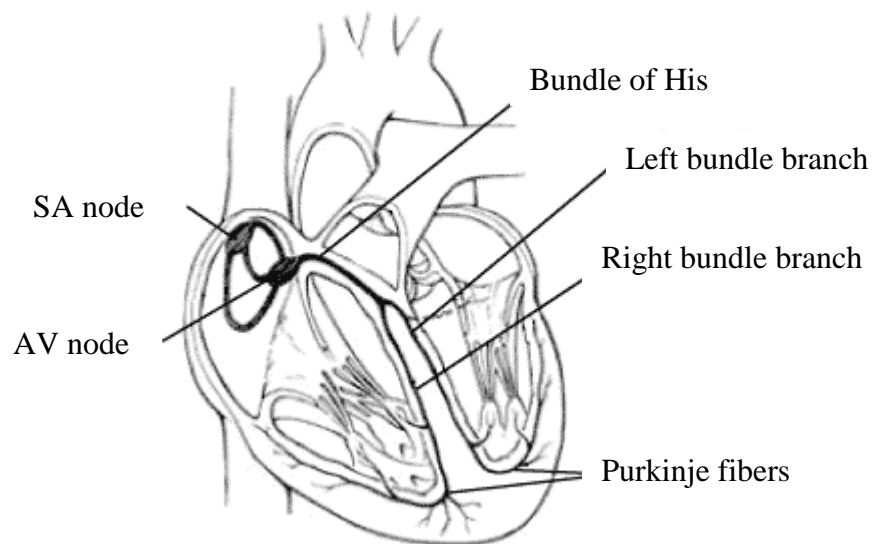


Figure 2-3: Conduction system of the heart [12].<sup>2</sup>

The following steps describe the conduction process shown in Figure 2-4 [13].

---

<sup>2</sup> Copyright © 2008 St. Jude Medical, Inc. All rights reserved

1. The SA node, called the pace maker, provides the electrical pulse that initiates the electric wave that traverses the heart.
2. The wave traverses toward the right and left atrium. These waves cause the atrial cells to conduct the electrical activity.
3. The wave passes through the AV node, which acts as an electrical relay station between the atria and the ventricles.
4. The wave traverses through the common bundle and the bundle branches to activate the ventricles.
5. The Purkinje fibers are activated, and the ventricular muscles are activated.
6. Finally, the ventricular cells start to repolarize, recover, and prepare for the next beat.

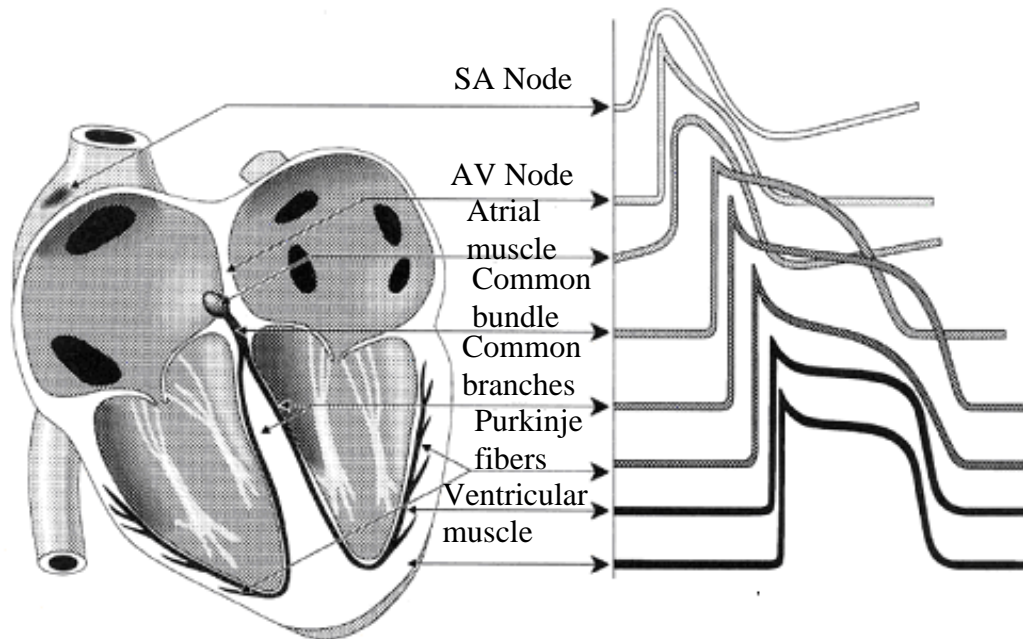


Figure 2-4 Electric Activity (activation sequence) of the heart cells generating an ECG signal [14].<sup>3</sup>

<sup>3</sup> Figure 2-4 is printed with permission from Jaakko Malmivuo.

Now that the cardiac cell activity and the cardiac activation and conduction sequence have been presented, the next section presents the electric activity measurement at the body surface.

### ***2.3 Electric Activity Measurement***

The electrical currents that initiate the contraction of the heart also spread through the body. This electrical activity can be recorded on the body surface and provides a noninvasive way to measure the electrical activity of the heart. The measured electrical activity is called an electrocardiogram (ECG) [11]. The ECG signals are captured by 12 electrodes. The measurement of the electrical potential between two limb (arm or leg) electrodes is called a lead. The modeling approach in this work uses this potential difference of the cardiac cell group activity between two electrodes to generate an ECG signal. The different electrode placements and the ECG features and properties are discussed in this section.

The leads between the three limb electrodes are called “Standard Lead I, II, and III” referring to the two arm electrodes and the left leg electrode. By connecting the points of the electrodes, the relationship between the standard leads is called Einthoven's triangle. The “Standard Leads” were first used by Einthoven to measure the ECG signal of a frog. Einthoven's triangle is used when determining the electrical axis of the heart, called the hexaxial reference system. The six leads consist of the bipolar leads (I, II, and III) and unipolar leads (aVR, aVL, and aVF) [11]. The 12 leads positioning and a sample ECG signal are shown in Figure 2-5 and Figure 2-6, respectively.

The bipolar leads are the measurement between two relatively distinctive points. Lead I measures the activity between + left arm and – right arm. Lead II measures the

activity between + left leg and – right arm. Lead III measures the activity between + left leg and – left arm.

The unipolar leads are "augmented vector" leads whose first letters are aV. The third letter refers to the positive pole (R right arm, L left arm, F foot or left leg). The negative pole is the area between the two remaining axis. The V leads or the precordial leads are considered as "probing electrodes" that measure the potential at specific locations and general body area. They are unipolar, and their usefulness depends on their placement as shown in Figure 2-5.

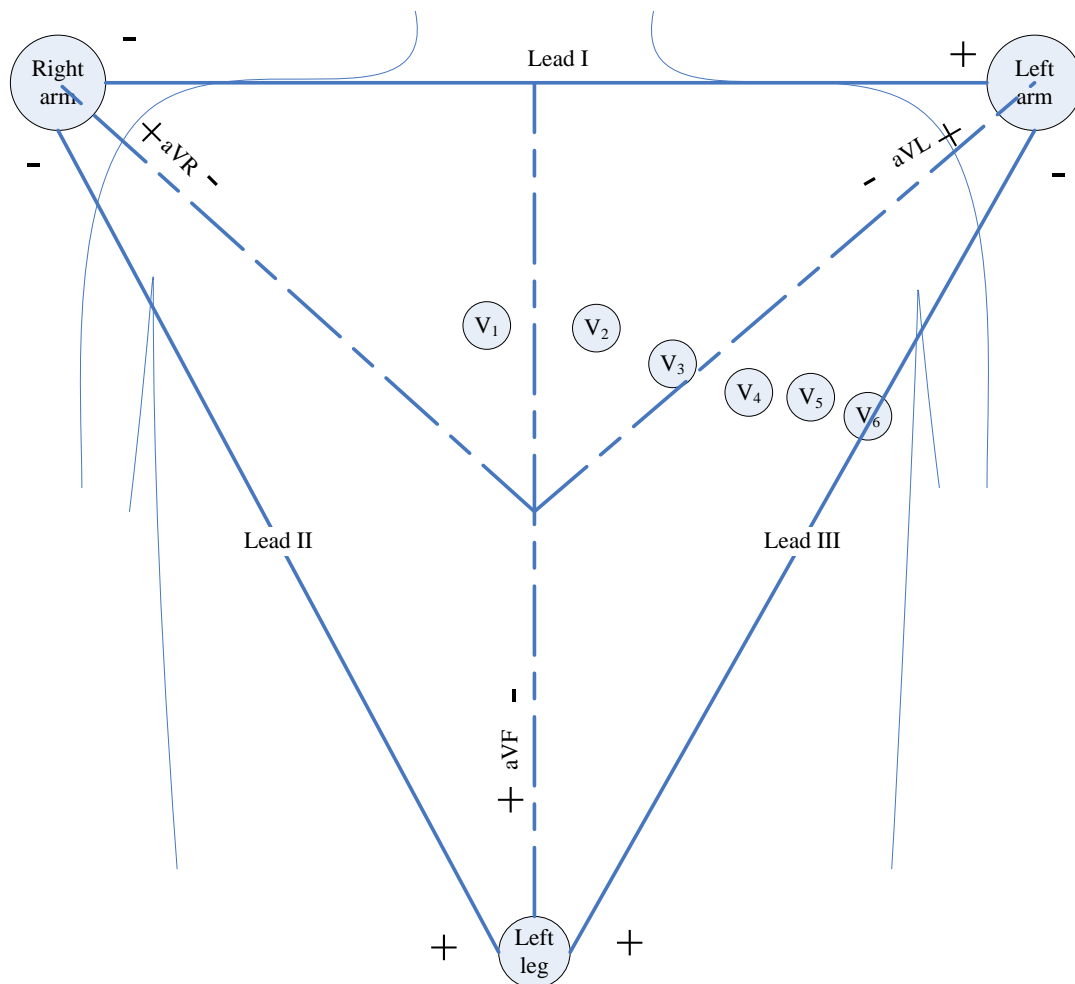


Figure 2-5: Electrocardiographic view of the heart.

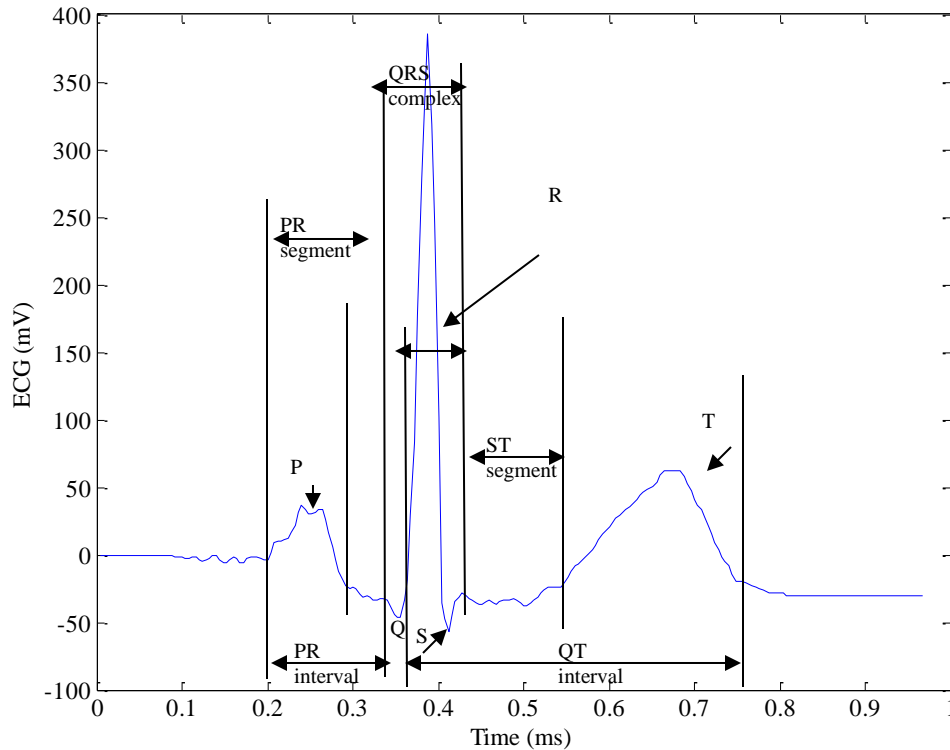


Figure 2-6: A sample annotated ECG signal at Lead I.

### 2.3.1 Wave Identification

An ECG, as seen in Figure 2-6, has different characteristics depending on the location of the electrode recording it. ECGs are characterized by those deflections below and above the baseline (the zero line) [8]. When the curve shows a negative deflection, below the baseline, it means the electric wave is moving away from the electrode. When the signal rises above the base line, i.e., positive deflection, the wave is moving toward the electrode.

The following sections describe the ECG waves. The ECG waves are the P wave, Q, R, and S waves (QRS complex), T wave, and U wave.

#### P Wave

The first wave in the ECG signal is called the P wave. The P wave represents the depolarization of the atria. The P wave is generally upright in leads I, II, aVf, and V3 through V6; and inverted in aVR, V1, and V2 [8].

### QRS Complex

The Q wave is the first downward deflection after the P wave. If there is no downward deflection, then the Q wave does not exist. The R wave is the first upright wave after the P wave regardless if the Q wave is present. The S wave is the negative deflection following the R wave. The combination of the Q, R, and S waves is called the QRS complex [8].

### T Wave

The T wave appears after the S wave and represents the ventricular repolarization. It follows the QRS complex and is generally upright and rounded in the hexaxial leads except for aVR, where it is downward [8].

### U Wave

The T wave might be followed by the U wave representing late ventricular repolarization or deficient levels of potassium [8].

## **2.3.2 Intervals and Segments**

In addition to the waves, the ECG consists of segments and intervals, which are identified by the beginning and end of the waves they enclose. The following sections describe the PR and the QT intervals and the ST segment.

### PR Interval

The PR interval is the time from the beginning of the atrial depolarization to the beginning of the ventricular depolarization, including the activation of the Purkinje fibers. It is measured from the beginning of the P wave to the beginning of the Q wave. The segment between the end of the P wave and the beginning of the Q wave is called the PR segment [8].

### QT Interval

The QT interval represents the ventricular depolarization and repolarization. It is measured from the beginning of the Q wave to the end of the T wave. The QT interval

varies with heart rate, sex, and age. Under normal conditions, the QT interval should be less than half of the distance between two consecutive R peaks (RR interval) [8].

### ST Segment

The ST segment occurs when the QRS complex returns to the baseline. The return point is called the J-point or junction point. Generally, the ST segment is isoelectric. However, it might slightly deviate above or below the baseline. It might also slope as a small curve gradually toward the T wave [8].

## **2.4 Cardiac Activity Summary**

Summarizing the heart activity, the cardiac mechanical and electrical systems are related in the sequence of which they operate. The relation between the electrical and mechanical systems and how they are represented on the ECG signal are presented in Table 2.1. The activation of the SA node denotes the beginning of the cycle for the heart activity. The atria cells depolarize, which cause the atrial muscles to contract. The effect of the atrial activity appears on the ECG as the beginning of the P wave. The electrical activity stops at the AV node. This signals the blood flow to the ventricles and appears on the ECG signal as the end of the P wave and beginning of PR segment. This denotes the end of the atrial activity and beginning of the ventricle activity. The ventricle activity begins by the electrical signal traveling from the AV node toward the bundle of His, which is seen as the beginning of the Q wave. The wave then travels to the bundle branches, which appears on the ECG signal as the rest of the Q wave. The signal travels through the Purkinje fibers, and the right and left ventricles depolarize, initiating the contraction of the ventricles that is seen as the R and the S waves. The repolarization of the ventricles denotes the relaxation of the ventricles and is shown as the ST segment and T wave.

Table 2.1: Sequence of mechanical and electrical events during a single cardiac cycle [15].

Sequence	Electrical Function	Mechanical Function	Electrical Representation
1	SA node emits electrical signal		
2	Atria depolarize	Atria contract	Start of P Wave
3	Electrical signal pauses at AV node	Blood flows to ventricles	End of P Wave
4	Electrical signal travels down Bundle of His to Bundle Branches		Q wave
5	Atria repolarize while ventricles depolarize	Atria relax, ventricles contract pumping blood to lungs and body	R and S wave
6	Ventricles repolarize	Ventricles relax	T wave

## 2.5 Coronary Artery Disease

Now that the cardiac electrical and mechanical systems have been presented, this section describes the stages of coronary artery disease: myocardial ischemia, injury, and infarction. These diseases are caused by the lack of oxygenated blood arriving at the cardiac cells. The next section describes the coronary circulation, i.e., circulatory system responsible for delivering oxygenated blood to the heart.

### 2.5.1 Coronary Circulation

The cardiac muscle requires oxygen during its operation; which demands its own circulatory system called the coronary circulation. The heart has its own arteries and veins to maintain its operation [11].

Two major arteries that branch from the aorta feed the cardiac muscle: the right and left coronary arteries. The right coronary artery delivers oxygen-rich blood to the

right atrium and right ventricle. The left coronary artery feeds the left chambers of the heart. The left coronary artery, unlike the right artery, splits into two vessels called the transverse and descending branches [11]. The amount of blood delivered to each side varies according to the individual. Generally, about one half of all people have a dominant right artery, three in ten have equal delivery on both sides, and the rest have a dominant left artery. In addition to the arteries, the heart has more than 2000 capillaries per  $6 \times 10^{-5} \text{ m m}^3$  that help provide the sufficient oxygen supply to the heart [11].

### **2.5.2 Myocardial Ischemia, Injury, and Infarction**

Now that the coronary circulation has been defined, this section presents the causes of coronary artery disease. Additionally, this section presents the effect of this disease on the ECG signal.

There are three stages of myocardial abnormalities related to coronary artery disease in humans. The first stage is known as ischemia, a transient reversible stage, which shows depression in the ST segment and/or inversion in the T wave. The second stage is myocardial injury, which is an intermediate stage that often appears in the elevation of the ST segment. The third stage is myocardial infarction, which is known as a permanent irreversible damage to the cardiac muscle that often appears as changes in the QRS complex.

Ischemia is the lack of sufficient blood supply from the coronary arteries to the surrounding cardiac cells. Generally, the cause can be traced to coronary artery disease caused by the blockage of the coronary artery due to fat buildup and cholesterol, known as plaque. The causes of ischemia can also be traced to trauma (a serious bodily injury), anemia (deficiency in red blood cells), or coronary vasospasm (a sudden contraction of a

blood vessel that reduces the blood flow). The stage following myocardial ischemia is myocardial injury [11, 15], a reversible condition.

Myocardial infarction is the sudden death of the myocardial tissue and cells due to the prolonged lack of blood supply to the ventricles. This condition is irreversible. If it becomes severe enough, the heart is not able to supply blood to the entire body. Figure 2-7 shows an example of one of the conditions for myocardial ischemia/infarction, where the blood flow is blocked in the coronary artery.

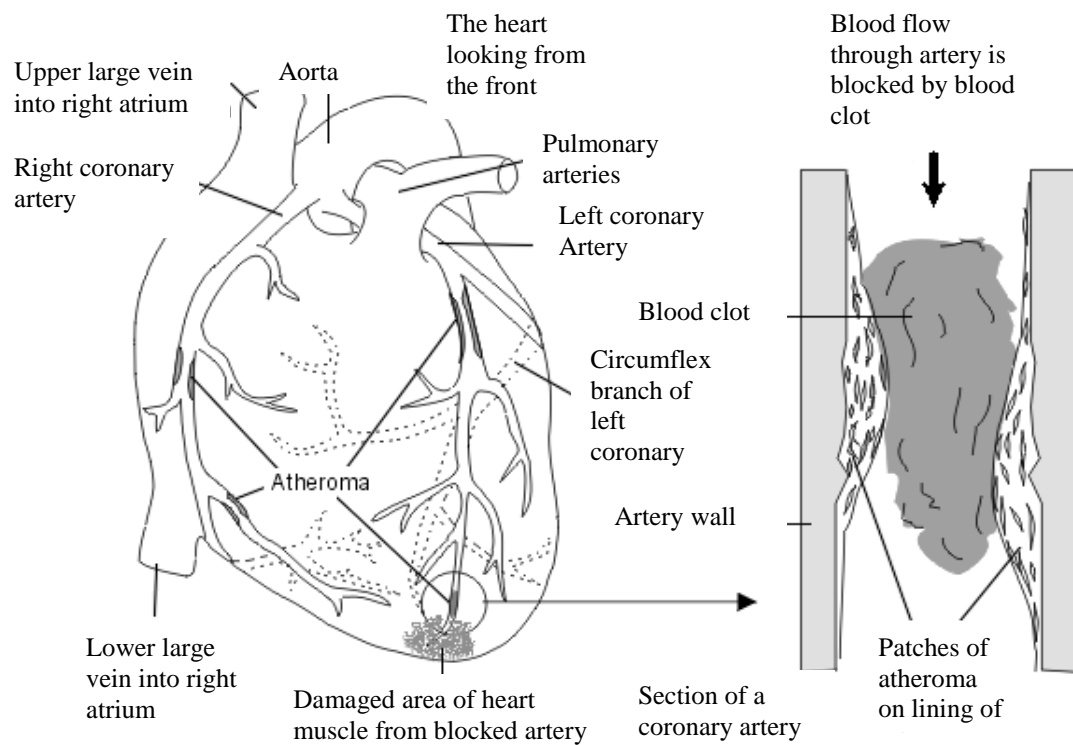


Figure 2-7: How myocardial infarction occurs [16]<sup>4</sup>.

### 2.5.3 Coronary Artery Disease ECG Effects

Now that the stages of coronary heart disease are defined, this section describes the effects of myocardial ischemia and myocardial infarction on ECG leads. Generally,

<sup>4</sup> Diagram copyright EMIS and PiP 2007, as distributed on [www.patient.co.uk](http://www.patient.co.uk)

the leads facing the area of involvement show the indicative changes. Additionally, the leads opposing the area of involvement show reciprocal changes, i.e., those changes are the exact reversals of the changes occurring in the leads directly over the injury.

The three indicative changes are the inversion of T wave, the elevation of depression of the ST segment, and the appearance of the Q wave. These changes occur in approximately 80% to 85% of patients with proven myocardial infarction. It is to be noted that the T wave is always normally inverted in aVR and might be normally inverted in leads III and V1 [11].

### **2.5.3.1 Myocardial Ischemia**

As mentioned previously, myocardial ischemia affect the ECG at the lead close to the ischemic region. The literature has established that there is a strong correlation between elevation and depression of the ST portion of the ECG signal and cardiac problems related to ischemia and infarction [17]. In 1920, Pardee first claimed that ST elevation was a sign of ischemic problems [17]. According to Fozzard and Janse, the abnormality is due to the way that ischemic tissue conducts electricity [18, 19]. It is generally accepted that an ST deviation or elevation greater than 1 millivolt may indicate the presence of ischemia. ST elevation and deviation have been used by cardiologists to identify myocardial ischemia. Now that the basis for ischemia detection has been presented, the next section describes the relation between the infarction location and 12 standard leads.

### **2.5.3.2 Localizing Infarcts**

The effects of myocardial infarction at the right ventricles are difficult to detect using the 12 standard leads. Therefore, this section presents the effect of myocardial

infarctions occurring at the left ventricles. The left ventricular chambers can be divided into areas: anterior, septal, apical, inferior, lateral, and posterior walls. The occurrence of infarcts in multiple locations can be called anteroseptal, anterolateral, inferolateral, and so on [11]. Figure 2-8 shows a sketch of the areas of the left ventricular chambers of the heart.

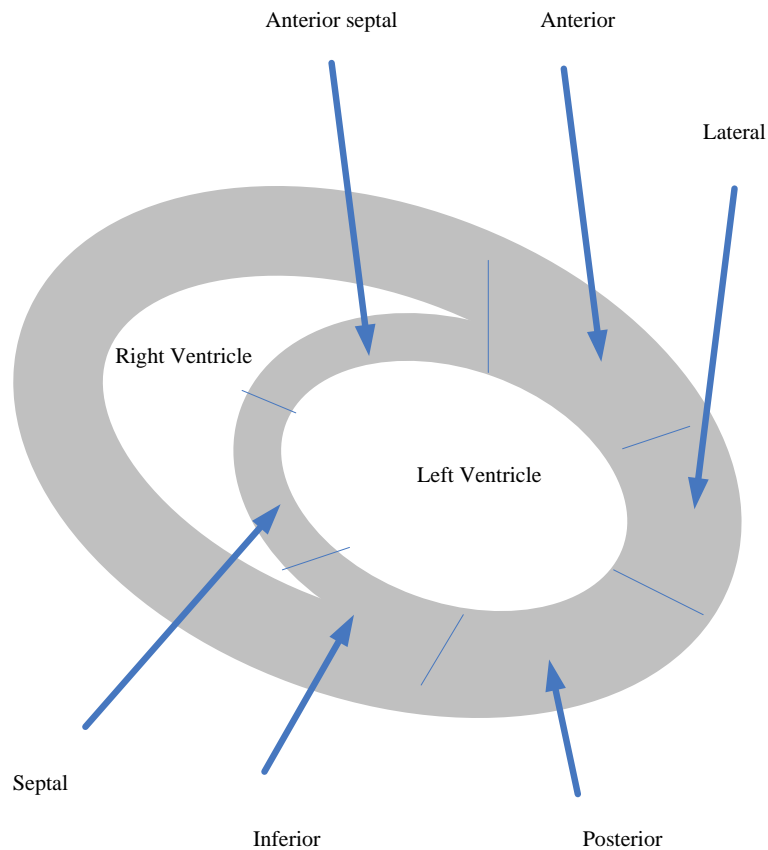


Figure 2-8: Left ventricular chamber areas.

In addition to ST segments, infarctions affect the Q waves of the ECGs measured at the leads close to the infarcted location. Two types of Q wave activity indicate the location of myocardial infarction. The first type causes significant changes in the Q wave in the leads close to the infarct. These infarcts are referred to as Q wave infarcts, and they

consist of 75% of all infarcts. The second is the disappearance of the Q wave in the leads close to the infarct. These infarcts are referred to as non Q wave infarcts.

### 2.5.3.3 Q wave infarcts

In the Q wave infarcts, the changes in the ECG leads generally appear as a series of stages that allows the evolution of the infarct to be observed. In the first 72 hours, the leads over the area of injury show ST elevation. The next 24 hours show significant Q wave changes in the same leads over the area of the infarct. The Q wave changes include a change in depth (Q wave duration  $\geq 0.04$ ) and in width (magnitude  $\geq 25\%$  of the R wave) [11]. Additionally, it might be possible to detect infarctions during the hyperacute phase by recognizing high ST elevation without the presence of the Q wave. These indicative changes can be seen for the first four to six hours following chest pains. The next stage is the fully evolved acute phase, where the ST segment remains elevated, and the T wave becomes inverted in the same leads located over the area of the infarct. Generally, the second stage lasts as long as seven to ten days [11]. Finally, in the last chronic phase, i.e. after 72 hours of the first chest pains, the ST segment returns to the baseline, the T wave returns to normal, and the Q wave remains abnormal. Table 2.2 shows a summary of the progressive phases of acute myocardial infarction and the relative changes appearing on the leads over the infarcted area.

Table 2.2: Progressive phases of acute myocardial infarction [11].

Phase	ECG Changes
Hyperacute (lasts 4-6 hours)	Elevation of the ST segment, tall and wide T waves
Fully evolved acute phase	Pathological Q waves, elevated ST segment, tall and wide T waves
Chronic	Pathological Q waves, ST segments return to normal

It is possible to differentiate between evolving myocardial infarctions and old ones [11]. For example, if the ST segment is elevated, the infarct is called acute. If the Q wave is seen with an inverted T wave and the ST segment at the baseline, the infarct is called age indeterminate. Finally, if the Q wave is seen in a lead where it should not normally be, the ST segment is at baseline, and the T wave is upright, then the infarct is considered old. The conditions for old infarcts can last for months or even years, making it impossible to determine the age of the infarct [11]. Because it is difficult to determine the age of the infarct, a series of ECGs is necessary to keep track of the evolution of the infarct.

#### **2.5.3.4 Non-Q wave infarcts**

As discussed earlier, non-Q wave infarcts, the second type of infarcts, occur in 25% of all acute myocardial infarctions [11], because they are partial-thickness infarcts. The indications that appear on the ECG are ST elevation/depression, deep T wave inversion, and no Q wave is seen. Generally, the patients with non-Q wave infarct experience repeated episodes of post-infarction chest pain and are more likely to have recurrent infarcts.

#### **2.5.3.5 Relation between Leads and Infarct Location**

Now that the changes caused by myocardial infarction have been presented, this section presents the relation between the infarcted location and the 12 standard leads. Table 2.3 shows the changes occurring in the ECG above the area of the infarct and their relation with respect to each of the areas of the left ventricular chamber [11].

Table 2.3: ECG changes seen in acute myocardial infarction [11].

Area	Changes and leads
Anterior	Q or QS in $V_2$ through $V_4$
Septal	Q or QS in $V_1$ through $V_3$
Lateral	Q or QS in I, aVL, and $V_5$ through $V_6$
Inferior	Q or QS in II, III, and aVF
Posterior	Tall R waves in $V_1$ through $V_3$

The posterior infarct can occur as the reduction of the S wave in  $V_1$  through  $V_3$  rather than the actual tall R wave. Also, the changes must be seen in at least two of the three leads over the suspected area. Changes in one lead will not be diagnosed as an acute posterior infarct [11].

In the case where more than one location is infarcted on the left ventricular free wall, the changes will occur in leads over multiple areas. For example, if the infarct is inferolateral, then ST elevation, T wave inversion, and Q wave changes appear in leads II, III, aVF, and  $V_4$  through  $V_6$ . Similarly, an anteroinferior myocardial infarction shows similar changes in leads  $V_2$  through  $V_6$ , and II, III, and aVF [11].

## 2.6 Summary of Chapter

This chapter presented a description of the cardiac mechanical and electrical systems. Additionally, a description of the lead system and electrocardiogram features are presented. Since this work applies the model in the detection of myocardial ischemia and localization of myocardial infarction. This chapter also presented a description of the causes and effects of these diseases on electrocardiograms.

The next chapter presents a history review of cardiac modeling, forward and inverse problem solutions, and automatic myocardial ischemia detection, as well as myocardial infarction localization.

## **Chapter 3      Background of the Problem**

The previous chapter described the anatomy of the heart, cardiac mechanical and electrical systems, and the causes of coronary artery diseases. This chapter, the second of the background chapters, presents a historical review and brief background of the cardiac modeling problem, the automatic ischemia detection problem, and the infarction localization problem. This chapter presents previous research methods used in the modeling of the cardiac electrical activity, solving the forward and inverse problem, and the detection of myocardial ischemia, and the localization of myocardial infarction.

This chapter is organized into two sections. The first section presents the current cardiac modeling methods. The cardiac modeling historical review includes geometric modeling, the modeling of the electrical activity cardiac cells and tissue, and the inverse and forward problems. The second section presents a historical review of current diagnostic methods for myocardial ischemia and myocardial infarction.

### ***3.1 Cardiac Modeling***

Cardiac modeling is divided into three problems: modeling the electrical activity of the cells and tissue and solving the inverse or forward problems. Current modeling approaches that solve the cardiac modeling problem require having a geometric model of the heart and torso of the patient and a model of the cells and tissue to solve for the forward and inverse problems.

This section on cardiac modeling is further subdivided into five subsections. The first subsection explains the current methods used to model the heart and torso geometrically. The following two subsections describe the current research related to

modeling the cardiac cell and tissue electrical activity. Finally, the current solutions for the forward and inverse problems are presented.

### 3.1.1 Geometric Modeling

As mentioned previously, the current modeling methods require geometric modeling of the heart and body torso. Current methods use finite element (interpolation) basis functions to generate continuous geometrical models of the heart and body torso. This section presents the current methods used in cardiac geometric modeling.

Generally, Lagrangian interpolation in one-, two-, and three-dimensions, and cubic Hermite basis functions are used in geometric modeling. The finite element methods generally divide the heart into a set of points called nodes. These nodes are interpolated using linear, quadratic, and higher order Lagrangian basis functions. However, the Lagrangian basis function does not provide continuity on the boundaries. Thus, Nielsen et al. [10] proposed the use of Hermite basis functions, which provided continuity at the boundaries.

To provide an accurate geometrical model of the heart, LeGrice et al. [10] provided a detailed structural measurement of the heart. Generally, cardiac geometrical models are determined from images using magnetic resonance imaging (MRI), computed tomography, or ultrasound. Moreover, the images of the heart are digitized and fitted with linear and nonlinear meshing techniques to create a continuous geometrical model of the heart. LeGrice et al. used linear fitting technique because it is a linear least square fit of the MRI measured data. In 1997, Bradley et al. used a nonlinear fitting technique on the MRI data [10]. In 1989, Young et al provided a smoothness constraint to the optimization function to have a smoother fit to the digitized data obtained from MRI.

In 1991, Nielsen et al. proposed the use of a prolate spheroid coordinate system to geometrically model a canine heart. The use of this coordinate system simplified the problem since it was dealing with just the radius to produce the shape, reducing the problem to a linear fitting one [10].

In 2002, Tomlinson et al. proposed the use of a Cartesian system to fit data from the canine heart. This coordinate system provides more flexibility in modeling the different cardiac surfaces. In 1999 and 2000, Young et al. presented a three-dimensional patient-specific heart model developed using cardiac MRI scans. In 2003, the same approach was applied by Stevens to model a porcine heart and by Schulte et al. to model a human heart [10].

Human torso models are used to provide an insight on the relation between the electrical activity of the heart and human torso. In 1996, the first human model was provided at Auckland using high resolution MRI data set, which was used to develop a fitted model by Pullan et al. in 2004 [10].

### **3.1.2 Cell Modeling**

Now that the current geometrical models of the heart and body torso have been presented, this section presents a historical overview and brief description of the current cell models. As mentioned in chapter 2, the electrical activity of the cardiac cell is the result of the chemical and electrical gradients across the outer membrane. Most of the components of the current cell models are based on the Hodgkin and Huxley model. The Hodgkin and Huxley model was first developed in 1952 to represent the behavior of a giant squid. Since the development of Hodgkin and Huxley model, more detailed models have been presented. The most widely known models are those developed by Noble et al.

in the 1960's and by Rudy et al. in the 1980's. Generally, the current models focus on modeling certain cells such as the original Noble model of the Purkinje fiber in 1962, the Beeler-Reuter ventricular cell model developed in 1977, the Difrancesco-Noble model of the Purkinje fiber in 1985, the mammalian ventricular cell models developed by Lou-Rudy in 1991 and 1994, and the Noble model of a guinea pig ventricular cells in 1998.

The Hodgkin and Huxley model and the cell models that follow are based on:

$$\frac{dy}{dt} = \alpha_y (1 - y) - \beta_y y . \quad (3.1)$$

Equation (3.1) describes the current flow resulting from the movement of the ions over the cell membranes. The activation and inactivation gating, threshold, voltage that cause the cells to activate and deactivate are  $m$  and  $h$ :

$$\frac{dm}{dt} = \alpha_m (1 - m) - \beta_m m , \quad (3.2)$$

$$\frac{dh}{dt} = \alpha_h (1 - h) - \beta_h h , \quad (3.3)$$

where  $\alpha$  and  $\beta$  are functions of the voltage

$$\begin{aligned} \alpha_m &= \frac{a(V_m + b)}{\exp^{[a(V_m + b)]} - 1}, \\ \beta_m &= c \exp\left[\frac{V_m}{d}\right], \\ \alpha_h &= f \exp\left[\frac{V_m}{g}\right], \\ \beta_h &= \frac{1}{e^{[a(V_m + e)]} + 1}, \end{aligned} \quad (3.4)$$

with variables  $a$ ,  $b$ ,  $c$ ,  $d$ ,  $e$ , and  $f$  depending on the cell activity.  $V_m$  is the magnitude of the ECG signal. By defining  $n$  as the activation gating variable, the outward current is described by

$$\frac{dn}{dt} = \alpha_n (1 - n) - \beta_n n, \quad (3.5)$$

where

$$\alpha_n = \frac{u (V_n + v)}{\exp^{[a(V_n + v)]} - 1}, \text{ and} \quad (3.6)$$

$$\beta_n = w \exp^{\left[\frac{V_m}{x}\right]},$$

with variables  $u$ ,  $v$ ,  $w$ , and  $x$  depending on the cell activity. Finally, by defining the leakage current  $I_L$  as

$$I_L = g_L (V_m) (V_m - E_L), \quad (3.7)$$

where  $g$  as the conductance of the ions

$$g_{Na} = \bar{g}_{Na} m^3 h, \text{ and} \quad (3.8)$$

$$g_K = \bar{g}_K n^4. \quad (3.9)$$

Therefore, the final Hodgkin and Huxley model is:

$$\begin{aligned} I_{NA} &= g_{NA} (V_m - E_{NA}) \\ I_K &= g_K (V_m - E_K) \\ I_L &= g_L (V_m) (V_m - E_L) \\ I_{ion} &= I_{NA} + I_K + I_L. \end{aligned} \quad (3.10)$$

The voltage for the heart cell activity can be determined by solving equation (3.11):

$$I_m = C_m \frac{\partial V_m}{\partial t} + I_{ion}. \quad (3.11)$$

The complexity of this model comes from the nonlinearity and the coupling of the differential equations (3.1) - (3.3). The number of unknown variables is more than 11, just to be able to determine  $I_{ion}$  and solve for  $V_m$ .

The difference between the Hodgkin and Huxley model and the current ones is in the level of complexity, which increases as the number of ionic currents increase. For example, in addition to the three currents ( $I_{Na}, I_K, I_L$ ) and the three gating variables ( $m, h, n$ ) in the Hodgkin and Huxley model, the Noble model (1962) used the Hodgkin and Huxley model to represent the cardiac cells. Moreover, the Beeler Reuter model used four currents ( $I_{Na}, I_{K1}, I_s, I_{x1}$ ) and six gating variables ( $m, h, j, d, f, x_1$ ). Similarly, the DiFrancesco and Noble model used 12 currents and 7 gating variables, while the Luo-Rudy model (1994) used 11 currents and 11 gating variables. Additionally, in 1998, Noble et al. used 27 ionic currents and 17 gating variables to model the cardiac cells.

In addition to the models presented above based on modeling the physiological activity of the cellular activity, Fitzhugh and Nagumo in 1961 developed a model based on cubic polynomial excitation. This model is a nonlinear differential equation. If it is excited by an external source  $I_{ext}$ , a spike occurs in  $v$  and  $\omega$  before they return to rest:

$$\begin{aligned}\dot{v} &= v - v^3 - \omega - I_{ext} \\ \tau \dot{\omega} &= v - a - b\omega.\end{aligned}\tag{3.12}$$

### 3.1.3 Tissue Modeling

Now that the existing models for the cell electrical activity have been presented, this section describes the latest modeling methods that represent the electrical activity of the cardiac tissue. Tissue modeling is defined as the combination of the cellular models to generate the electrical activity at the heart surface. The multi-cellular tissue modeling can be either discrete or continuous. The discrete approach uses the cell as a building block to generate a complex model of the whole heart. The cells are considered to be connected by

resistances. This type of modeling is known as the network model and has been used by van Capelle and Durrer in 1980, Leon and Roberge in 1991, and Trayanova in 1996, and Rudy in 2000. These models contain over  $10^5$  cells, yet this represents a small fraction of the total muscle volume. With this huge number of cells and with the number of unknowns as shown above, and with even the current computational power, the computational complexity of using the cellular models presented above for modeling the forward and inverse problem is very computationally expensive. In 2007, Farina et al. reported that it took three minutes to compute the electrical activity at the tissue and 17 minutes to generate a single beat ECG for every iteration of the forward problem solution on a workstation with a PowerPC G5 processor and 2 GB of memory [7].

The continuous models developed by Pullan et al. in 2004 require accurate models of the heart and its boundaries. Generally, the cable model, series of cells connected in series with resistances in between, is used to represent the continuous models. Due to the nonlinearity of the cardiac tissue, the propagation of the electric activity of the cardiac cells is governed by coupled nonlinear differential equations (Bidomain equations). A finite difference method was used by Quan et al. in 1998 to solve the differential equations governing the electrical activity of the heart cells. Additionally, in 1994 Culloch et al. and Vigmond et al. in 1998 used finite elements to solve the Bidomain differential equations. Finite difference methods were also used to solve for these differential equations by Buist et al. in 2003.

### **3.1.4 Forward Problem**

Now that the current cardiac electrical activity modelling methods have been presented, this section describes the previous forward solutions, i.e. electrocardiogram

(ECG) generation. The modelling of the electrical fields over the body surface from the cardiac electrical activity is called the forward problem of electrocardiology. However, since the cardiac electrical activity at the heart surface cannot be measured using easily, researchers have defined the forward problem as the generation of the electrical activity at the body surface from estimates of the cardiac region activity [10].

To solve the forward problem, researchers developed wave propagation models through the heart, tissues of the human body, and the body surface. The propagation models are highly nonlinear integral equations derived from Maxwell's equations. The most commonly used solutions use finite element methods.

To solve the governing equations, certain assumptions have been made regarding the modeling of the electric source on the heart surface. In 1933, Wilson et al. used a single dipole, while in 1966, Boineau et al. used a multi-polar source to describe the cardiac activity [10]. In 1978, Miller et al. used a multiple dipole approach to model the different regions of the heart [10]. To improve the computational complexity, the dipolar source is used to model a group of myocytes. This is achieved by scaling the action potential at each nodal point. Wei et al. in 1995 used 54 dipoles to represent 50,000 cells. After using the dipoles as a model for the electric source, finite element, finite difference, or a combined finite element-derived finite difference method is used [10].

### **3.1.5 Inverse Problem**

The inverse problem is the estimation of the electrical activity at the cardiac surface from measurements performed at the body surface. Since measuring the electrical activity at the surface of the heart is invasive, researchers have been studying the ability

to estimate the electrical activity at the heart surface from densely sampled electrocardiographic signals at the body surface.

Several studies have investigated the effect of the torso geometry on the solution of the inverse problem. One of the earliest studies was performed by Rudy et al. in 1986. The model used involving Rudy's method is a set of eccentric spheres to represent the heart. Due to the simplicity of the Rudy's geometrical model of the heart, it was easy to determine the electrical activity over the sphere. This allowed them to determine the changes of the electrical propagation over the sphere for different sphere locations and sizes.

Additionally, in 1995 Throne et al. used the eccentric spheres system to look at the effect of errors in geometry and conductivity to the inverse problem. Four different configurations were used to solve the inverse problem. Their results showed that the inverse solution was slightly affected by the heart size effect, while the position has significant effect [10].

In 1989, Huiskamp et al. considered realistic torso geometries created from three patients using MRI images and triangularisation techniques. The model included the skin surface, lungs, and heart. They compute an inverse solution from the patient's ECG recordings and from ECG recordings of another patient. Their results show that the inverse solution is highly dependent on the patient's model. Similar results were determined by Johnston et al. in 1995, where they performed the study using 16 realistic torso models with variant sizes and heart positions [10].

In 2001, Rmanathan and Rudy studied the effects of using a zero order Tikhonov method [10]. By solving the inverse problem with different torso configurations including

different material properties, the authors showed that the configurations had minimal effects on the solution [10].

Now that the previous cardiac modelling methods have been presented, the next section describes the current diagnostic methods used in the detection of myocardial ischemia and localization of myocardial infarction.

### ***3.2 Diagnoses of Myocardial Ischemia, Injury, and Infarct***

Several methods are used for the diagnosis of myocardial ischemia and infarcts. The cost of these methods varies from being very accurate, yet very expensive, to less accurate, yet inexpensive. Each of the methods to be discussed later has advantages and disadvantages. Thus, the physician must select the diagnosis method on a patient-by-patient basis. The most commonly used methods are cardiac catheterization (angiography), echocardiograms, Magnetic Resonance Imaging (MRI), and monitoring ST elevations and QRST complexes in ECGs during exercise stress testing. The first three methods are known for their higher accuracy compared to the later method, although they are much more expensive. These diagnostic methods are described in turn.

#### **3.2.1 Cardiac Catheterization**

Cardiac catheterization is a combined hemodynamic and angiographic invasive procedure that provides a detailed anatomy of the condition of the heart. There are several different approaches to perform this procedure. The first, the direct method involves inserting a catheter in the antecubital area, which provides access to the brachial artery and vein. The catheterization of the right heart is done via the brachial vein, and the left heart is done via the brachial arteries. The direct approach is used with patients with peripheral vascular disease, obesity, hypertension, and wide pulse pressure. The

advantage of this approach is the increased catheter control. The major disadvantage is that if the artery is not repaired properly, it leads to haemorrhaging. The second approach, Seldinger approach, is the most popular approach because it does not involve atrial cutdown or repair. During this procedure, catheters are inserted using a guide wire via an introducer into the femoral artery and vein through the groin. The blood pressure is monitored using a stopcock system. After the procedure is performed, the catheters are removed, and pressure is applied for 20-30 minutes to insure clotting in the injection site. The advantages of this method are that the catheters can be left in place so that there is easy access to the coronary arteries for interventional purposes, and no artery repair is required. The major disadvantages include required bed rest after the procedure and less control of the catheters. A diagram showing the Seldinger approach is presented in Figure 3-1.

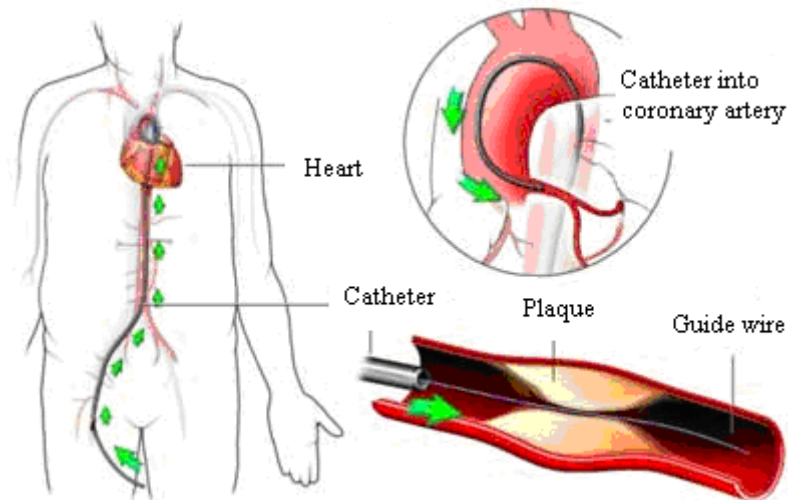


Figure 3-1: The Seldinger approach catheterization method [20]<sup>5</sup>.

<sup>5</sup> Copyright © 2005 Nucleus Communications, Inc. All rights reserved.

After the catheters are inserted using either method, the guide wire is removed leaving the catheters, which are used to measure the blood pressure within the blood chambers and to take blood samples. Additionally, special X-ray sensitive dye is released, and X-ray images are taken. Cardiologists use the X-ray image to diagnose the heart condition highlighting any constrictions or blockages of the arteries. The process is repeated for several locations to make an accurate diagnosis. The catheterization method has a high accuracy in locating a blocked artery, with sensitivity ranging between 90% and 98%, and specificity between 95% and 98%. The average cost for this diagnosis method is about \$17,000.

### **3.2.2 Echocardiogram**

Echocardiogram is a highly accurate method for diagnosing myocardial ischemic disease. During this procedure, the patient lies in the left lateral decubitus position, i.e., left side. Coupling gel is applied on the chest, and a transducer that transmits a sweeping wave of ultrasound is used. By measuring the Doppler effect and the time delay of ultrasound reflected/scattered off the heart, a fan shaped image is formed by the echocardiogram machine. The image reveals detailed information regarding the shape, size, and activity of the structures within the plane being imaged. From these images, cardiologists are able to diagnose abnormalities in the cardiac tissue. The accuracy of the echocardiogram is lower than that of the catheterization method. The sensitivity ranges between 80% and 90%, while the specificity ranges between 75% and 100% depending on the degree of the ischemic changes. The average cost for this diagnosis method ranges between \$500 and \$1000. A sample echocardiogram is shown in Figure 3-2.

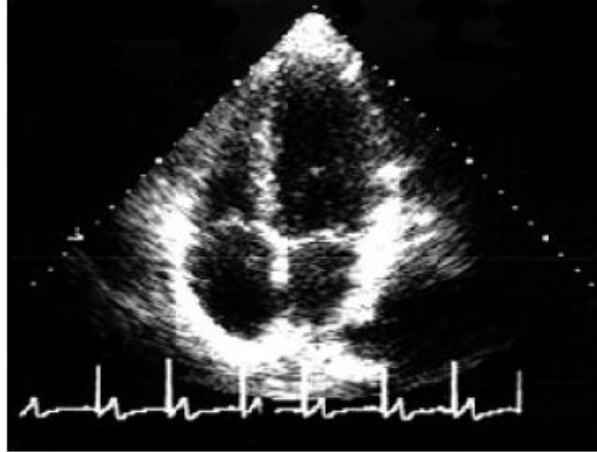


Figure 3-2: A sample echocardiogram [21]<sup>6</sup>.

### 3.2.3 Magnetic Resonance Imaging

Magnetic resonance imaging (MRI) is widely used in visualizing soft tissue structure. The MRI has finer detail and is safer than echocardiograms and X-rays since there is no ionizing radiation. The MRI creates cross-sectional images or slices through the plane of the body. MRI is easier for stationary organs such as the brain compared to the heart, a moving organ. The motion of the heart creates blurred images on regular MRI scans. To compensate for the heart motion, the MRI session lasts for an hour or longer. A gadolinium-based contrast material is used as a reliable indicator of myocardial infarction in MRI. This contrast helps indicate the altered cells due to myocardial infarction.

The accuracy for detecting myocardial infarction using MRI is moderate with sensitivity of 88% and specificity that ranges between 17% through 67%. The average cost for the cardiac MRI is more than that of the regular MRI. The cost of regular MRI ranges between \$400 to over \$2000. Figure 3-3 shows a sample cardiac MRI. The higher level of detail provided compared to echocardiograms and X-rays can be seen.

---

<sup>6</sup> Copyright © 2006 heartfailure.org. All rights reserved. All rights reserved

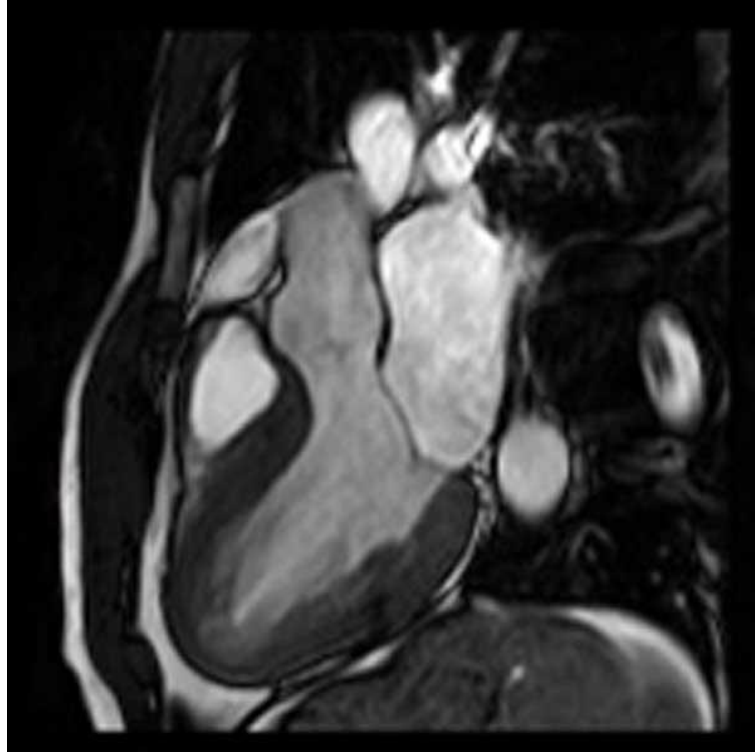


Figure 3-3: Cardiac MRI image [22].

### **3.2.4 Electrocardiograms**

As presented in chapter 2, electrocardiograms act as an indicator for myocardial ischemia myocardial infarctions. The following sections present the latest methods used in automatic ischemia detection and infarction localization.

#### **3.2.4.1 Myocardial Ischemia**

Significant research has been undertaken to develop a more accurate, less invasive, and less expensive method for detecting myocardial ischemia. Much of this research focuses on the use of ECG signals. This section discusses automatic methods used in the detection of myocardial ischemia. Having an accurate automatic method for detecting ischemic beats can help save physicians' time and patients' money. Various automatic methods have been proposed by researchers since 1983. However, these

methods have either been applied to a small dataset or required long duration of the ECG signal to make a decision.

In 1983, Pitas et al. applied a method to detect ischemic beats by modeling each beat using a mathematical model of two parameters. The parameters were used to distinguish the ischemic beats from healthy ones. The system was evaluated in a rather small dataset of eight ischemic and eight normal beats. The accuracy of this method was 87.5% [23].

In 1989, Shook et al. estimated the absolute ST segment deviation from the isoelectric line. The average of the ST deviation and slope was measured in every 30 seconds of the ECG signal. The rules used in the classification process were: 1 mm for the absolute deviation, 0.75 mm for the deviation, and zero for the slope. Another set of rules were used to decide the probability of the ischemic episode: 1 mm for the absolute deviation, 1 mm for the deviation, and zero for the slope. The first rule decides if the episode is "definite," while the second decides if it is "probable" [24]. The final system's output is the margins of the "definite" and "probable" ischemic episodes. The system was evaluated using 18 24-hour ambulatory ECGs, and the authors achieved sensitivity and positive predictive accuracy of 90% and 96%, respectively. The system employs rules that refer to ST-segment depression only.

In 1992, Badilini et al. used frequency analysis of the ST segment to diagnose ischemia. They concluded that the ischemic beats contain lower frequencies than the normal ones. This system has been tested on a dataset of 20 normal and 24 ischemic Holter ECGs, and the method achieved sensitivity and specificity of 95.8% and 90%, respectively [25].

In 1992, Jager et al. used Principal Component Analysis (PCA) of the ECG beat to detect ischemic beats from normal beats. The first five principal components for the QRS complex and the first five of the ST segment were used in the diagnosis process. The diagnosis process used a threshold analysis to decide if the beat is ischemic or healthy. Their system was evaluated using the European ST-T database. The obtained sensitivity and specificity were 85.2% and 86.2%, respectively. Additionally, Laguna et al. used the same approach for the analysis of the effect of the whole ST-T interval on ischemic beats [26].

In 1995, Senhadji et al. used a wavelet transform for the diagnosis of cardiac rhythms. Wavelets were used to examine both time and frequency information of the signal simultaneously since they are both oscillatory and localized in time. The features obtained from the wavelet transformation were used to classify beats as normal, ischemic due to ST-segment deviation, or premature ventricular contraction. The system was evaluated in a small dataset containing 20 ischemic and 20 normal beats and achieved sensitivity and specificity of 95% and 100%, respectively [27].

In the same year, Taddei et al. designed a rule-based system for two-lead ECG recordings that employs a geometric algorithm that calculates a 2D loop for the ST segment. For each cardiac beat, the ST-segment deviations are estimated in the two leads, and each pair of values is graphically represented sequentially in time. A graphical rule is used to identify ischemic episodes. The system was tested using the European ST-T database. The achieved sensitivity and specificity were 82% and 81% [28].

In 1997, Vila et al. performed a time-frequency domain analysis of the heart rate variability. The generated spectrum was divided into three frequency bands: very low,

low, and high. The diagnosis of the ST-segment was decided on the minimum and maximum values of these bands and their energies. The system was evaluated using 14 out of 90 recordings of the European Society of Cardiology (ESC) ST-T database. However, quantitative results were not reported [29].

Additionally in the same year, T. Stamkopoulos et al. proposed an approach using PCA and neural networks in the identification of ischemic beats. The system was evaluated on 60 out of 90 recordings of the European ST-T dataset. The accuracy of this approach was 84.4% and 78.8% for ischemic and healthy beats, respectively [1]. In a later work, Stamkopoulos et al. used PCA and radial basis neural networks to identify ischemic beats, and the accuracy is 90 [1].

In another work, Silipo and Marchesi proposed three more sophisticated ANN methods for ischemia detection with accuracies of 85% and 88%.

In 2003, Papaloukas used four different training algorithms with Multi-Layer Perceptrons (MLP) for beat classification. The approach was applied to the European ST-T database which were diagnosed beat-by-beat by three experienced cardiologists. The result of taking a majority vote of four systems resulted to 90% sensitivity and 89% specificity [30-32].

In 2003, Victor-Emil Neagoe applied a Neuro-Fuzzy Approach and PCA for the classification of myocardial ischemia. The accuracy shown in the paper was 100% for 50 features. However, the paper dealt with only identifying ischemic and normal patients, the features were extracted using template signals from the patients' healthy and ischemic beats, and the number of training and testing data were 40 patients, half used for training and half for testing [33].

### 3.2.4.2 Myocardial Infarction

ECGs are the most used tools in the diagnosis of myocardial infarction (MI). The advantages of the ECGs are that they provide an insight of the location and the extent of the infarct from the Q waves, especially at the left ventricular walls. More than 50 years ago, in 1949, Myers et al. reported the correlation between pathological Q waves and the location of the infarct. The results were confirmed in 1971 by Horan et al. The developed criteria is that the presence of abnormal Q waves in leads V1 and V2 is related to septal wall MI; in V3 and V4 to anterior wall MI; in V5 and V6, I, and aVL to lateral wall MI (I, aVL high lateral; V5 and V6, low lateral); and in II, III, and aVF to inferior wall MI.

Recently, to generalize a standard in the localization of MI, the American Heart Association agreed to divide the left ventricles into 4 walls: septal, anterior, lateral, and inferior; divided into 17 segments: 6 basal, 6 mid, 4 apical, 1 segment being the apex.

In 1989, Selvester et al. used a computer application to generalize the relation between the variations in the Q wave at the leads the location and extent of the infarct. These relations were later called Selvester's criteria. In 2002, Bayés de Luna et al. confirmed Selvester's criteria by using cardiac magnetic resonance imaging (CMR) as a gold standard. Bayés de Luna et al. studied the most frequent infarction patterns and their effects on electrocardiograms. These patterns have shown a specificity of at least 90% and sensitivity at least 80%, except for the patterns of the mid-anterior and lateral MI, which showed a sensitivity of at least 66%.

MRS Reddy et al. developed an approach based on the QRS measurement and neural networks to classify healthy and patients with inferior myocardial infarction. The accuracy was 79% with a specificity of 97% [34].

---

HL Lu et al. used a neuro-fuzzy logic approach for the classification of myocardial infarction. The ST elevation and magnitude of the T wave were measured manually and used as features during the classification process. The approach identified if the 12 leads are infarcted, and based on that, the infarct location is determined. The accuracy for detecting healthy patients was 89.4% and for detecting infarcted patients was 95.0% [35].

In 2007, Mneimneh et al. proposed the use of a reconstructed phase space with Gaussian mixture models to automatically localize myocardial infarctions. The details of this approach are described in appendix B.

The next chapter presents the data sets used in this work for the diagnosis of myocardial ischemia and myocardial infarction. Additionally, a simulated dataset is described for the testing the accuracy of the proposed forward problem solution.

## Chapter 4 Datasets

The previous chapter describes the current methods used in cardiac modeling, ischemia detection, and myocardial infarction localization. This work proposes an electrophysiological model and applies it to solve the forward and inverse problems, myocardial ischemia detection, and myocardial infarction localization. This chapter describes the datasets used in this work. The datasets presented in this chapter are the Long Term ST (LTST) database, used for the detection of ischemic and normal beats, the Physikalisch-Technische Bundesanstalt (PTB) dataset, used for the localization of myocardial infarcts, and a simulated dataset based on Clifford's model is used to for testing the accuracy of the forward problem solution.

### 4.1 PTB Dataset

The dataset was donated to Physionet by the Physikalisch-Technische Bundesanstalt (PTB), the National Metrology Institute of Germany. This dataset consists of digitized electrocardiograms (ECGs) collected at the Department of Cardiology of University Clinic Benjamin Franklin in Berlin, Germany from healthy volunteers and patients with various cardiac diseases [36].

The ECGs were recorded using the PTB recorder. The recorder has 16 input channels, (14 for ECGs, 1 for respiration, 1 for line voltage). The input voltage is  $\pm 16$  mV with an offset voltage of up to  $\pm 300$  mV. The recordings have a 16 bit resolution with synchronous sampling of 1 kHz [36].

The database consists of 549 records taken from 294 subjects. Each record includes 15 simultaneously measured signals: the conventional twelve leads (I, II, III, aVR, aVL, aVF, V<sub>2</sub>, V<sub>3</sub>, V<sub>4</sub>, V<sub>5</sub>, and V<sub>6</sub>), and the three Frank leads (V<sub>x</sub>, V<sub>y</sub>, V<sub>z</sub>).

Along with each recording, a header file containing a detailed clinical summary, including age, gender, and diagnosis is provided. The dataset contains 148 subjects with myocardial infarction, 54 healthy controls, 18 subjects with cardiomyopathy/heart failure, 15 with Bundle branch block, 14 with dysrhythmia, 7 with myocardial hypertrophy, 6 with valvular heart disease, 4 with myocarditis, and 5 miscellaneous [36].

## ***4.2 Long Term ST Dataset***

The Long-Term ST Database consists of 86 ECG recordings taken from 80 human subjects [36]. The database was contributed by different sources: the Laboratory for Biomedical Computer Systems and Imaging at the University of Ljubljana, Slovenia and the European ST-T (EST) database gathered by the Pisa group. For the purpose of consistency, the analog recordings of the EST were redigitalized for the LT-ST Database. Additionally, Zymed, Inc. contributed 18 recordings to the LTST database. The LTST database was contributed to Physionet on two dates. The first half, 42 records, was contributed on February 2003, and the second half was contributed on May 2007 [36].

Detailed annotation and clinical notes are provided for each ST deviation for all the 86 records. The duration of the records is between 21 to 24 hours. Each record contains two to three ECG leads. The records are digitized at 250Hz with 12 bit resolution. The LT-ST database is used in the differentiation between ischemic and healthy beats. The recordings contain signals with four different ST segment changes [36]:

1. ischemic ST episodes
2. axis-related non-ischemic ST episodes
3. slow ST level drift
4. mixtures of the above phenomena

The recordings were annotated by professional annotators using SEMIA, an interactive graphical user interface to a semi-automated algorithm for the measurement of ST levels written by the group in Ljubljana. Each recording was reviewed independently by expert annotators using SEMIA at each of the three sites (Ljubljana, Pisa, and Cambridge). Participants met several times annually to obtain the consensus reference annotations. The rules used during the annotation process are based on the reference function defined by Physionet. The reference function is patient independent. The standard value, called the ST deviation, is calculated as the difference between the ST level and a predefined ST reference function (shown in Figure 4-1) [36]. The steps taken to determine the reference function are [36]:

1. the initial value of the reference function is taken from the stable ST level at the beginning of the record
2. an expert must annotate the record labeling points of ST deviation
3. the resulting ST deviation is then labeled as ischemic or healthy

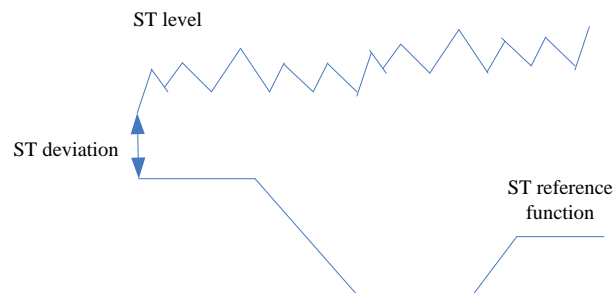


Figure 4-1: Example of ST deviation calculation

The criterion for determining the ischemic ST segments shown in Figure 4-2 is defined as [36]:

1. the ST event begins when the ST deviation exceeds  $50\mu\text{V}$ .
2. the ST deviation must exceed  $100\mu\text{V}$  for at least 30 seconds during the event.
3. the ST event ends when the ST deviation drops below  $50\mu\text{V}$  for at least 30 seconds.

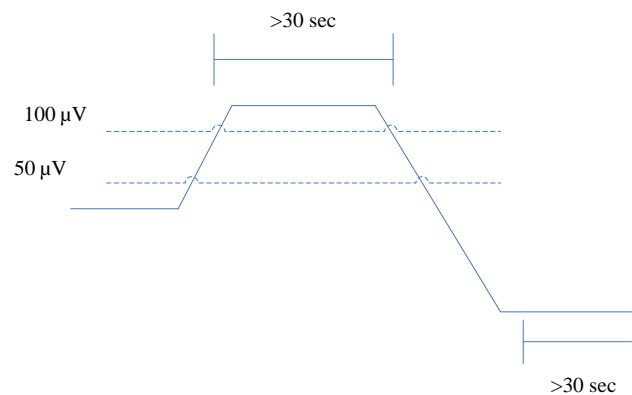


Figure 4-2: Definition of ST event

### 4.3 A General Gaussian Signal Model

The general Gaussian signal model (GGSM) has been developed by G. Clifford et al. The GGSM is based on the assumption that the ECG signal is varying smoothly and contains symmetric and asymmetric turning points, i.e. the ECG waves P, Q, R, S, and T can be represented by a set of Gaussian functions. The P, the Q, the R, and the S waves are assumed to be symmetric and thus represented by a single Gaussian, while the T wave is assumed to be asymmetric and is represented by two Gaussians. The Gaussian function used to represent the ECG features is [37]:

$$f(a, b, \Delta t, Z) = \left(\frac{a}{2b}\right) e^{\frac{\Delta t^2}{2b^2} + zt}, \quad (4.1)$$

where  $\Delta t = t - t_{wave}$  represent the position of the wave at time  $t_{wave}$ ,  $a / 2b$  is a normalization constant,  $z$  represent a baseline offset,  $a$  represents the magnitude of the wave, and  $b$  represents the width of the wave [37].

The cumulative ECG represented by the GGSM is [37]:

$$ECG = \sum_{i=\{P,Q,R,S,T^-,T^+\}} \left(\frac{a_i}{2b_i}\right) e^{\frac{\Delta t_i^2}{2b_i^2} + z_i t}, \quad (4.2)$$

where T- and T+ are the two Gaussians used to describe the asymmetric T wave.

The GGSM is used in this dissertation to generate synthetic ECG signals. The synthetic signal acts as a tool to test the accuracy of the forward problem solution. For this purpose, additional white, pink, and brown noise has been added at different noise levels.

White Gaussian noise is defined to have a flat spectral density function over all frequencies; i.e. it is not correlated over time. However, in practice noise does not have flat spectral densities; noise is called colored when the noise samples are correlated in time. This work uses the noise model discussed in [38] to generate colored noise and realistic ECG artifacts. The noise model is characterized by a single parameter representing the slope of a spectral density function that decreases monotonically with frequency [38]:

$$S(f) \propto \frac{1}{f^\beta}, \quad (4.3)$$

where  $f$  is the frequency, and  $\beta$  is a measure of noise color. White noise ( $\beta = 0$ ), pink noise ( $\beta = 1$ ) or flicker noise, and brown noise ( $\beta = 2$ ) or the random walk process, are

three of the most commonly referenced noises. Colored noise is generated by taking samples of white noise and performing a frequency domain transform using the Discrete Fourier Transform (DFT). The frequency components of the DFT are then reshaped and an inverse DFT is used to transform it back to the time domain.

Table 2.1 shows the parameters used to generate the simulated electrocardiogram. The simulated ECG is then perturbed with white, pink and brown noise at difference noise levels. The signal to noise ratio, measured at the ST level, ranges between -25dB to 5dB. The white and pink noise simulates electrical interference noise. The brown noise simulates electrical interference and baseline wandering noise.

Table 4.1: Parameters of the GGSM used to simulate an ECG.

Index ( $i$ )	P	Q	R	S	T <sup>-</sup>	T
$\theta_i$	$-70^\circ$	$-15^\circ$	$0^\circ$	$15^\circ$	$83^\circ$	$90^\circ$
$a_i$	0.8	-5.0	30.0	-7.5	0.5	1.5
$b_i$	0.2	0.1	0.1	0.1	0.4	0.2

#### 4.4 Summary

This chapter presented the datasets used in this work along with the initial preprocessing applied to each of the datasets. These datasets are used in measuring the model's accuracy, and the two diagnostic applications: myocardial ischemia detection, and myocardial infarction localization. The following chapter presents the electrophysiological cardiac model and describes the forward problem solution.

## Chapter 5                      Cardiac Modeling

Chapter 3 reviewed the current cardiac modeling methods used to solve the forward and inverse problems. These cardiac modeling methods cannot be used to solve the forward and inverse problem rapidly due to the computational complexity and required patient geometrical models. Therefore, a cardiac model that solves the forward and inverse problems sufficiently fast is required.

This chapter is the first of two chapters that present a novel sufficiently fast solution for the cardiac modeling problem. As mentioned in chapter 1, the modeling problem contains two sub problems. The first is modeling the electrical activity of the cardiac regions. The second is solving the forward and inverse problems. This chapter presents the mathematical formulation for the electrophysiological cardiac model (ECM) that accounts for six major cardiac regions: sinoatrial (SA) node, atrioventricular (AV) node, bundle branches (Bb), Purkinje fibers (Pf), and left ventricle (LV) and right ventricle (RV). These regions are chosen because of to the importance of their role in the conduction process as will be discussed further in the next section. Additionally, a novel direct solution for the forward problem based on the ECM is presented in this chapter.

The advantage of the ECM is that it can provide a direct solution for the forward problem independent of the geometry of the heart and body torso. Additionally, the ECM can be used as a basis for sufficiently fast clinical diagnostic applications such as myocardial ischemia detection and myocardial infarction localization that will be presented later in the dissertation.

This chapter is divided into three sections. The first section presents the mathematical formulation for the ECM. It starts by presenting the cardiac model. It then

presents the difference of two sigmoid functions used to model the cardiac region electrical activity. The second section presents the direct solution for the forward problem. This second section presents the mathematical formulation for ECG generation using the ECM. The third section discusses the model in comparison with the previous models.

### ***5.1 Electrophysiological Cardiac Model***

The electrophysiological cardiac model is based on the hypothesis that the heart can be represented by its main regions. Since an individual cell's voltage is low and considering millions of cardiac cells is computationally expensive, the ECM divides the heart into six important regions. Each region consists of a combination of cells at the SA node, the AV node, the bundle branches (Bb), the Purkinje fibers (Pf) and the left ventricle (LV), and right ventricle (RV). These regions are chosen because of the importance of their role in the activation and conduction sequence of the heart. The SA node initiates the activation sequence. The AV node maintains the sinus (normal) cardiac rhythm by regulating the delay between the atrial and ventricular activity. The bundle branch is the first region to conduct in the ventricular activity. The Purkinje fibers conduct the electrical activity to the right and left ventricles. The electrical activity of the left and right ventricles initiates the contraction of the largest portion of the heart muscle.

The ECM is divided into two models: atrial and ventricular. The regions that represent the atrial activity are

- SA, which represents the activity of the SA node, and
- AV, which represents the activity of the AV node.

The regions that model the ventricular activity are

- *Bb* and *Pf*, which represent the activity of the bundle branches and Purkinje fibers, respectively, and
- *LV* and *RV*, which represent the activity of the left and right ventricles, respectively.

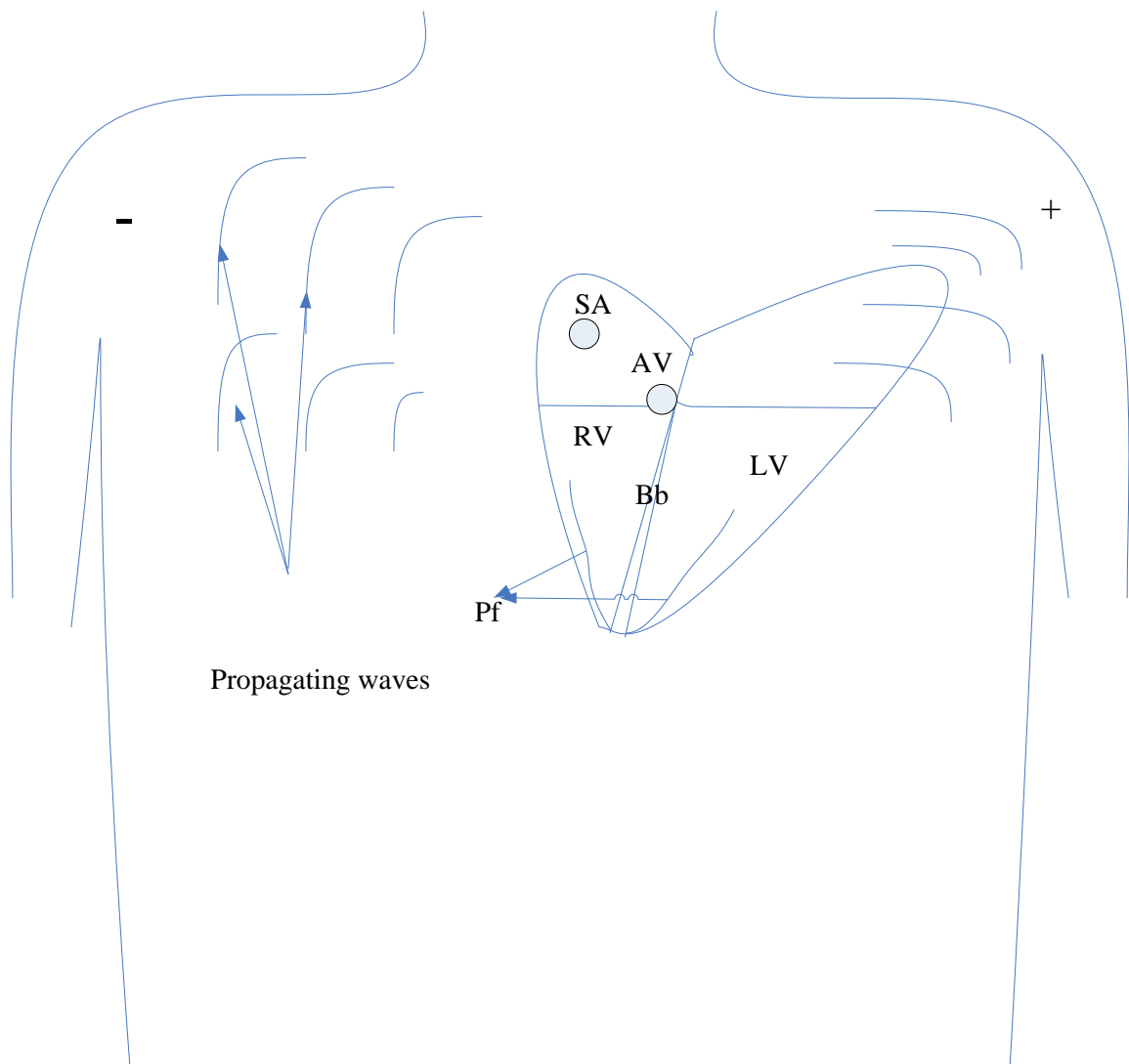


Figure 5-1: Sketch of the human body and the heart model.

To clarify the solution of the cardiac modeling problem, Figure 5-1 shows a sketch of the human body and the cardiac model, ECM. Additionally, the figure shows the modeled cardiac regions. Each of these regions is modeled as a signal generator. The

generated waves propagate from each of the regions to leads present at surface of the body, which are noted by the “+” and “-“. The leads capture the waves propagating from the heart, which appear as the electrocardiogram. The electrocardiogram is generated by the potential difference between the waves arriving at the positive and negative electrodes of the lead. The appearance of an electrocardiogram, shown in Figure 5-2, is due to the delay of the electric waves arriving at the positive and negative electrodes.

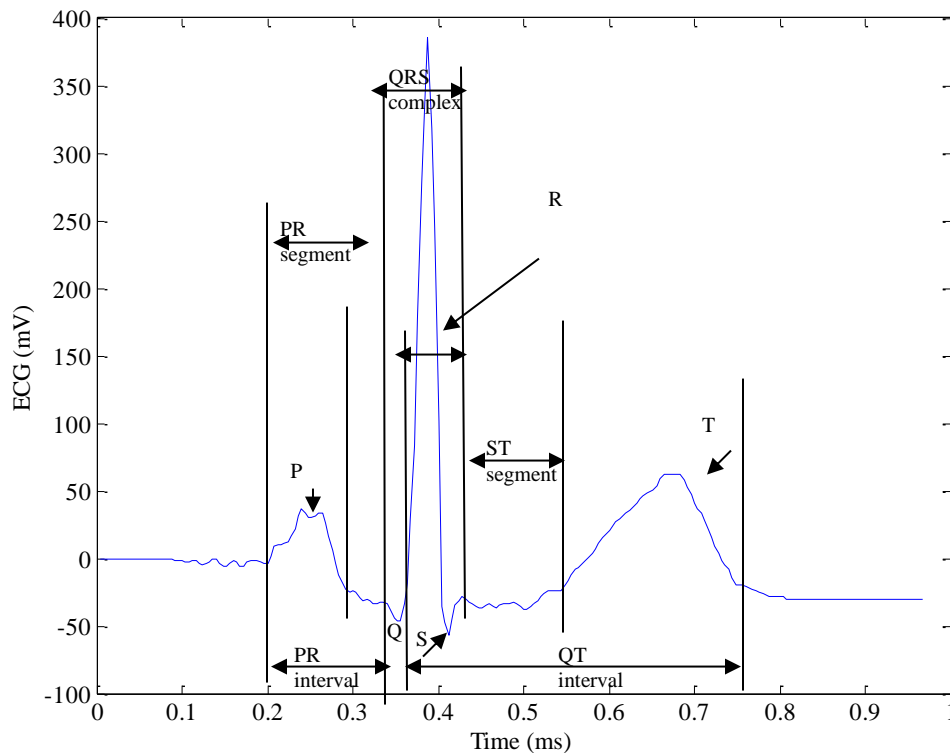


Figure 5-2: A ECG signal at Lead I.

The ECM models the waves arriving at the positive and negative electrodes as a delayed version of the signal generated by each region. This modeling method is based on the assumption that the generated signals maintain their properties during the propagation phase and that there exist a path between the regions and the leads. Following these assumptions, the ECM is be used to solve the forward and inverse

---

problems by developing a cardiac region model that can account for the time delays of the electrical activity arriving at the positive and negative electrodes.

### **5.1.1 Cardiac Region Electrical Activity Model**

Now that the overall heart model is presented, this section presents a model of cardiac region electrical activity. Before presenting the model, the most advanced cardiac cell model is described to provide a basis for comparison. As described in Chapter 2, the electric activity of the myocardial cells is caused by the variation of the positively and negatively charged ions at the cell membrane. The Luo-Rudy model is the most advanced and applied myocardial cell model published to date [39]. It has been extensively validated against measured cardiac cell activity. As such, it is used here as the gold standard for describing cardiac cell activity. As presented by Rudy et al. [39], the electric activity of the cell is given in Figure 5-3. It is to be noted as the downward spike is a numerical error due to the initial condition.

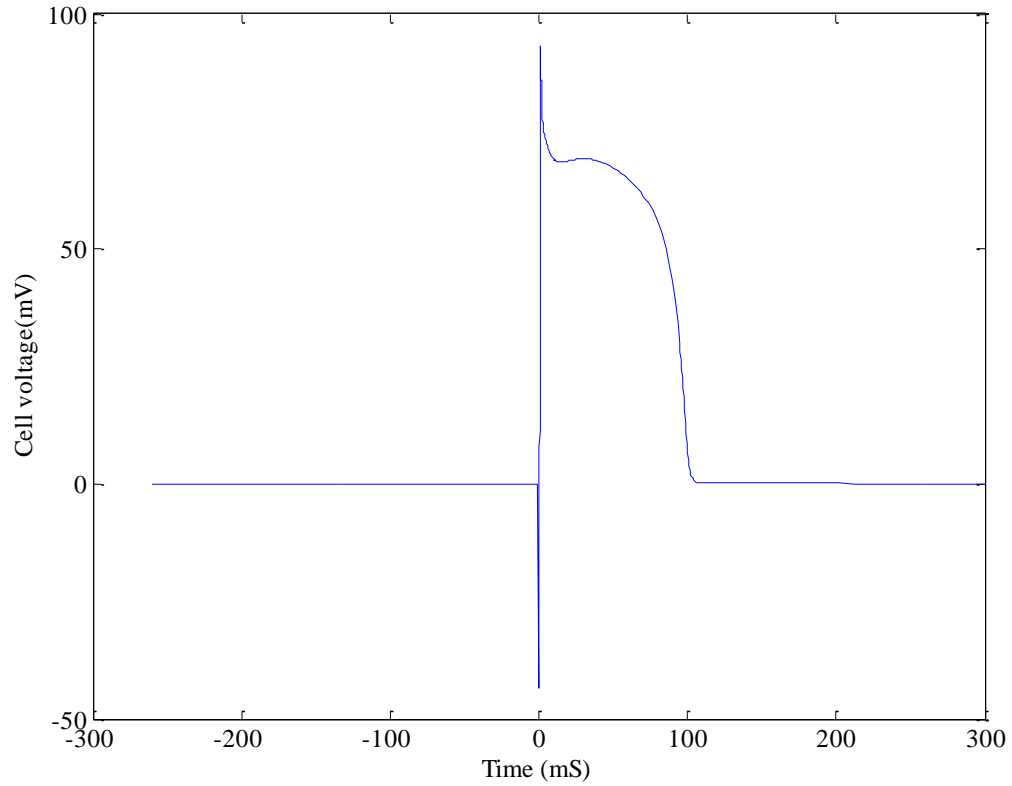


Figure 5-3: Conduction activity of the heart.

The Luo-Rudy model captures the cardiac cell electro chemical dynamics as a set of 29 nonlinear coupled differential equations. The parameters of the Luo-Rudy model are the ion concentrations and tissue conductivity. The details of this model are provided in Appendix A.

The drawback of this model is that these equations do not have a closed form solution and must be solved numerically. Additionally, the model parameters do not indicate the time and degree of activation and deactivation of the cardiac cell activity. Along this trend, the Luo-Rudy model cannot be used to provide a closed form forward problem solution.

In contrast to the Luo-Rudy model, this work proposes a closed form solution based on the difference of two sigmoid functions (diffsig) to model the electrical dynamics of the cardiac regions, which is described by

$$f(t, a_1, c_1, a_2, c_2, k) = k \left( \frac{1}{1 - e^{-a_1(t-c_1)}} - \frac{1}{1 - e^{-a_2(t-c_2)}} \right), \quad (5.1)$$

where  $k$  represents the magnitude of the wave,  $a_1$  and  $a_2$  control the rising slope, and  $c_1$  and  $c_2$  control the translation in the direction of the  $t$  axis as shown in Figure 5-4.

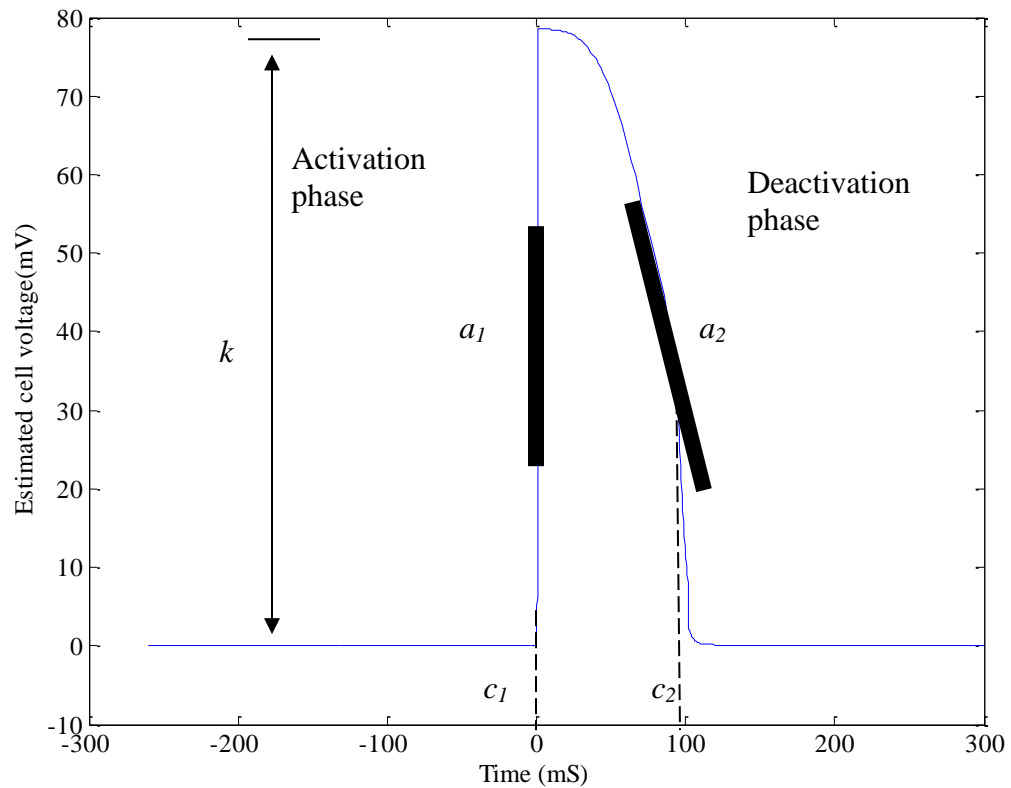


Figure 5-4: Model for cardiac region electrical activity.

The diffsig is chosen because its parameters closely correspond to important electrical dynamics of the cardiac cells. The parameters  $c_1$  and  $c_2$  represent the time of the depolarization/activation and repolarization/deactivation of the cardiac region.

Additionally, the parameters  $a_1$  and  $a_2$  represent quantitatively the rate of depolarization and repolarization, which are crucial in determining if the cells are ischemic.

A comparison between the Luo-Rudy and diffsig model is shown in Figure 5-5. The error between the two model generated signals is shown in Figure 5-6. The modeled activity is noted by the solid line, while the Luo-Rudy modeled activity is the dotted line. It can be seen the signal match at the activation and deactivation time and slope and that the major error is at the spike of the activation phase.

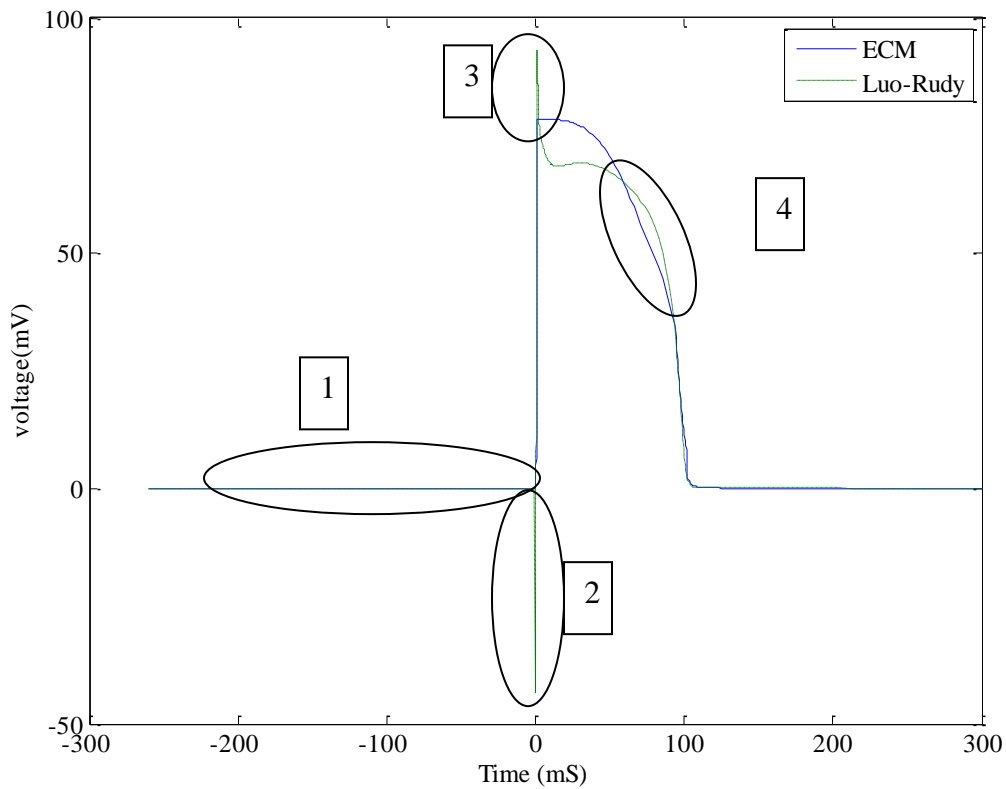


Figure 5-5: Comparison between the diffsig model and Luo-Rudy model

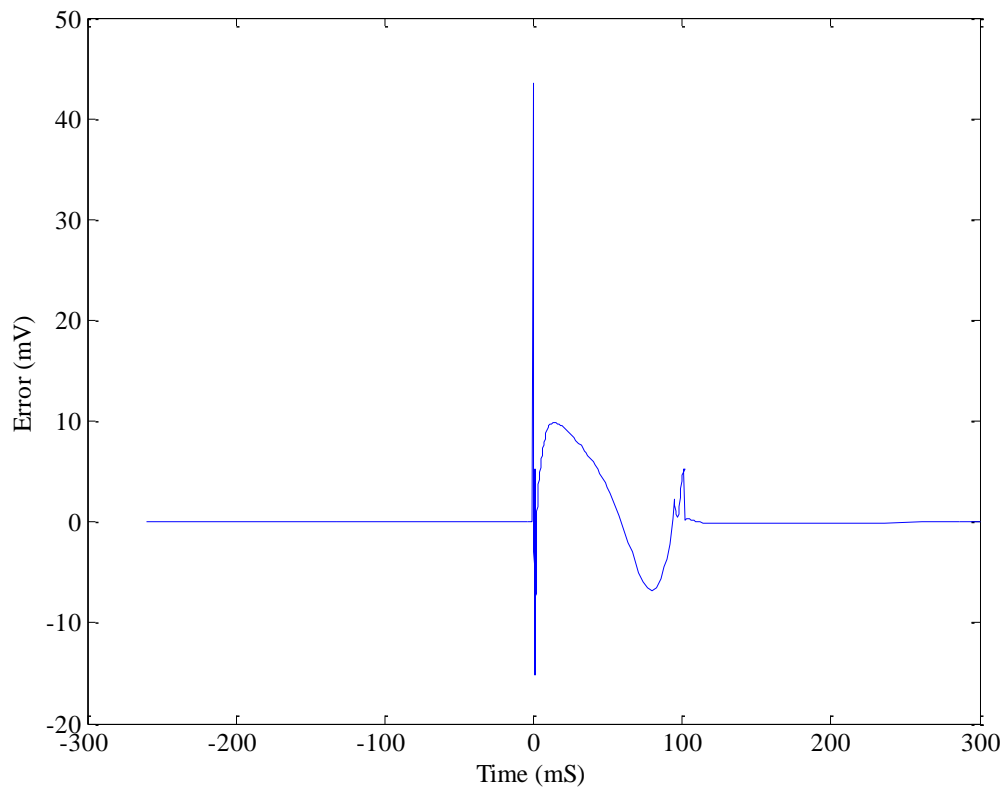


Figure 5-6: Error between the Luo-Rudy and diffsig cell activity.

The circles noted in Figure 5-5 represent the major differences between the Luo-Rudy model and the diffsig model. In circle one, the segment between  $[-250,0)$  was added to the signal at the same level as the interval between  $[100-300]$ . As mentioned in chapter 2, this was added because the polarization levels must be the same. In circle 2, the downward shift is a numerical error due to the initial condition [39]. Moreover, the upward spike is due to the potassium current in the ion channels. The variation of the spike magnitude is directly proportional to the potassium ion concentration. The fourth circle identifies the error during the repolarization phase.

## ***5.2 Forward Problem Solution***

Now that the cardiac model is presented, this section presents the solution for the forward problem. As presented in chapter 2, ECGs are the measurement of the sequential activation and conduction of the cardiac cells' electrical activity at the body surface. The ECM uses the same electrophysiological sequence to solve the forward problem. In this case, the forward problem is described as the generation of an ECG at a certain lead from the electrical activity at the cardiac regions. The ECM is used to generate the P wave, the PR segment, the Q, the R, the S waves (QRS complex), the ST segment, and the T wave. After generating each of the ECG features, the mathematical representation for a single lead ECG is presented.

### **5.2.1 ECG Generation**

The ECG features, i.e. waves and segments, are generated from the potential difference at the positive and negative electrodes of the cardiac cells electric activity. The previous section proposed the use of the diffsig to represent the cardiac region's electric activity. The ECG generation is performed by following the same rules described in chapter 2 that relate the cardiac electrical activity to the ECG features. Before presenting solution to the forward problem, the electrophysiological rules are presented briefly.

The rules governing the cardiac conduction process are [13]:

1. The SA node, called the pace maker, provides the electrical pulse that initiates the electric wave that traverses the heart.
2. The wave traverses toward the right and left atrium causing the atrial cells to conduct.

3. The wave passes through the AV node, which acts as an electrical relay between the atria and the ventricles.
4. The wave traverses through the common bundle and the bundle branches to activate the ventricles.
5. The Purkinje fibers are activated, which activates the ventricular muscles.
6. The ventricular cells start to repolarize, recover, and prepare for the next beat.

Now that the electrophysiological rules are presented, the solution for the forward problem can be described. As mentioned previously, the ECM is divided into an atrial model and a ventricular model. The atrial activity appears in the ECG signal as the P wave and the PR segment. The ventricular activity appears in the ECG signal as the Q wave, R wave, S wave (known as the QRS complex) the ST segment, and the T wave. The SA node and AV node are used to generate the P wave and PR segment, while the Bb, Pf, LV, RV are used to generate the QRS complex, T wave, and ST segment.

### 5.2.1.1 Method Concept

The concept behind the method for ECG generation is that when a cardiac region generates an electrical wave, there exists a delay in the arrival time at the positive and negative electrodes. As mentioned previously, the modeled electrical activity at each cardiac regions is defined as  $f$ , see (5.1). Therefore, the delayed activity arriving at the positive and negative electrodes at the body surface are represented by  $f_i^+$  and  $f_i^-$ ,

$$f^+ = f(t, a_1, c_1 + \delta_1^+, a_2, c_2 + \delta_2^+, k), \text{ and} \quad (5.2)$$

$$f^- = f(t, a_1, c_1 + \delta_1^-, a_2, c_2 + \delta_2^-, k), \quad (5.3)$$

where  $\delta_1^+$  and  $\delta_1^-$  represent the activation delay at the positive and negative electrodes, respectively. The parameters  $\delta_2^+$  and  $\delta_2^-$  represent the delay of the deactivation timing at the positive and negative electrodes, respectively. The modeled electrical activity of each region at each electrode is described as

1.  $(f_{SA}^+, f_{SA}^-)$  represents the activity of the *SA* node at the positive and negative electrodes, respectively.
2.  $(f_{AV}^+, f_{AV}^-)$  represents the activity of the *AV* node at the positive and negative electrodes, respectively.
3.  $(f_{Bb}^+, f_{Bb}^-)$  represents the activity of the bundle branch at the positive and negative electrodes, respectively.
4.  $(f_{Pf}^+, f_{Pf}^-)$  represents the activity of the Purkinje fiber at the positive and negative electrodes, respectively.
5.  $(f_{Lv}^+, f_{Lv}^-)$  represents the activity of the left ventricle at the positive and negative electrodes, respectively.
6.  $(f_{Rv}^+, f_{Rv}^-)$  represents the activity of the right ventricle at the positive and negative electrodes, respectively.

Now that the functions describing the electrical activity of the cardiac regions are defined and knowing that an ECG is the potential difference of the cardiac electrical activity at the body surface, the ECG features can be generated using the difference between  $f_i^+$  and  $f_i^-$ . The mathematical representation for generating the ECG features is described in the following sections.

### 5.2.1.2 P Wave Generation

As noted earlier, the P wave is generated from the measurement of the potential difference of the electric conduction activity of the atrial cells at the positive and negative electrodes. In the modeling approach, the same concept is followed where the  $P$  wave is generated from the estimate of the SA node activity by

$$P_{wave} = (f_{SA}^+ - f_{SA}^-). \quad (5.4)$$

The generation of the P wave using the diffsig is shown in Figure 5-7. The two graphs at the top of the figure represent the diffsig model of the SA node at the positive and negative electrodes of a single lead. The annotations on the figure refer to the activation delays  $\delta_1^+$  and  $\delta_1^-$  and the deactivation delays  $\delta_2^+$  and  $\delta_2^-$  at the positive and negative electrodes. The bottom graph of Figure 5-7 represents the generated P wave resulting from the difference between the modeled SA node activity at the positive and negative electrodes. Additionally, the annotations at the bottom figure show the beginning and end of the P wave and their respective positions on the diffsigs in the top graphs. The beginning and end of the P wave are at the point of intersection between  $f_i^+$  and  $f_i^-$ .

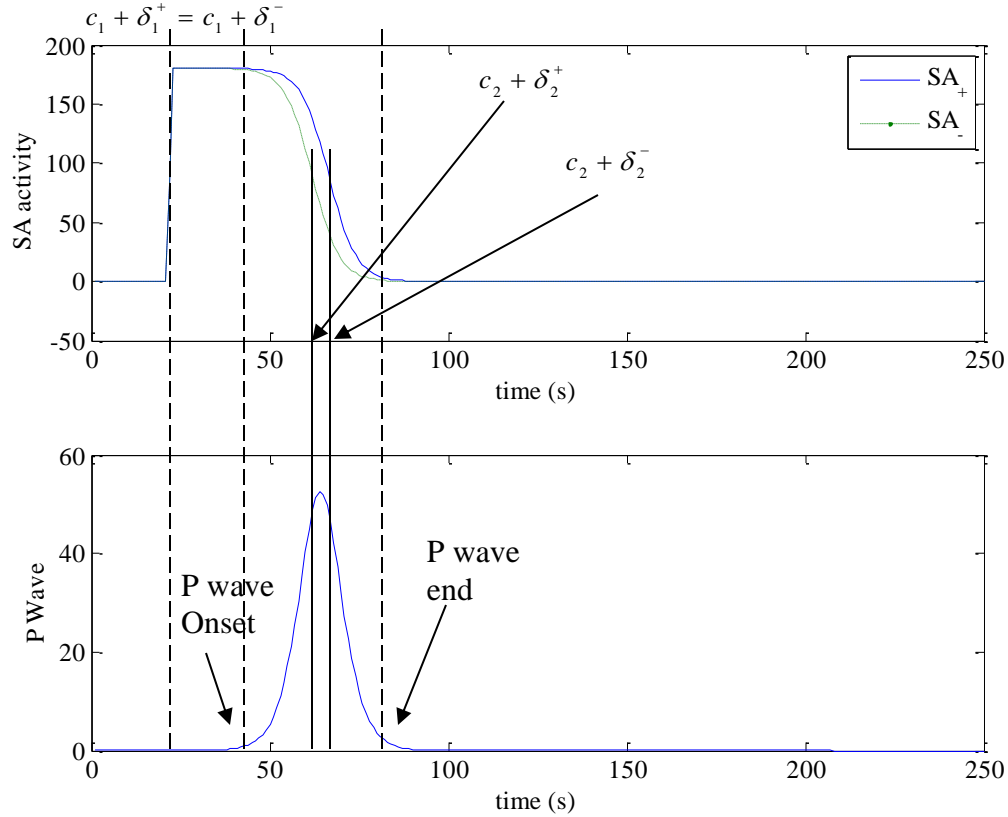


Figure 5-7: P wave modeled as the difference between two sigmoids.

### 5.2.1.3 PR segment Generation

As noted in Chapter 2, the PR segment is the measurement of the wave propagating from the AV node at the lead terminals. The duration of the PR segment is due to the delay of the AV node activation that synchronizes the heart beat. In this work, the same concept is followed to generate the PR segment as the potential difference between the electric activity of the AV node at the positive and negative electrodes as presented by

$$PR_{segment} = (f_{AV}^+ - f_{AV}^-). \quad (5.5)$$

Similar to the procedure shown in Figure 5-7, the PR segment is generated as shown in Figure 5-8. The top figure represents the electrical activity measured at the positive and negative electrodes. The annotations on the figure refer to the activation

delays  $\delta_1^+$  and  $\delta_1^-$ , and the deactivation delays  $\delta_2^+$  and  $\delta_2^-$  at the positive and negative electrodes. The bottom graph of Figure 5-8 shows the generated PR segment of a sample ECG. Figure 5-8 shows the annotations of the beginning and end of the PR segment, which are at the intersection of the  $f^+$  and  $f^-$ .

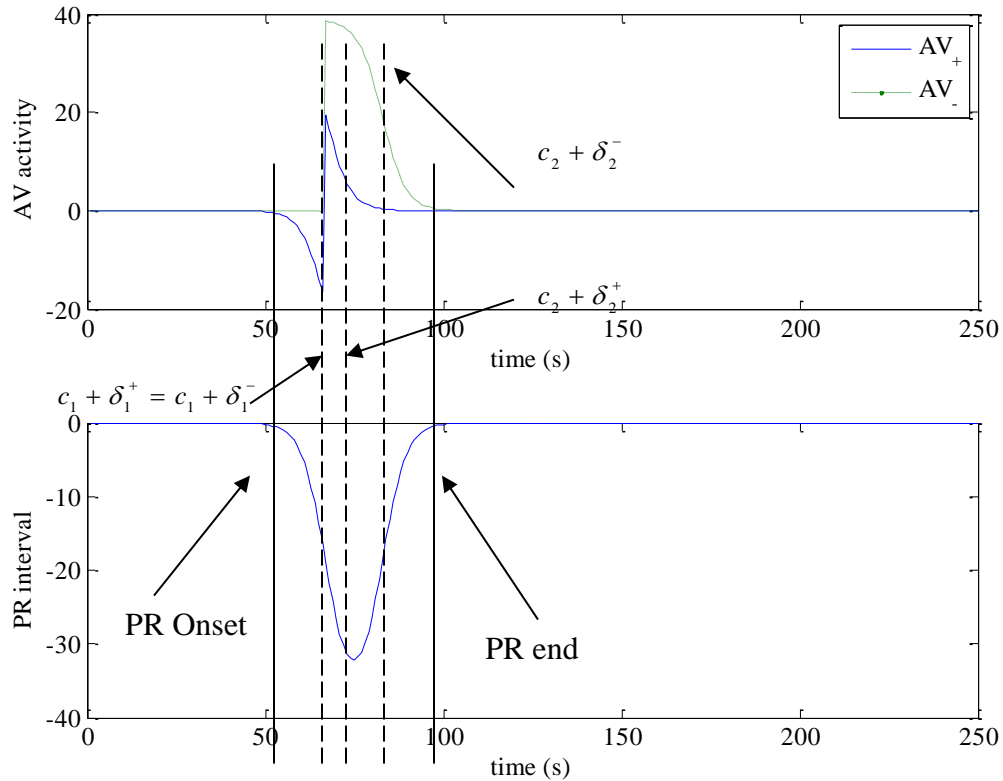


Figure 5-8 PR interval generation using the differential sigmoid model

#### 5.2.1.4 QRS Complex and T Wave Generation

The QRS complex and the T wave denote the interval for the beginning and end of the ventricular electrical activity. The generated QRS complex and T wave are the result of the difference between the diffsig representation at the positive and negative electrodes of the selected regions. In this work, the QRS complex is generated by the activation part of the diffsig representation of the activity of the bundle branches, Purkinje fiber, and the activation phase of the left and right ventricles at the positive and

negative terminals of the lead. The T wave is modeled by the deactivation phase of the diffsig representation of the left and right ventricles. The Q wave is generated as the difference between the diffsig representation of the electrical activity of the bundle branches at the positive and negative electrode given by

$$Q_{wave} = (f_{Bb}^+ - f_{Bb}^-). \quad (5.6)$$

The R wave and T wave is generated by the activation and deactivation of the Pf diffsig representation, respectively at the positive and negative lead terminals given by

$$R_{wave} \& T_{wave} = (f_{Pf}^+ - f_{Pf}^-). \quad (5.7)$$

Similar to the  $R_{wave}$  &  $T_{wave}$  generation method, the S wave and the T wave are generated using the diffsig model. The S wave is generated during the activation part of the diffsig, and the T wave is represented during the deactivation phase as follows

$$S_{wave} \& T_{wave} = (f_{Lv}^+ - f_{Lv}^-). \quad (5.8)$$

Figure 5-9 through Figure 5-11 show the models representing the QRS complex and the T wave using the diffsig model and cardiac electrophysiology. The top graphs in these figures show the diffsig at the positive and negative terminals of the lead. The annotations on the figures refer to the activation delays  $\delta_1^+$  and  $\delta_1^-$  and the deactivation delays  $\delta_2^+$  and  $\delta_2^-$  at the positive and negative electrodes. The bottom graphs show the result of the difference between the two diffsigs at the positive and negative terminals. Moreover, the annotations of the beginning and end of the Q wave are shown in Figure 5-9. Additionally, Figure 5-10 shows the annotations for the beginning and end of the R wave. Finally, Figure 5-11 shows the beginning and end of the S and T waves.

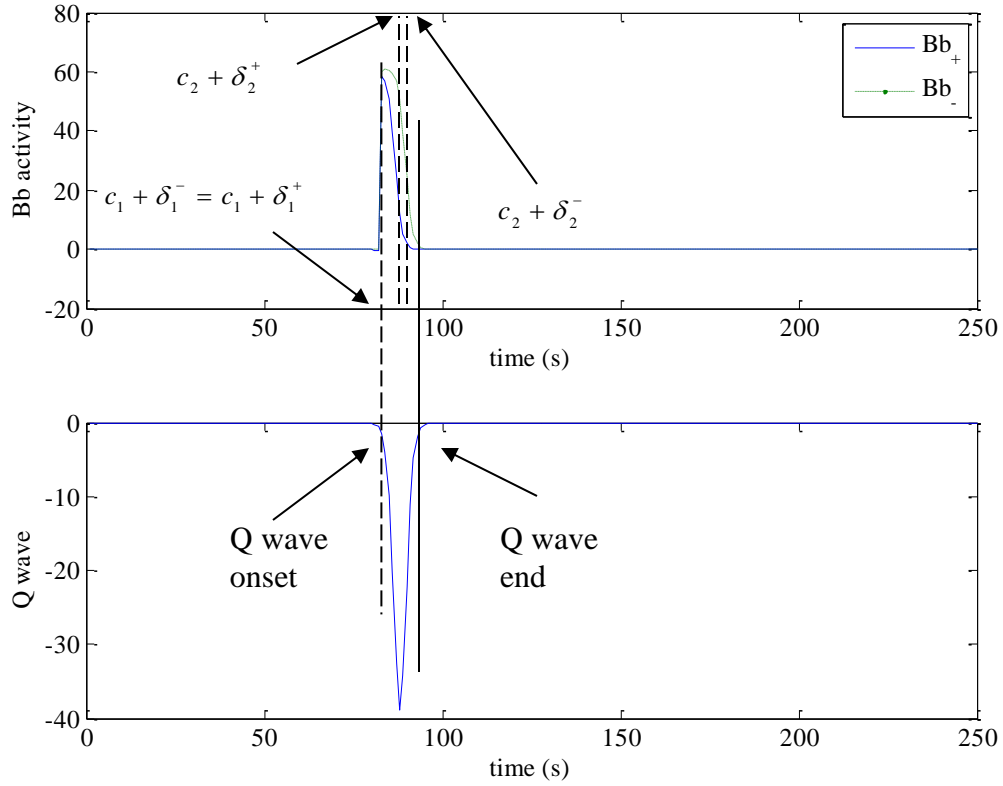


Figure 5-9: Q wave generation

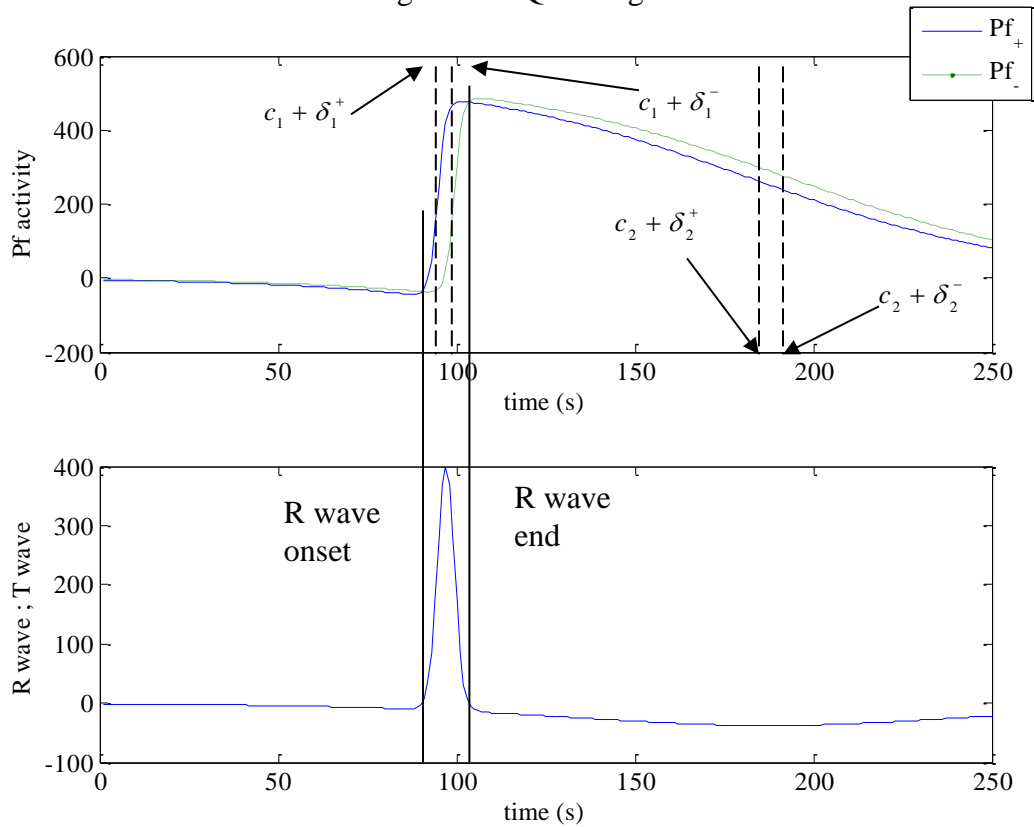


Figure 5-10: R wave and T wave generation.

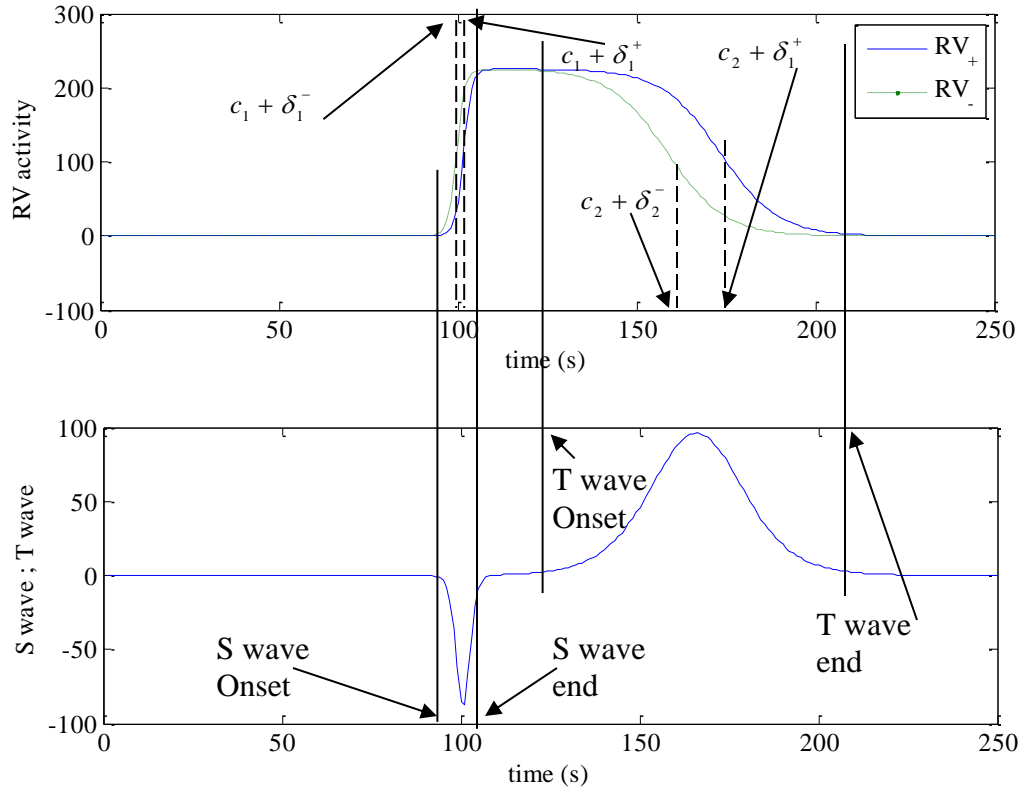


Figure 5-11: S wave and T wave generation

### 5.2.1.5 ST Segment

Due to the importance of the ST segment elevation or deviation to the detection of myocardial diseases, the ST segment is modeled by the potential difference of the deactivation phase of diffsig of the *RV*. The ST segment is given by

$$ST_{segment} = (f_{RV}^+ - f_{RV}^-). \quad (5.9)$$

Figure 5-12 shows the modeling of the ST segment. The top graph in Figure 5-12 represents the diffsig estimate of the electrical activity at the positive and negative terminals. The annotations on the figure refer to the activation delays  $\delta_1^+$  and  $\delta_1^-$  and the deactivation delays  $\delta_2^+$  and  $\delta_2^-$  at the positive and negative electrodes. The resulting difference between the diffsig at the positive and negative terminal is shown in the ST

wave model on the bottom of Figure 5-12. The annotations for the beginning and end of the ST segment are displayed with respect to the modeled signals.

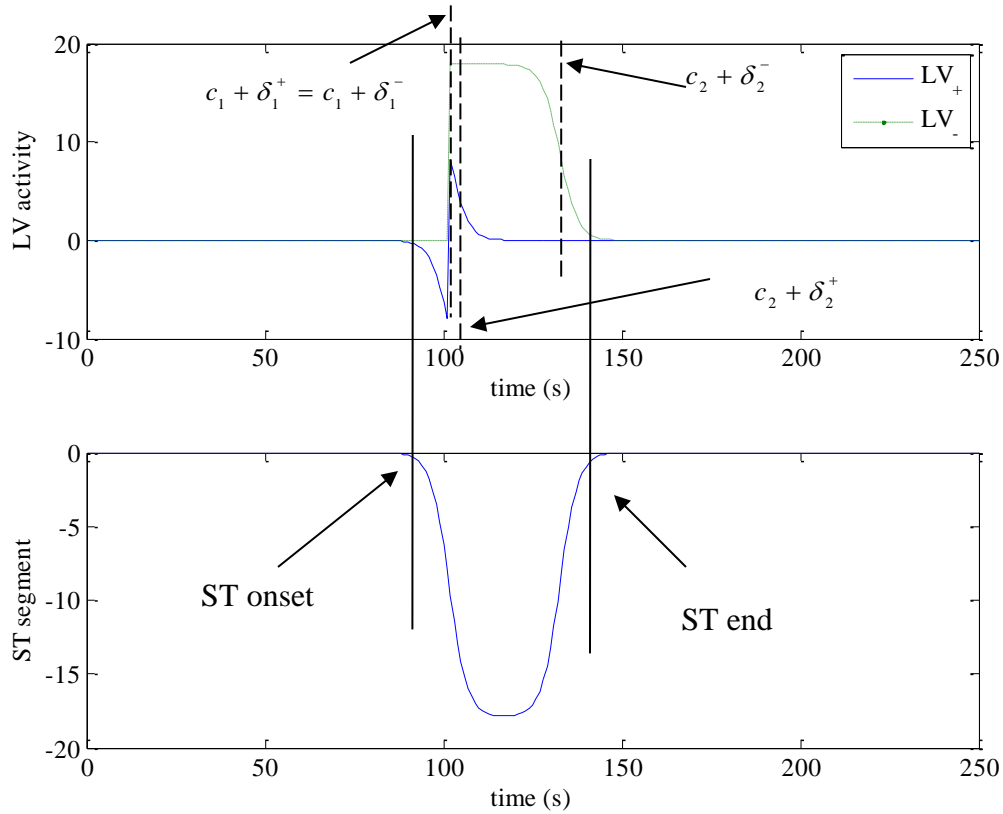


Figure 5-12: ST segment generation

### 5.2.1.6 Single Lead ECG Generation

Now that the generation of each of the ECG features has been described, the cumulative direct solution for the forward problem is presented. The ECG signal is generated as the sum of the features presented in sections 5.2.1.2-5.2.1.5. Thus, an ECG signal is written as

$$\hat{f}_{ECG} = P_{wave} + PR_{segment} + Q_{wave} + R_{wave} + S_{wave} + ST_{segment} + T_{wave} . \quad (5.10)$$

By replacing each feature representation by its respective value presented in (5.4) through (5.9), the ECG representation becomes

$$\begin{aligned} \hat{f}_{ECG} = & (f_{SA}^+ - f_{SA}^-) + (f_{AV}^+ - f_{AV}^-) + (f_{Bb}^+ - f_{Bb}^-) \\ & + (f_{Pf}^+ - f_{Pf}^-) + (f_{Lv}^+ - f_{Lv}^-) + (f_{Rv}^+, f_{Rv}^-). \end{aligned} \quad (5.11)$$

Therefore, the mathematical formulation for generating an ECG signal and the solution to the forward problem solution is

$$\hat{f}_{ECG} = \sum_{i \in [SA, AV, Bb, Pf, Lv, Rv]} (f_i^+ - f_i^-), \quad (5.12)$$

where  $\hat{f}_{ECG}$  is the generated ECG signal,  $SA, AV, Bb, Pf, LV, RV$  represent the modeled cardiac regions,  $f_i^+$  and  $f_i^-$  represent cardiac electrical activity at the positive and negative electrodes. By replacing  $f_i^+$  and  $f_i^-$  with (5.1) and accounting for the delays  $\delta_1^+$ ,  $\delta_1^-$ ,  $\delta_2^+$ , and  $\delta_2^-$ ,  $\hat{f}_{ECG}$  becomes

$$\hat{f}_{ECG} = \sum_{i=SA, AV, Bb, Pf, Lv, Rv} k_i \left[ \left( \left( \frac{1}{1 - e^{a_{(i)1}(t-c_{(i)1}-\delta_{1i}^+)}} - \frac{1}{1 - e^{a_{(i)2}(t-c_{(i)2}-\delta_{2i}^+)}} \right) - \left( \frac{1}{1 - e^{a_{(i)1}(t-c_{(i)1}-\delta_{1i}^-)}} - \frac{1}{1 - e^{a_{(i)2}(t-c_{(i)2}-\delta_{2i}^-)}} \right) \right) \right]. \quad (5.13)$$

It can be seen in (5.13) that the ECM can be used to generate an ECG based on the cardiac electrophysiology by accounting for the time delays in the arrival of the electrical activities at the positive and negative electrodes. Moreover, the same concept for generating a single lead ECG can be applied to generate a multilead ECG.

### 5.2.1.7 Multilead ECG Generation

The multilead model is based on the same concept presented earlier, where the ECM model generates the simulated electrical cardiac activity, which arrives at the positive and negative electrodes at the body surface with the delays  $\delta_1^+$ ,  $\delta_1^-$ ,  $\delta_2^+$ , and  $\delta_2^-$ .

This concept can be extended to multiple lead ECG generated simultaneously by knowing the time delays of the activation sequence of each lead. In this case, the scalar time delays  $\delta_1^+$ ,  $\delta_1^-$ ,  $\delta_2^+$ , and  $\delta_2^-$  will be replaced by a vector of delays. Each element of the vector of delays represents a lead. For example, assume leads I, II, and III are being generated. The vector of delays becomes

$$\begin{bmatrix} \delta_{1 I}^+ \\ \delta_{1 II}^+ \\ \delta_{1 III}^+ \end{bmatrix}, \begin{bmatrix} \delta_{2 I}^+ \\ \delta_{2 II}^+ \\ \delta_{2 III}^+ \end{bmatrix}, \begin{bmatrix} \delta_{1 I}^- \\ \delta_{1 II}^- \\ \delta_{1 III}^- \end{bmatrix}, \begin{bmatrix} \delta_{2 I}^- \\ \delta_{2 II}^- \\ \delta_{2 III}^- \end{bmatrix}. \quad (5.14)$$

The formulation of the forward problem solution at leads, *I*, *II*, and *III* is

$$\begin{bmatrix} \hat{f}_{ECG I} \\ \hat{f}_{ECG II} \\ \hat{f}_{ECG III} \end{bmatrix} = \sum_{i=SA,AV,Bb,Pf,Lv,Rv} \begin{bmatrix} k_i \left( \left( \frac{1}{1 - e^{-a_{(i)l}(t-c_{(i)l}-\delta_{1 I}^+)}} - \frac{1}{1 - e^{-a_{(i)2}(t-c_{(i)2}-\delta_{2 I}^+)}} \right) - \left( \frac{1}{1 - e^{-a_{(i)l}(t-c_{(i)l}-\delta_{1 II}^-)}} - \frac{1}{1 - e^{-a_{(i)2}(t-c_{(i)2}-\delta_{2 II}^-)}} \right) \right) \\ k_i \left( \left( \frac{1}{1 - e^{-a_{(i)l}(t-c_{(i)l}-\delta_{1 III}^+)}} - \frac{1}{1 - e^{-a_{(i)2}(t-c_{(i)2}-\delta_{2 III}^+)}} \right) - \left( \frac{1}{1 - e^{-a_{(i)l}(t-c_{(i)l}-\delta_{1 III}^-)}} - \frac{1}{1 - e^{-a_{(i)2}(t-c_{(i)2}-\delta_{2 III}^-)}} \right) \right) \\ k_i \left( \left( \frac{1}{1 - e^{-a_{(i)l}(t-c_{(i)l}-\delta_{1 III}^+)}} - \frac{1}{1 - e^{-a_{(i)2}(t-c_{(i)2}-\delta_{2 III}^+)}} \right) - \left( \frac{1}{1 - e^{-a_{(i)l}(t-c_{(i)l}-\delta_{1 III}^-)}} - \frac{1}{1 - e^{-a_{(i)2}(t-c_{(i)2}-\delta_{2 III}^-)}} \right) \right) \end{bmatrix} \quad (5.15)$$

This formulation can be extended to generate the standard 12 leads or even the body surface map 356 leads. The advantage of this formulation is the lower number of parameters compared to generating a single lead ECG at a time. This shows that the heart model, ECM, can generate multilead ECG signals based on the delay of arrival at each lead.

### 5.3 Discussion

This chapter presents a novel heart model based on the hypothesis that the heart can be divided into six main regions. Each region's electrical activity is modeled as the difference of two sigmoid functions (diffsig). In comparison with the previous cell models, the advantage of the diffsig model is that it provides a closed form representation of the cardiac region electrical dynamics compared to solving 11 nonlinear coupled differential equations [10]. Moreover, it can be noticed in the literature that the number of differential equations has been increasing due to the focus on accurately modeling the chemical dynamics of the ion channels.

This chapter presents a solution for the forward problem based on the cardiac electrophysiology and using the ECM. The major advantage of the presented solution is that it provides a direct solution for the forward problem independent of the geometry of the heart and body torso. The model parameters represent important information such as the activation and deactivation of the cardiac electrical activity that can be related to the beginning and end of the ECG features.

The ECM reduces the computational complexity of the forward problem solution faced in finite element models by considering the crucial cardiac regions in the modeling process instead of millions of cell or solving the scattering and wave propagation equations. Additionally, the number of parameters of the diffsig that represent the cardiac cell activity is lower than that of the nonlinear differential equations of that describe the cardiac cell's chemical dynamics, and thus the number of parameter, 54, for the ECM is lower than that of the earliest model, Hodgkin and Huxley model [10], 132 parameters. It

is to be noted that later models contained more parameters, which adds to the complexity of obtaining the solution.

The next chapter presents the optimization method use to solve the inverse problem, i.e. determination of the cardiac cell electrical activity. The next chapter proposes the use of nonlinear constraint optimization for the estimation of the diffsig parameters from real ECGs.

## **Chapter 6      Inverse Problem Solution (through optimization)**

The previous chapter presents a novel approach, electrophysiological cardiac model (ECM), to solve the forward problem. The ECM uses the difference of two sigmoid functions to model the cardiac cell electrical activity and the cardiac electrophysiology to generate electrocardiograms. This chapter, the second of the series, presents a novel method for solving the inverse problem, i.e. estimating the cardiac electrical activity at the heart surface from that at the body surface, electrocardiograms (ECG).

As presented in Chapter 3, previous methods require the geometrical modeling of the heart and body torso and solving the wave scattering and propagation equations to determine the cardiac cell electrical activity. The first drawback of such methods is that geometrical modeling requires magnetic resonance imaging of patients' torso, which requires two to four hours. The second drawback is the computational complexity of solving the nonlinear coupled integral and differential equations that represent the scattering and wave propagation problems, respectively whose solution requires up to several days with the current computation power.

This chapter presents a novel method that uses the ECM and a sum squared error minimization to solve for the inverse problem sufficiently fast. This minimization problem is solved using a nonlinear constrained optimization technique that accounts for the cardiac electrophysiology.

This chapter is divided into three main sections. The first section presents an overview of the inverse problem solution. The second section describes the mathematical

formulation of the optimization problem. The third section describes the initial condition applied during the optimization process. The fourth section presents the nonlinear constrained optimization technique used to solve the inverse problem.

### ***6.1 Inverse Problem Solution***

This section presents an overview of the inverse problem solution using the minimization of sum squared error between the ECM-generated ECG and the actual patient ECGs. Figure 6-1 shows a block diagram of the inverse problem solution. The solution is based on an iterative approach that estimates the cardiac region electrical activity from actual ECGs. The steps of the approach as shown in Figure 6-1 are

1. An initial condition is selected depending on the ECG signal under consideration.
2. The ECM generates an estimate of the actual ECG by modeling the cardiac regions and solving the forward problem.
3. The sum squared error between the generated ECG and the actual ECG is calculated.
4. If the sum squared error fits the convergence criteria, the ECM parameters are returned for post processing.
5. If the convergence criteria are not met, an optimization technique is used to update the model parameters, and steps 2-5 are repeated.

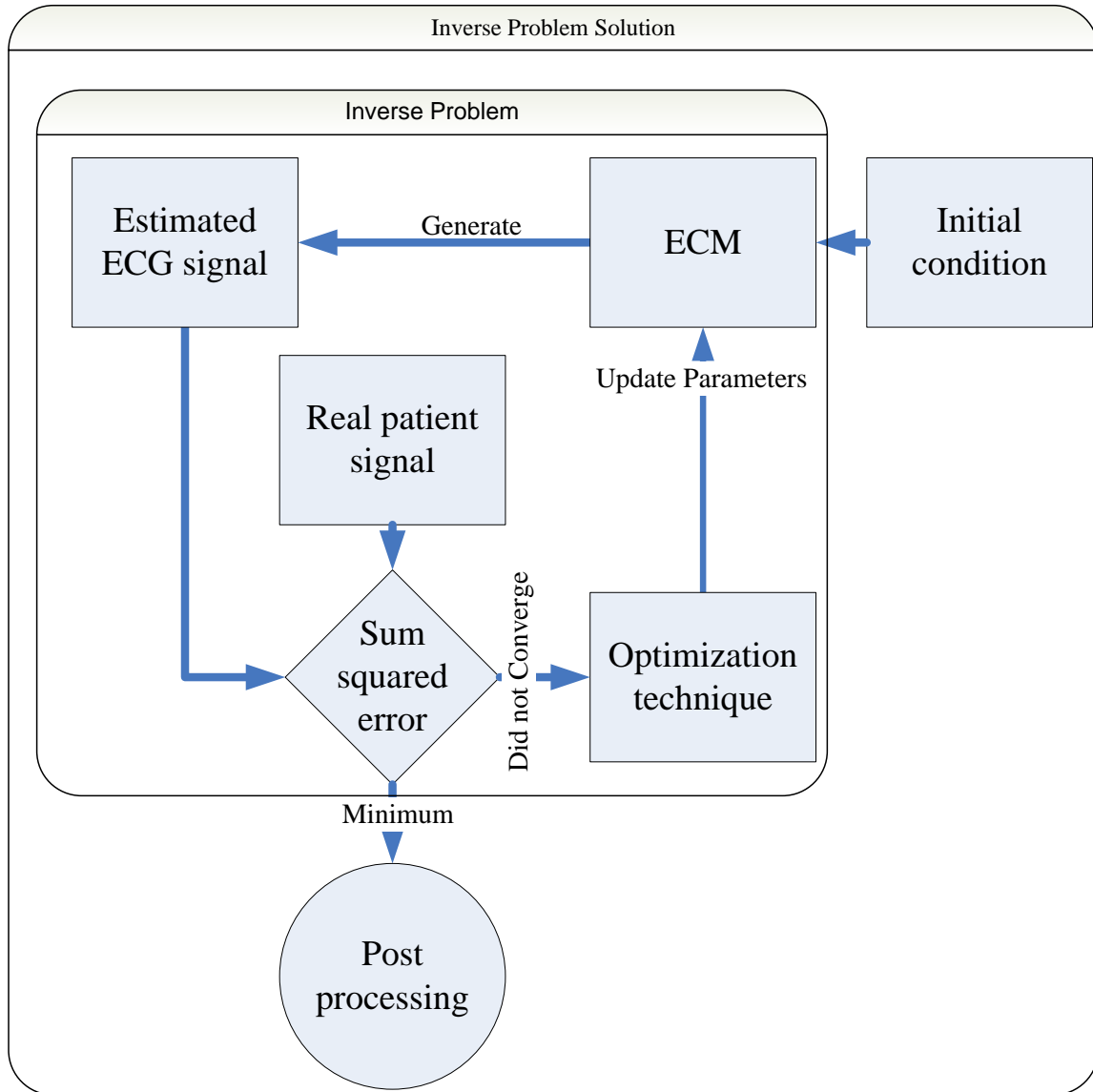


Figure 6-1: Block diagram of inverse problem solution.

Now that an overview of the inverse problem solution is presented, the following sections identify each of the components of the approach. The next section presents the mathematical formulation of the inverse problem.

## 6.2 Inverse Problem Setup (Optimization Problem)

This section presents the mathematical formulation of the inverse problem. The inverse problem is set up as an optimization problem, which minimizes the sum squared error between the forward problem solution and an actual ECG given in (6.1). Before presenting the optimization problem, a brief review of the forward problem solution is presented below. As presented in Chapter 5, the mathematical formulation for the ECM-generated ECG is

$$\hat{f}_{ECG} = \sum_{i \in [SA, AV, Bb, Pf, Lv, Rv]} (f_i^+ - f_i^-), \quad (6.1)$$

where  $f_i^+$  and  $f_i^-$  are the difference between two sigmoid functions (diffsig) model used to represent the cardiac cell electrical activity arriving at the positive and negative electrodes, respectively. The diffsig is represented by

$$f(t, a_1, c_1, a_2, c_2, k) = k \left( \frac{1}{1 - e^{a_1(t-c_1)}} - \frac{1}{1 - e^{a_2(t-c_2)}} \right), \quad (6.2)$$

where  $[SA, AV, Bb, Pf, Lv, Rv]$  are the modeled cardiac regions representing the sinoatrial (SA) node, (atrioventricular) AV node, bundle branches (Bb), Purkinje fiber (Pf), left ventricle (LV) and right ventricle (RV). The  $f_i^+$  and  $f_i^-$  are defined as

$$f^+ = f(t, a_1, c_1 + \delta_1^+, a_2, c_2 + \delta_2^+, k), \quad (6.3)$$

$$f^- = f(t, a_1, c_1 + \delta_1^-, a_2, c_2 + \delta_2^-, k), \quad (6.4)$$

where  $\delta_1^+$  and  $\delta_1^-$  represent the delay of the activation timing at the positive and negative electrodes, respectively. The delays  $\delta_2^+$  and  $\delta_2^-$  represent the delay of the deactivation timing at the positive and negative electrodes, respectively.

Now that the formulation of ECG generation is presented, the inverse problem, i.e. the sum squared error between the ECM simulated ECG presented in (5.12) and real ECG is defined as

$$Error = \sum_{time} \left( ECG - \hat{f}_{ECG} \right)^2, \quad (6.5)$$

where  $\sum_{time}$  is the sum over time samples and  $ECG$  represents an actual electrocardiogram. By substituting (5.12) into (6.5), the error becomes

$$Error = \sum_{time} \left( ECG - \sum_{i \in [SA, AV, Bb, Pf, Rv, Lv]} (f_i^+ - f_i^-) \right)^2. \quad (6.6)$$

From (5.1) -(6.4) and (6.6), the optimization problem is

$$\min_x \left\{ Error = \sum_{time} \left( ECG - \sum_{i \in [SA, AV, Bb, Pf, Lv, Rv]} k_i \left[ \left( \frac{I}{I - e^{a_{(i)1}(t-c_{(i)1}-\delta_{1i}^+)}} - \frac{I}{I - e^{a_{(i)2}(t-c_{(i)2}-\delta_{2i}^+)}} \right) - \left( \frac{I}{I - e^{a_{(i)1}(t-c_{(i)1}-\delta_{1i}^-)}} - \frac{I}{I - e^{a_{(i)2}(t-c_{(i)2}-\delta_{2i}^-)}} \right) \right] \right)^2 \right\}, \quad (6.7)$$

where  $x$  represents the ECM parameters defined as  $x = [t, a_1, c_1, a_2, c_2, k, \delta_1^+, \delta_1^-, \delta_2^+, \delta_2^-]$  at each of the modeled regions  $[SA, AV, Bb, Pf, Lv, Rv]$ . The aim of this optimization problem is to solve for the ECM parameters  $x$  that minimize the sum squared error between the ECM-generated and an actual ECG. The inverse problem solution is based on the hypothesis that the resulting ECM parameters can be used to model the actual cardiac region activity.

The inverse problem (6.7) can be generalized to account for multilead ECGs by using a vector of delays  $\delta_1^+, \delta_1^-, \delta_2^+$ , and  $\delta_2^-$ . These delays represent the arrival time of the generated cardiac region activity at the positive and negative electrodes of the

multiple leads. For example, assume leads I, II, and III are available for the inverse problem. In this case, the vector of delays is

$$\begin{bmatrix} \delta_{1 I}^+ \\ \delta_{1 II}^+ \\ \delta_{1 III}^+ \end{bmatrix}, \begin{bmatrix} \delta_{2 I}^+ \\ \delta_{2 II}^+ \\ \delta_{2 III}^+ \end{bmatrix}, \begin{bmatrix} \delta_{1 I}^- \\ \delta_{1 II}^- \\ \delta_{1 III}^- \end{bmatrix}, \begin{bmatrix} \delta_{2 I}^- \\ \delta_{2 II}^- \\ \delta_{2 III}^- \end{bmatrix}. \quad (6.8)$$

By replacing the scalar time delays in (6.7) with the vectors in (6.8), the inverse problem becomes

$$\min_x \left\{ Error = \sum_{time} ECG - \sum_{i=SA,AV,BB,Pf,Lv,Rv} k_i \left[ \left( \frac{I}{1 - e^{a_{(i)}(t-c_{(i)}-\delta_{1i}^+)}} - \frac{I}{1 - e^{a_{(i)}(t-c_{(i)}-\delta_{2i}^+)}} \right) - \left( \frac{I}{1 - e^{a_{(i)}(t-c_{(i)}-\delta_{1i}^-)}} - \frac{I}{1 - e^{a_{(i)}(t-c_{(i)}-\delta_{2i}^-)}} \right) \right] \right\}^2. \quad (6.9)$$

Although this formulation is an example, it shows that the inverse problem setup can be extended to account for the 12 standard leads or any number of leads.

Now that we have set up the optimization problem, four sets of constraints are required to enforce the cardiac electrophysiology. The first set is used to maintain the same firing sequence as the cardiac electrophysiology. Equations (6.10) - (6.11) represent the constraints requiring the activation and deactivation of the SA node prior to that of the AV node.

$$c_{(SA)1} < c_{(AV)1} \quad \text{and} \quad (6.10)$$

$$c_{(SA)2} < c_{(AV)1} . \quad (6.11)$$

Equations (6.12) - (6.15) force the arrival time of the wave generated by the SA node at the positive and negative electrodes to precede that of the AV node.

$$c_{(SA)1} + \delta_{(SA)1}^+ < c_{(AV)1} + \delta_{(AV)1}^+ , \quad (6.12)$$

$$c_{(SA)2} + \delta_{(SA)2}^+ < c_{(AV)1} + \delta_{(AV)1}^+ , \text{ and} \quad (6.13)$$

$$c_{(SA)1} + \delta_{(SA)1}^- < c_{(AV)1} + \delta_{(AV)1}^- , \text{ as well as} \quad (6.14)$$

$$c_{(SA)2} + \delta_{(SA)2}^- < c_{(AV)1} + \delta_{(AV)1}^- . \quad (6.15)$$

Equations (6.16) - (6.19) represent the constraints that the atrial activity occurs prior to the ventricular activity. In this case, the deactivation of the AV node occurs prior to that of the bundle branches, the Purkinje fibers, and the right and left ventricles.

$$c_{(AV)2} < c_{(Bb)1} , \quad (6.16)$$

$$c_{(AV)2} < c_{(Pf)1} , \quad (6.17)$$

$$c_{(AV)2} < c_{(Lv)1} , \quad (6.18)$$

$$c_{(AV)2} < c_{(Rv)1} , \quad (6.19)$$

Equations (6.20) - (6.27) constrain the waves generated by the AV node to arrive prior to those of the Bb, Pf, and RV and LV at the positive and negative electrodes,

$$c_{(AV)2} + \delta_{(AV)2}^+ < c_{(Bb)2} + \delta_{(Bb)2}^+ , \quad (6.20)$$

$$c_{(AV)2} + \delta_{(AV)2}^- < c_{(Bb)1} + \delta_{(Bb)1}^- , \quad (6.21)$$

$$c_{(AV)2} + \delta_{(AV)2}^+ < c_{(Pf)2} + \delta_{(Pf)2}^+ , \quad (6.22)$$

$$c_{(AV)2} + \delta_{(AV)2}^- < c_{(Pf)1} + \delta_{(Pf)1}^- , \quad (6.23)$$

$$c_{(AV)2} + \delta_{(AV)2}^+ < c_{(RV)2} + \delta_{(RV)2}^+, \quad (6.24)$$

$$c_{(AV)2} + \delta_{(AV)2}^- < c_{(RV)1} + \delta_{(RV)1}^-, \quad (6.25)$$

$$c_{(AV)2} + \delta_{(AV)2}^+ < c_{(LV)2} + \delta_{(LV)2}^+, \text{ and} \quad (6.26)$$

$$c_{(AV)2} + \delta_{(AV)2}^- < c_{(LV)1} + \delta_{(LV)1}^-. \quad (6.27)$$

Now that the atrial activity has been set to occur prior to the ventricular activity, the constraints regarding the activation sequence of the ventricles is described. Equations (6.28) - (6.29) represent the constraints that the activation and deactivation of the bundle branches occur prior to those of the Purkinje fibers.

$$c_{(Bb)1} < c_{(Pf)1}, \text{ and} \quad (6.28)$$

$$c_{(Bb)2} < c_{(Pf)1}. \quad (6.29)$$

The bundle branch activity must arrive at the positive and negative electrodes prior to the wave generated by Purkinje fibers:

$$c_{(Bb)1} + \delta_{(Bb)1}^+ < c_{(Pf)1} + \delta_{(Pf)1}^+, \quad (6.30)$$

$$c_{(Bb)2} + \delta_{(Bb)2}^+ < c_{(Pf)1} + \delta_{(Pf)1}^+, \text{ and} \quad (6.31)$$

$$c_{(Bb)1} + \delta_{(Bb)1}^- < c_{(Pf)1} + \delta_{(Pf)1}^-, \text{ as well as} \quad (6.32)$$

$$c_{(Bb)2} + \delta_{(Bb)2}^- < c_{(Pf)1} + \delta_{(Pf)1}^-. \quad (6.33)$$

The activity of the Purkinje fibers must occur prior to that of the right and left ventricles:

$$c_{(Pf)2} < c_{(LV)1} \text{ and} \quad (6.34)$$

$$c_{(Pf)2} < c_{(RV)1}. \quad (6.35)$$

The arrival time of the Purkinje fibers activity at the positive and negative electrodes must be prior to that of the left and right ventricles:

$$c_{(Pf)2} + \delta_{(Pf)2}^+ < c_{(LV)1} + \delta_{(LV)1}^+, \quad (6.36)$$

$$c_{(Pf)2} + \delta_{(Pf)2}^- < c_{(LV)1} + \delta_{(LV)1}^-, \text{ and} \quad (6.37)$$

$$c_{(Pf)2} + \delta_{(Pf)2}^+ < c_{(RV)1} + \delta_{(RV)1}^+, \text{ as well as} \quad (6.38)$$

$$c_{(Bb)2} + \delta_{(Bb)2}^- < c_{(Pf)1} + \delta_{(Pf)1}^-. \quad (6.39)$$

The activation of LV occurs prior to that of the RV, as seen in (6.40), while the deactivation occurs after that of the RV, as shown in (6.41):

$$c_{(LV)1} < c_{(RV)1}, \quad (6.40)$$

$$c_{(RV)2} < c_{(LV)2}. \quad (6.41)$$

Equations (6.42)-(6.45) constrain the arrival time of the RV and LV generated waves at the positive and negative electrodes:

$$c_{(LV)1} + \delta_{(LV)1}^+ < c_{(RV)1} + \delta_{(RV)1}^+, \quad (6.42)$$

$$c_{(LV)1} + \delta_{(LV)1}^- < c_{(RV)1} + \delta_{(RV)1}^-, \text{ and} \quad (6.43)$$

$$c_{(RV)2} + \delta_{(RV)2}^+ < c_{(LV)2} + \delta_{(LV)2}^+, \text{ as well as} \quad (6.44)$$

$$c_{(RV)2} + \delta_{(RV)2}^- < c_{(LV)2} + \delta_{(LV)2}^-. \quad (6.45)$$

The second set forces the activation to occur before the deactivation. These set of constraint are formulated as

$$c_{(i)1} < c_{(i)2}, \quad (6.46)$$

$$c_{(i)1} + \delta_{(i)1}^+ < c_{(i)2} + \delta_{(i)2}^+, \quad (6.47)$$

$$c_{(i)1} + \delta_{(i)1}^- < c_{(i)2} + \delta_{(i)2}^-, \quad (6.48)$$

where  $i \in [SA \quad AV \quad Bb \quad Pf \quad Lv \quad Rv]$ .

Finally, the third set forces the slopes of the activation to be higher than those of the deactivation curves:

$$a_{(i)1} < a_{(i)2}. \quad (6.49)$$

As a summary, this section presented the optimization problem used to solve the inverse problem. Additionally, the cardiac electrophysiological constraints are presented.

### 6.3 Initial Condition

Now that the optimization problem is defined, the initial condition used in this work is presented in this section. When solving any numerical optimization technique, a good initial condition is required for a more accurate and faster solution. For this case, a template initial condition with known parameters for  $\hat{f}_{ECG}$  is used to set the initial condition for the optimization process. Additionally, a dynamic template is generated. The initial condition adapts the chosen initial parameters to the magnitude and sign of the R peak. The sign of the ECM R peak is chosen to match the sign of the R wave peak in the signal.

In addition to the above setup for the template initial condition, a time alignment is required between the initial signal and actual ECG. The alignment between the template initial condition and the actual ECG signal is performed by choosing the highest cross-correlation between the two. Four steps are applied to ensure the minimal error between the initial condition and actual ECG. First, the initial template ECG is setup and generated. Second, the original signal is zero padded at the beginning and end. Third, the

difference between the initial template and the original signal is calculated. In the fourth step, the signal is time-shifted and step three is repeated until the minimum error between the two is reached.

Figure 6-2 shows an actual ECG measured at lead II. Figure 6-3 shows the initial condition signal built according to the actual signal shown in Figure 6-3. Figure 6-4 shows the initial condition signal with the actual signal.

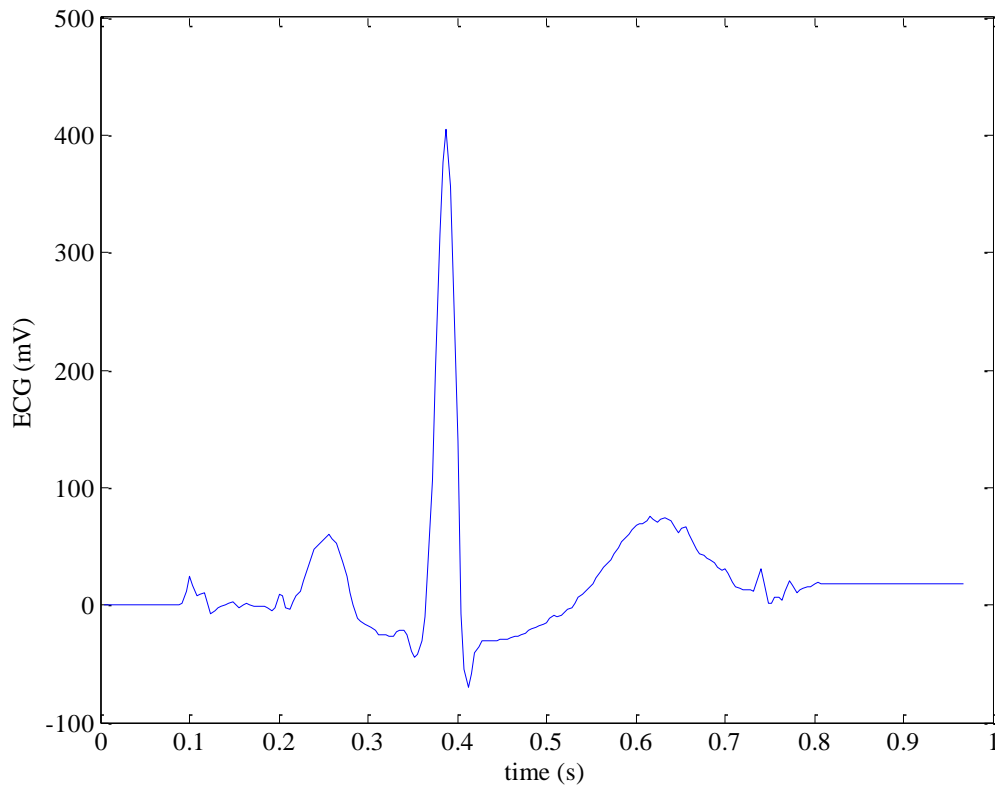


Figure 6-2: Actual ECG signal at lead II.

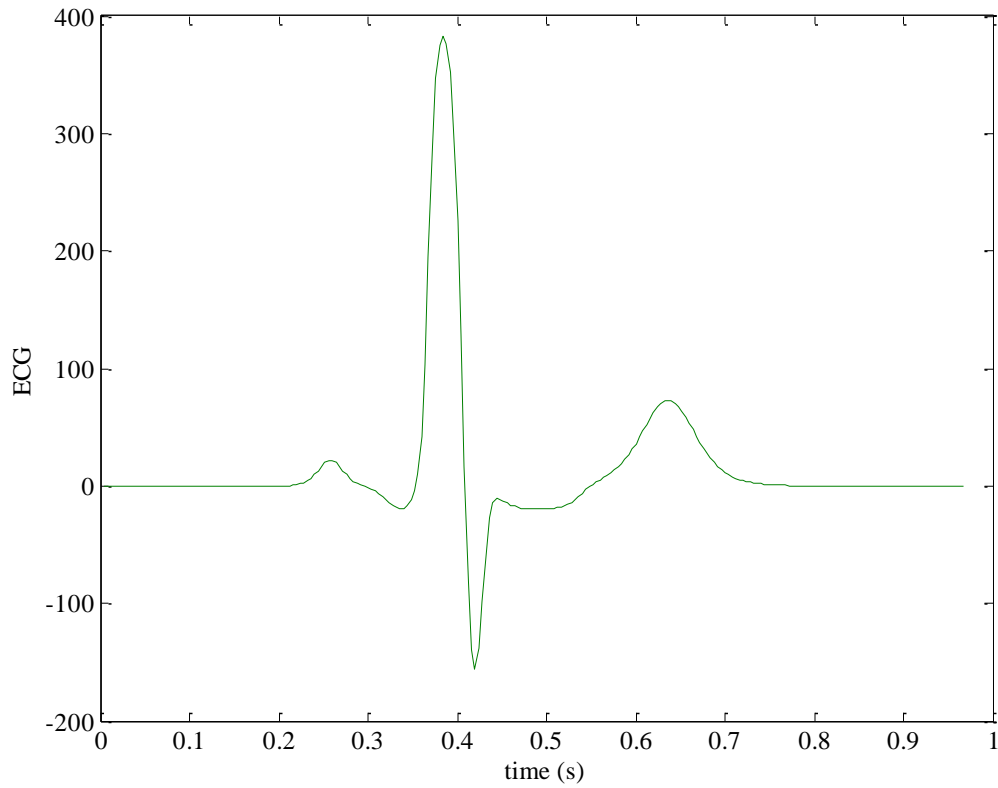


Figure 6-3: Initial condition signal.

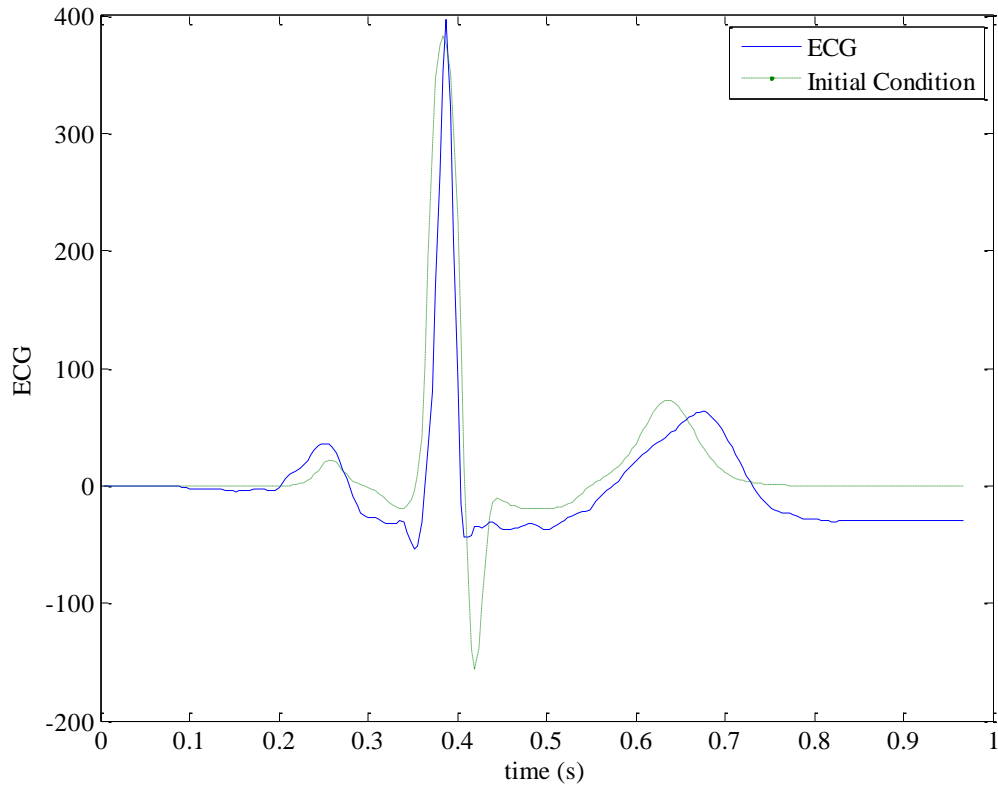


Figure 6-4: Initial condition signal compared to the signal to be fitted.

## 6.4 Nonlinear Constrained Optimization

Now that the optimization problem (6.7) and the initial conditions are defined, the optimization technique used to solve the inverse problem is described in this section. This work uses a nonlinear constrained optimization technique based on a line search method. The optimization technique solves (6.7) with the constraints presented in (6.10) - (6.49). As mentioned previously, these constraints enforce the cardiac electrophysiology on the solution to the inverse problem. The nonlinear constrained solver `fmincon` in Matlab is applied to the problem (6.5) with the constraints (6.10) - (6.49). The line search algorithm used in `fmincon` is described below.

The line search algorithm is an iterative gradient descent optimization technique used to find a minimum  $x^*$  of an objective function  $f: \mathbb{R}^n \rightarrow \mathbb{R}$  [40]:

1. Set iteration counter to  $k = 0$
2. Make an initial guess  $x_0$  for the minimum.
3. Compute a descent direction  $p_k$ .
4. Choose  $\alpha_k$  to “loosely” minimize  $\phi(\alpha) = f(x_k + \alpha p_k)$  over  $\alpha \in \mathbb{R}$ .
5. Update  $x_{k+1} = x_k + \alpha_k p_k$  and  $k = k + 1$ .
6. If  $\|\nabla f(x_k)\| \leq \textit{tolerance}$  stop, else go to step 2.

The minimization of  $\phi$  can be performed exactly by solving for  $\phi(\alpha_k) = 0$  or by determining a sufficient decrease in  $\phi$ . The latter can be performed by using the Wolfe conditions [40].

The stopping criteria can include more than one condition. The stopping criteria used in this work are  $\|\nabla f(x_k)\| \leq 10^{-10}$  and  $k < 10^6$ . The first criterion is the difference

between the two consecutive function evaluations. The second criterion is the maximum number of iterations.

## **6.5 Discussion**

This chapter presents a novel approach for solving the inverse problem. This approach uses the electrophysiological cardiac model and a numerical optimization technique to solve for the inverse problem. The main advantage of this approach is the ability to constraint the activation timing of the cardiac regions to maintain cardiac electrophysiological rules. In contrast to the previous methods, this approach is independent of the heart and body geometry.

Furthermore, the presented approach has lower computational complexity compared to previous methods due to the lower number of parameters. Previous methods, using the same number of cardiac regions and the Hodgkin and Huxley model as a cell model, solve for at least 132 parameters compared to 54 in the presented approach. However, previous methods use more than 100,000 cells to solve for the inverse problem and require for at least 356 leads.

Now that the solution for the cardiac modeling problem has been presented, the following chapter presents the two diagnostic methods applied to the detection of myocardial ischemia and localization of myocardial infarction.

## **Chapter 7      Ischemia Detection and Infarction Localization**

The previous chapters present a novel method for solving the inverse problem based on the minimization of the sum squared error between the electrophysiological cardiac model (ECM) generated electrocardiogram (ECG) and an actual ECG. The presented inverse problem solution estimates the ECM parameters, which indicate the properties of the cardiac region electrical activity. This chapter presents two diagnostic methods that use the inverse problem solution, the principle component analysis (PCA) of the ECG, and a decision tree classifier. The first is used for the detection of myocardial ischemia. The second is for the localization of myocardial infarction. The rest of the chapter describes each the diagnostic methods.

### **7.1 *Methods***

As mentioned previously, this work presents two clinical applications using the ECM. The first application is the detection of myocardial ischemia. The second application is the localization of myocardial infarction. This section presents an overview of the diagnostic methods. These diagnostic methods are based on a beat to beat classification approach that detects the condition of a single beat. The ischemia detection method uses a beat to beat classifier to detect if a beat shows signs of ischemia. The infarction localization method uses a beat to beat classification approach to detect if a beat at each of the 11 leads shows signs of infarction.

The methods section is divided into two subsections. The first describe the ischemia detection method. The second subsection presents the infarction localization method.

### 7.1.1 Ischemia Detection

The ischemia detection method uses the inverse problem solution of an actual electrocardiogram and principle component analysis of the patient's ECM as features for a decision tree classifier to detect myocardial ischemia. Figure 7-1 shows a block diagram of the ischemia detection method presented in this work. First, the electrocardiogram is measured at the patient's body surface. Second, an automatic beat annotator 'WQRS', provided by the Physionet Toolkit [36], is used to obtain beat by beat signals automatically from the records. Third, each beat is passed through a preprocessor. Fourth, the preprocessed beat is passed to a classification method that decides if a beat shows signs of myocardial ischemia. Each of the blocks in Figure 7-1 is described in the following subsections.

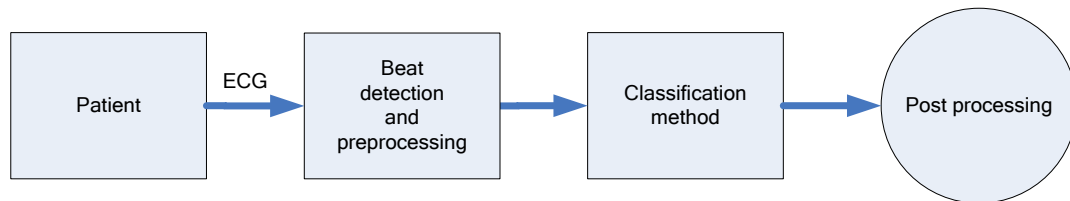


Figure 7-1: Block diagram of the ischemia detection method.

#### 7.1.1.1 Beat Detection and Preprocessing

The beats are detected from the ECG record using an automatic ECG annotator 'WQRS', which detects the beginning and end of a single beat. The beginning and end of the detected beat may contain a nonzero isoelectric line, which requires preprocessing prior to solving the inverse problem. The inverse problem solution requires the isoelectric line prior to the P wave to be zero padded to align with the initial ECM-generated ECG during the optimization process.

Figure 7-2 shows the preprocessing steps for the ischemia detection method. The upper graph in the figure shows the original beat. The bottom graph shows the

preprocessed figure. The two rectangles on the upper graph represent the modified areas of the measured ECG. In rectangle 1, the beginning of the ECG is translated to zero. Additionally, the signal in rectangle 1 is zero padded from zero to 40 ms. Similarly, in rectangle 2, the ECG signal is zero padded from 200 to 240 ms. These changes are indicated in the bottom graph of Figure 7-2 as indicated by the arrows.

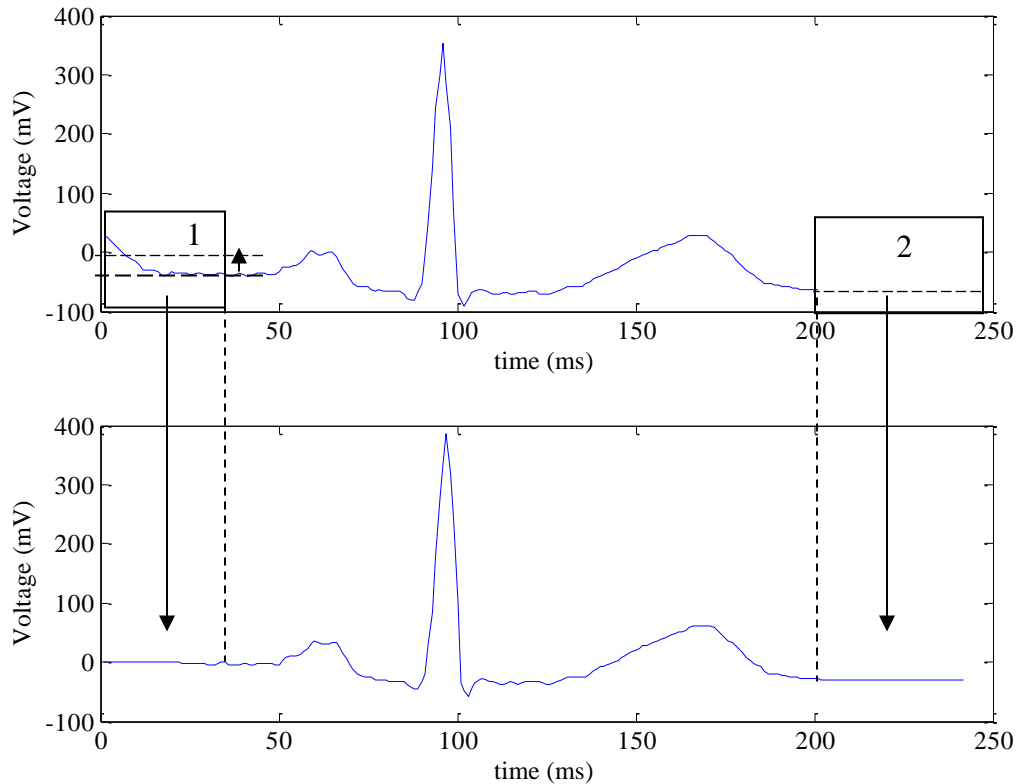


Figure 7-2: Preprocessing representation of the ECG signals.

Now that the beat detection and preprocessing is performed, the classification method that detects if a beat shows signs of ischemia is presented.

#### 7.1.1.2 Classification Method

This section describes the classification method (ECM-PCA/C4.5) used to detect if a beat shows signs of myocardial ischemia. The presented classification method utilizes

the ECM parameters, obtained using the inverse problem solution, and principle component analysis (PCA) of a patient's ECG as features for a decision tree classifier.

Figure 7-3 shows a block diagram of the classification method. First the ECM generates an initial ECG. Second, using a nonlinear constrained optimization technique, the model parameters are updated until reaching a certain error with the pre-processed patient's ECG beat. The estimated model parameters are then used with the PCA components as features in the C4.5 decision tree classifier. The decision tree classifies the beat under consideration and checks if the beat is ischemic.

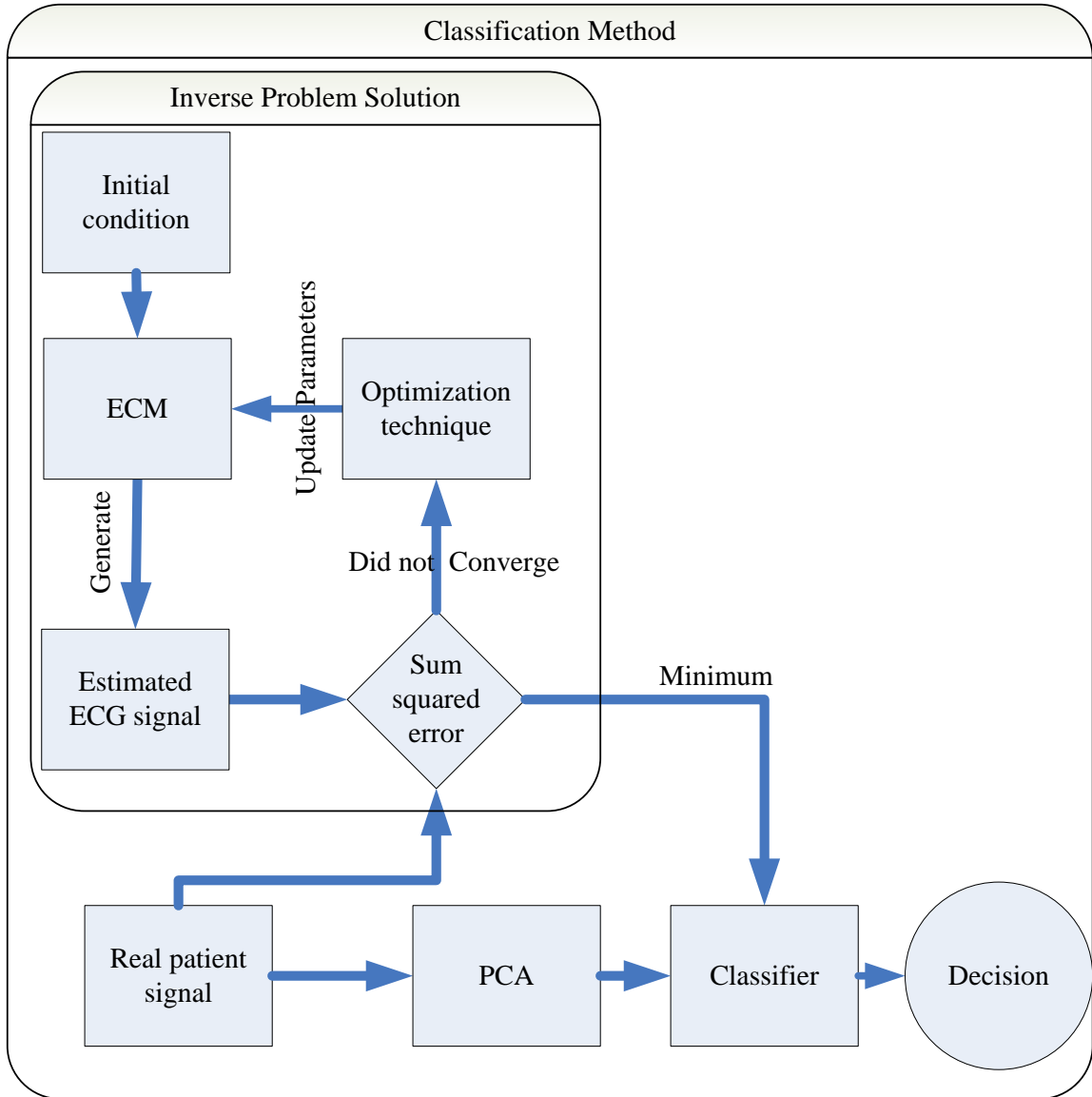


Figure 7-3: Block diagram of the beat diagnostic method.

The following sections describe each of the components of the beat diagnostic method. The next section presents a brief overview of the inverse problem followed by a description of principle component analysis and decision trees.

#### 7.1.1.2.1 Inverse Problem Solution

The model parameters are determined using the inverse problem solution presented in chapter 6. As mentioned the previous chapter, the solution is based

minimization of the sum squared error between the ECM-generated ECG beat and a real patient ECG. The optimization problem is defined as

$$\min_x \left\{ Error = \sum_{time} \left( ECG - \sum_{i=[SA,AV,Bb,Pf,Lv,Rv]} k_i \left[ \left( \frac{I}{1 - e^{a_{(i)1}(t-c_{(i)1}-\delta_{1i}^+)}} - \frac{I}{1 - e^{a_{(i)2}(t-c_{(i)2}-\delta_{2i}^+)}} \right) - \left( \frac{I}{1 - e^{a_{(i)3}(t-c_{(i)1}-\delta_{1i}^-)}} - \frac{I}{1 - e^{a_{(i)4}(t-c_{(i)2}-\delta_{2i}^-)}} \right) \right] \right)^2 \right\}, \quad (7.1)$$

where  $x$  represents the ECM parameters defined as  $x = [t, a_1, c_1, a_2, c_2, k, \delta_1^+, \delta_1^-, \delta_2^+, \delta_2^-]$  at each of the modeled regions  $[SA, AV, Bb, Pf, Lv, Rv]$ . The aim of this optimization problem is to solve for the ECM parameters,  $x$ , which yields the minimum sum squared error between the ECM-generated and an actual ECG. The inverse problem solution, presented in chapter 6, is based on the hypothesis that the resulting ECM parameters can be used to model the actual cardiac region activity.

### 7.1.1.2.2 Principle Component Analysis

Principle Component Analysis (PCA) is a linear transform of a signal, where the basis functions are taken from the statistics of the signal [41]. It is optimal in the sense of energy compaction, i.e., it places as much energy as possible in as few coefficients as possible. The PCA is typically implemented using singular value decomposition. The transform is not separable, and thus the full matrix multiplication must be performed [41]:

$$X = U^T x \quad \text{and} \quad (7.2)$$

$$x = UX, \quad (7.3)$$

where the  $U$  is the basis for the transform.  $U$  is estimated from a number of  $x_i$ , where

$i \in [0 \cdots k]$ :

$$U \Sigma V^T = [x_1 \quad x_2 \quad \cdots \quad x_k] = A, \text{ and} \quad (7.4)$$

$$U = \text{eigvec}(AA^T). \quad (7.5)$$

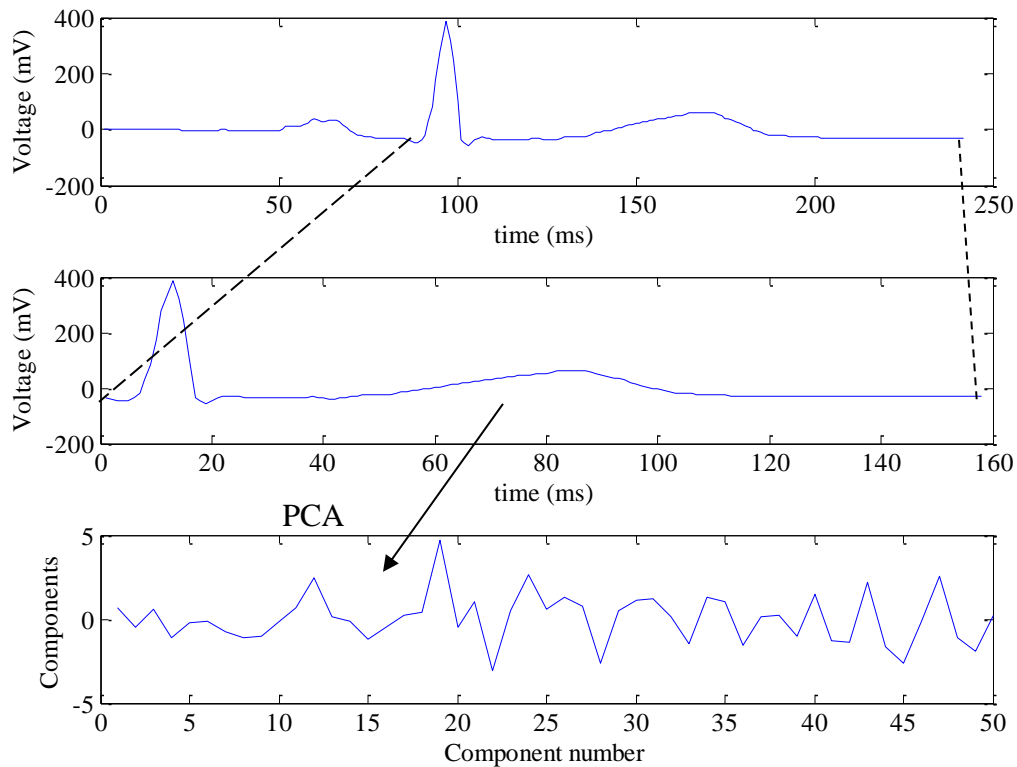


Figure 7-4: Demonstration of the PCA process.

As mentioned previously, the PCA is applied to the beat under consideration. As shown in Figure 7-4, first the beginning of the Q wave is identified using the automatic annotator ‘WQRS’. Second, the ECG is trimmed from the beginning of the Q wave until the end of the signal as shown in the middle graph of Figure 7-4 to account for the ischemic changes occurring in ventricular activity. The P wave and PR segment are dropped because they represent the atrial activity and show no changes in the detection of

myocardial ischemia [4]. The PCA is applied to the resulting signal as shown in the bottom of Figure 7-4. As recommend by [1, 33], fifty components are extracted from the signal to be used in the classification process.

### ***7.1.1.2.3 C4.5 Decision Tree***

The C4.5 algorithm was developed by Ross Quinlan in 1996 [42]. The C4.5 algorithm is a classifier that builds a decision tree from a training set based on the statistics of the data. During the testing phase, the algorithm uses the rules of the decision tree to reach a verdict. This work uses a C4.5 decision tree classifier because is one of the simplest and effective classifiers as applied in the fields of radar signal classification, medical diagnosis, expert systems, and speech recognition [43]. In the presented diagnostic approach, the C4.5 decision tree classifier uses the model parameters to generate rules based on the cardiac electrophysiology to classify whether a beat indicates myocardial ischemia. The implementation of the C4.5 classifier in the Weka classifier package [44] is used in this work. The rest of this section describes the training phase followed by the testing phase. Finally, a description of the application of the decision tree in the ischemia detection method is presented.

#### ***Training Phase***

The training dataset is defined as  $S = s_1, s_2, \dots, s_n$ , where each sample  $s_i = x_1, x_2, \dots, x_n$  is a vector of features or attributes  $x_i$ . The training dataset is associated with a vector  $C = c_1, c_2, \dots, c_n$ , where  $c_1, c_2, \dots, c_n$  is the set of classes corresponding to each sample. The C4.5 algorithm is based on the concept that the attributes can be used to

divide the data into smaller sets. The attribute with the lowest entropy,  $I_E$ , is chosen to subdivide the dataset. If a feature  $x$  belongs to a class,  $c_i$ , its information entropy is:

$$I_E(x) = -\sum_i p(x|c_i) \log_2 p(x|c_i), \quad (7.6)$$

where  $p(x|c_i)$  is the probability that an attribute  $x$  can classify a sample selected at random from a class  $c_i$ . The C4.5 training algorithm is:

1. Initialize the set of attributes  $X = x_1, x_2, \dots, x_i$
2. Loop for all attributes in set  $X$  and calculate the information entropy  $I_E$ .
3. Chose the attribute,  $x_{\min}$ , with the least information entropy.
4. Create a tree node that splits the data according to  $x_{\min}$ .
5. Terminate the tree growth if the stopping criteria are met, else remove  $x_{\min}$  the set of attributes  $X = X - x_{\min}$  and iterate over the remaining attributes.
6. Prepruning is used as stopping criterion of a decision tree. The tree growth is stopped when there is no longer sufficient data to make reliable decisions, i.e. individual nodes are being created with no relation to previous or following node.

### Testing Phase

Now that the training algorithm has been described, the test phase is presented. During the testing phase, each test example is passed through the decision tree by following a path that makes the test at each node true. The example is then assigned to the class at the last node (leaf) of the tree.

### Application of C4.5 in Ischemia Detection

The ischemia detection approach uses the decision tree training algorithm to generate a decision tree that classifies the condition of a certain beat. The estimated ECM parameters and the first fifty PCA components of the trimmed ECG signal, shown in previous section, are used as attributes in the training process. The classes corresponding to the samples are ischemic or healthy.

### **7.1.2 Infarction Localization**

Now that the ischemia detection method is presented, this section describes the infarction localization method. The infarction localization method is based on analysis first presented by Selvester [45] and the classification method described in the classification method section 7.1.1.2. This analysis proposes that the 12 ECG leads can indicate the location of the myocardial infarction. Figure 7-5 shows a block diagram of the infarction localization method. First, the 12 lead ECG signals are measured. The aVR lead is ignored due to its irrelevance in clinical diagnostics [45]. Each of the captured leads are passed to the WQRS beat detector [36]. The detected beats are then averaged per lead. Each of the resulting averaged beats is passed to the classification method, presented in the classification method section 7.1.1.2, to determine if it shows infarctions. The predicted results at each of the leads are passed through a localizer that determines the location of the infarct.

This section is divided into three subsections. First, the preprocessing of the ECG signal is described. The second subsection describes the procedure of applying the classification method, presented in section 7.1.1.2, to the localization method. Finally, the localizer method used to predict the infarction location is described.

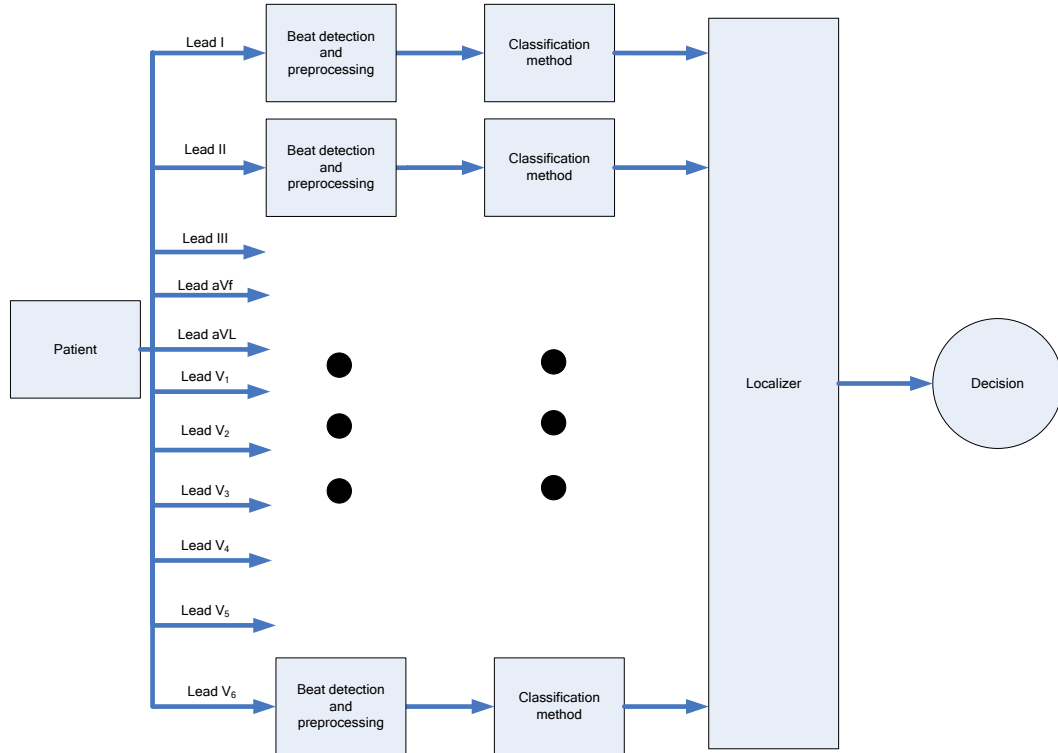


Figure 7-5: Block diagram of the infarction localization method.

### 7.1.2.1 Preprocessing

Ensemble averaging is performed in this approach to minimize the power line noise and temporal artifacts in the signal. Additionally, ensemble averaging maximizes the infarction patterns appearing at the leads. Moreover, the baseline wandering was removed using a median filter of order  $N=200$ .

The ensemble averaging is performed by averaging all good beats, where the start of the P wave and the end of the T wave are indicated by the automatic annotator. Four steps are applied to perform time averaging process. First, the beats are detected using the “WQRS” [8]. Second, one beat is fixed while another is shifted until a high cross-correlation between the detected good beats is reached. Third, the best match is saved, and the process is applied for all detected beats. Fourth, the matching beats are averaged.

Finally, the averaged beats are zero padded prior to the P wave as described in the beat detection and preprocessing section 7.1.1.1.

### 7.1.2.2 Classification Method

Now that the preprocessing of the ECG signal has been presented, this section describes the application of the classification method, presented in 7.1.1.2, to the 11 leads: I, II, III, aVL, aVF, V<sub>1</sub>, V<sub>2</sub>, ..., V<sub>6</sub>. First, the inverse solution of the ECM is applied to each beats of the 11 leads. Second, the principle component analysis, described in section 7.1.1.2.2, of the averaged beats at each of the leads is performed. The resulting ECM parameters and PCA components at each of the 11 leads are used as features in a C4.5 decision tree classifier to predict if a lead shows changes due to an infarct. The decision of the C4.5 classifier is either 1 for infarcted or 0 for healthy. The classifier decisions are stored in a 1x11 vector, which is passed to a localizer that decides the infarction location. The localizer is described in the next section.

### 7.1.2.3 Localizer

The localizer is a method used to transform the diagnosed leads to the location of the infarct. The localizer determines the infarct location based on the Selvester criteria. Table 7.1 shows the relations between the leads and the respective location in the left ventricle muscles as described by [45]. The changes in leads V<sub>2</sub>, V<sub>3</sub>, and V<sub>4</sub> are caused by anterior infarcts. Infarcts in the septal region change the ECG at leads V<sub>1</sub>, V<sub>2</sub>, and V<sub>3</sub>. Moreover, changes in the I, aVL, V<sub>5</sub>, and V<sub>6</sub> are attributed to lateral infarcts. The changes in II, III, and aVF are due to inferior infarcts. Furthermore, a combination of the infarcts can appear the respective leads of those infarcts. For example, the changes caused by anteroseptal infarcts appear in leads V<sub>2</sub>, V<sub>3</sub>, and V<sub>4</sub>, and V<sub>1</sub>.

Table 7.1: ECG changes seen in acute myocardial infarction [45].

Area	Changes and leads	Binary representation
Anterior	Q or QS in V2 through V4	[0 0 0 0 0 0 1 1 1 0 0]
Septal	Q or QS in V1 and V2	[0 0 0 0 0 1 1 0 0 0 0]
Lateral	Q or QS in I, aVL, and V5 and V6	[1 0 0 1 0 0 0 0 0 1 1]
Inferior	Q or QS in II, III, and aVF	[0 1 1 0 1 0 0 0 0 0 0]

Additionally, Table 7.1 shows the binary representation of the Selevester criteria, where the leads showing infarction signs are represented by 1, and healthy lead are represented by 0. As mentioned in the classification method, the resulting predictions at each of the leads are stored in a 1x11 vector. The location of the infarct is determined using the minimum distance between the predicted binary vector and the Selvester criteria binary representation.

## 7.2 Discussion

This chapter presented two diagnostic applications for the ECM model. These applications are based on the beat diagnostic method. This method uses the ECM, principle component analysis, and a decision tree classifier to diagnose a beat. The advantage of the diagnostic methods is that they use the electrophysiology of the heart, cardiac region electrical activity, and the principle components of the signal to extract the classification features. This provides an accurate, automatic, and inexpensive method for the detection of myocardial ischemia and localization of myocardial infarction.

Now that the ECM, the solutions for the forward and inverse problems, and the diagnostic applications have been described, the next two chapters present the results of the presented methods. Chapter 8 presents and analyses the forward and inverse

problems' solutions. Chapter 9 presents the results for the ischemia detection and infarction localization methods.

## Chapter 8      **Results of Modeling Problem Solution**

This chapter presents the experimental results of the electrophysiological cardiac model (ECM) and the forward and inverse problems solutions described in chapters 5 and 6. Three experiments have been applied to evaluate the ECM. The first is the application of the solution to actual single lead electrocardiograms (ECGs). The second experiment is the application of the ECM to simulated ECGs with different levels of white, pink, and brown noise. The third experiment is the application of the ECM to multilead ECGs. Each section contains explanation of the experiment, results, and discussion and analysis of the results.

The first section presents the experiment used to validate the forward and inverse problem solutions using actual single lead ECGs. The second section presents analyses the variation of the forward and inverse problems solution under different noise levels. The third section presents the results of the multilead forward and inverse problem solutions. The fourth section presents a summary and discussion of the results.

### ***8.1 Actual Electrocardiogram Experiment***

This section presents the experimental results of the forward and inverse problem solutions. The experiment is applied to healthy, ischemic, and infarcted electrocardiograms. The beats used in this experiment are selected at random from the Long Term ST and PTB diagnostic databases presented in chapter 4.

The first step in the experiment is to detect the beats using WQRS [36]. The second step is to apply the inverse and forward problem solutions presented in chapters 5

and 6. The third step is to analyze the estimated cardiac region activity and detected ECG features.

The next section presents the experimental results of the forward and inverse problems solutions applied to healthy beats. Sections 8.1.2 and 8.1.3 present the experimental results of the ECM applied to ischemic and infarcted beats, respectively.

### **8.1.1 Healthy ECG**

Figure 8-2 shows the results of the inverse problem solution described in chapter 6 applied to a healthy ECG shown in Figure 8-1. These graphs show the cardiac region electrical activity at the SA and AV nodes, the bundle branches (Bb), the Purkinje fibers (Pf), and left and right ventricle (LV and RV). These results are used by the ECM to generate an estimate of an actual healthy ECG signal. It can be seen that the cardiac electrophysiology is maintained in the ECM, where the sequence of activations of the cardiac region activity is the same as an actual heart.

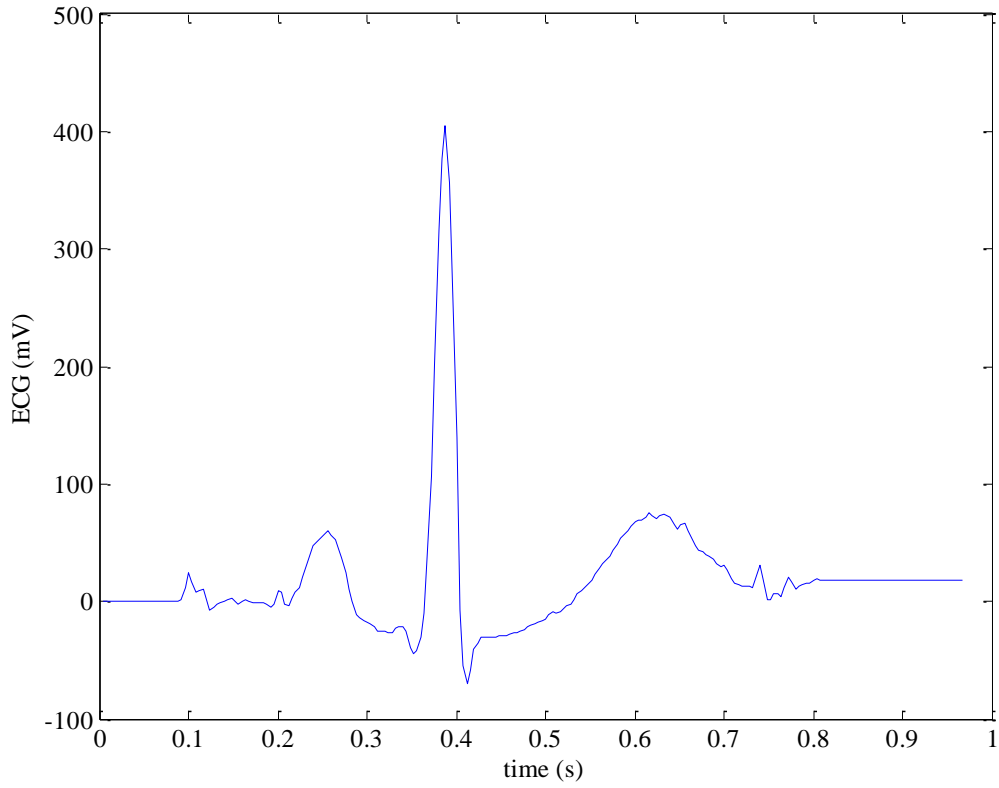


Figure 8-1: Actual healthy beat at lead II.

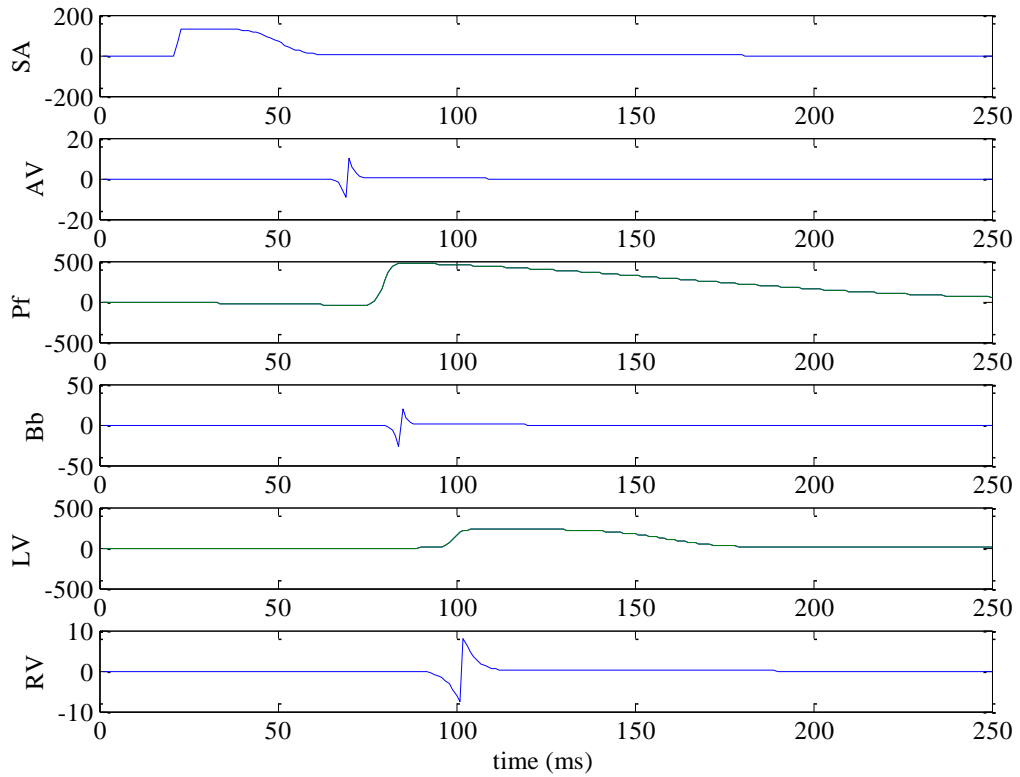


Figure 8-2: Cardiac region activity, inverse problem solution.

Figure 8-3 shows the forward problem solution. The upper six graphs represent the cardiac region electrical activity arriving at the positive and negative electrodes. The bottom graph shows the ECM-generated ECG. Figure 8-4 shows a comparison between the actual and the ECM-generated ECG. The error between the two signals is shown in Figure 8-5. It can be seen that the error indicated by the ovals are attributed to additional noise in the ECG. Moreover, the error at the QRS complex is less than 10%, which is clinically negligible [46]. The error at the end of the signal is due to the zero padding during the pre processing of the signal.

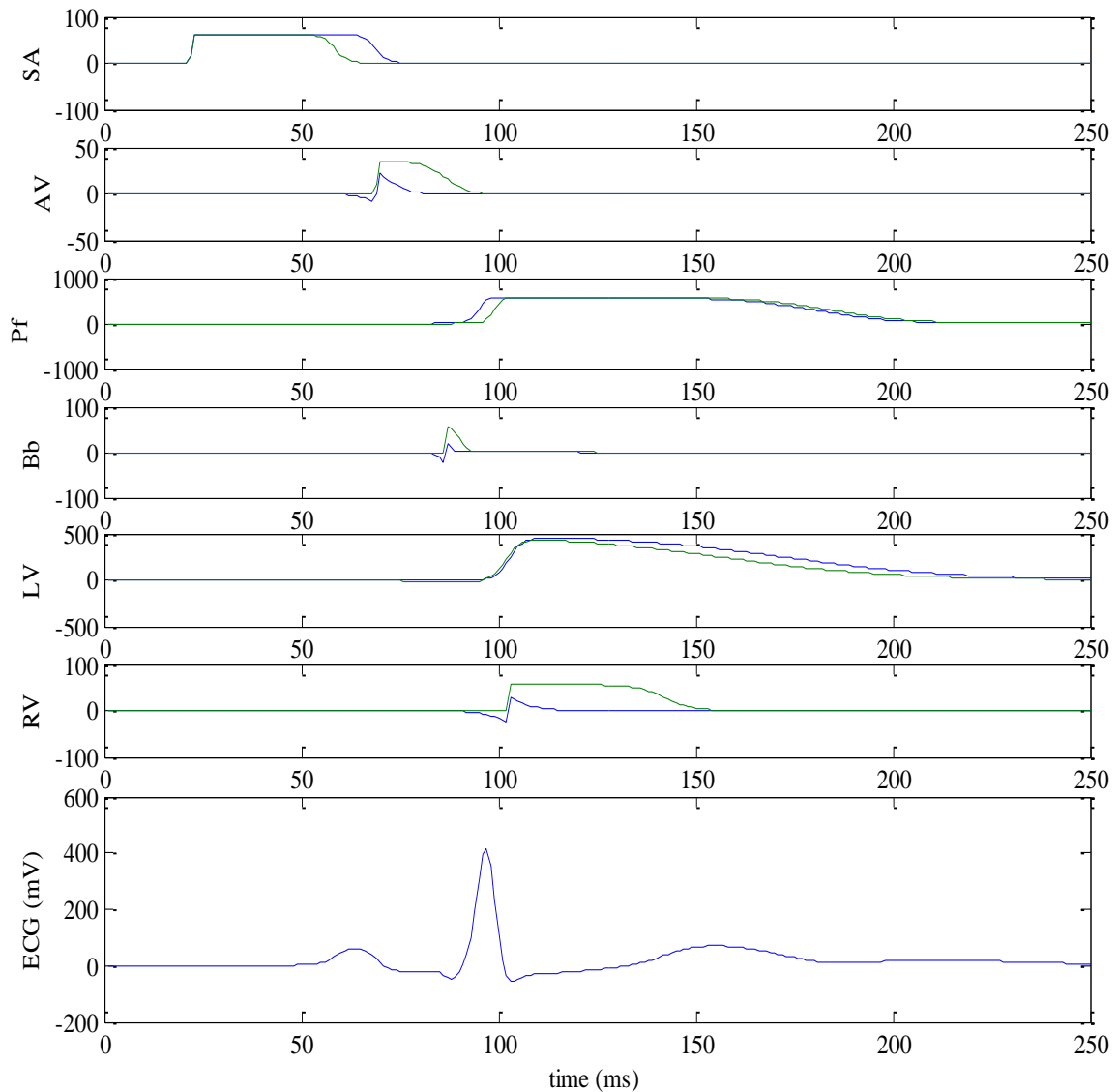


Figure 8-3: ECM-generated ECG, forward problem solution.

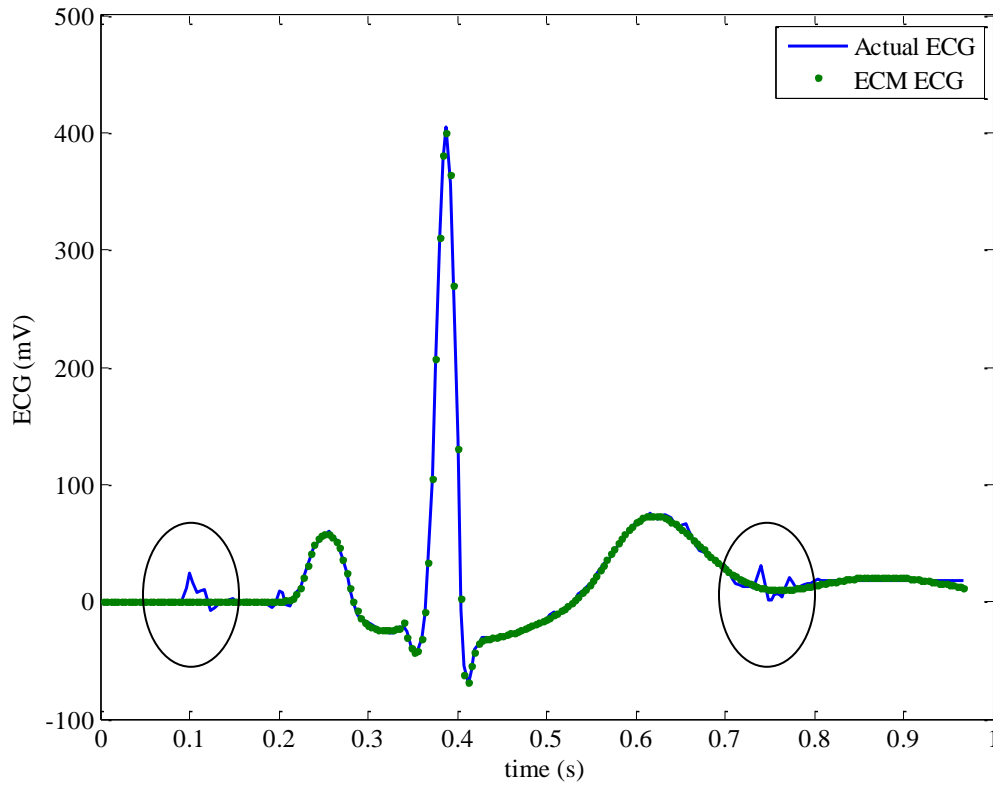


Figure 8-4: A comparison between an actual ECG and ECM-generated ECG.

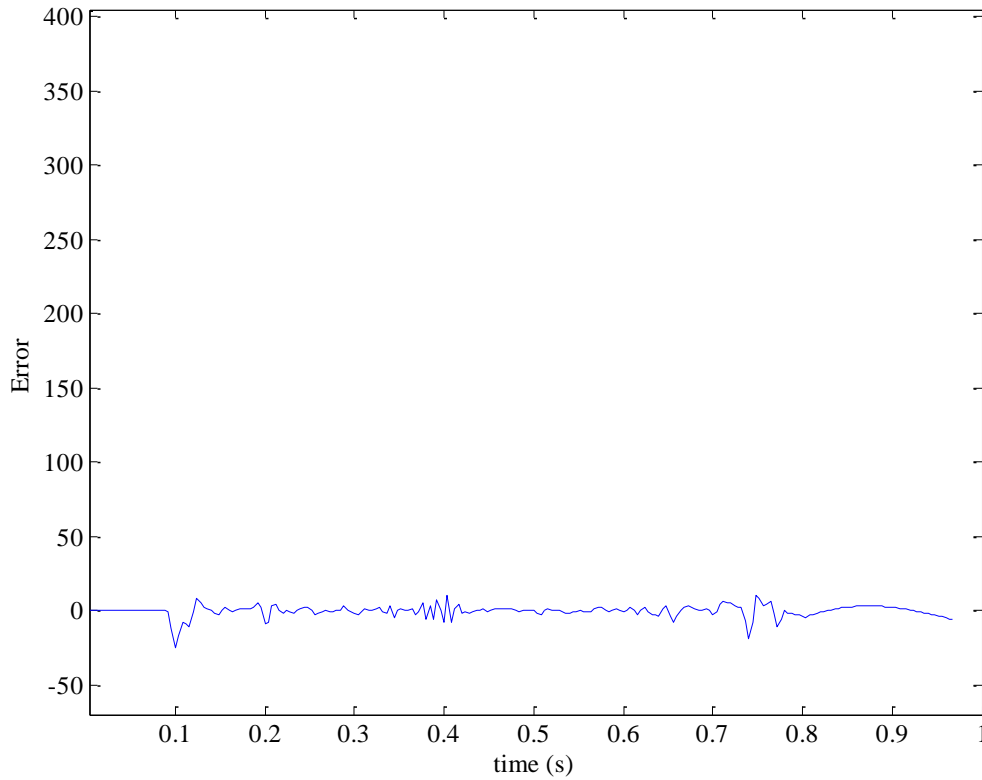


Figure 8-5: The error between the actual and ECM-generated ECG.

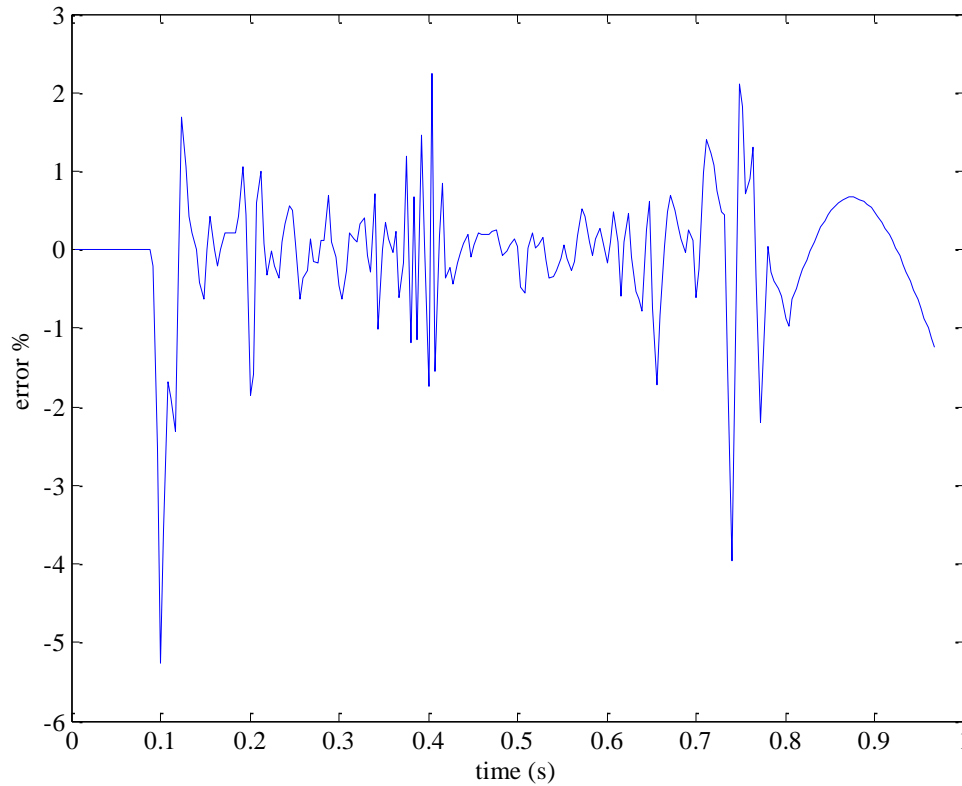


Figure 8-6: Percentage error between the actual and ECM-generated ECG.

Figure 8-7 shows normal density function fit to the distribution of the error shown in Figure 8-5. It can be seen that the resulting error between the original signal and ECM-generated ECG is close to a normal distribution. The null hypothesis that the residual is a random sample from a normal distribution is rejected by a Kolmogorov-Smirnov goodness of fit. Although, the Kolmogorov-Smirnov goodness of fit test resulted in rejecting the null hypothesis, the normal fit had the lowest root mean squared error and highest  $p$  value compared to uniform, Laplace, and Rayleigh distributions. The rejection of the null hypothesis can be attributed to the high frequency noise affecting ECGs at 50Hz-60Hz.

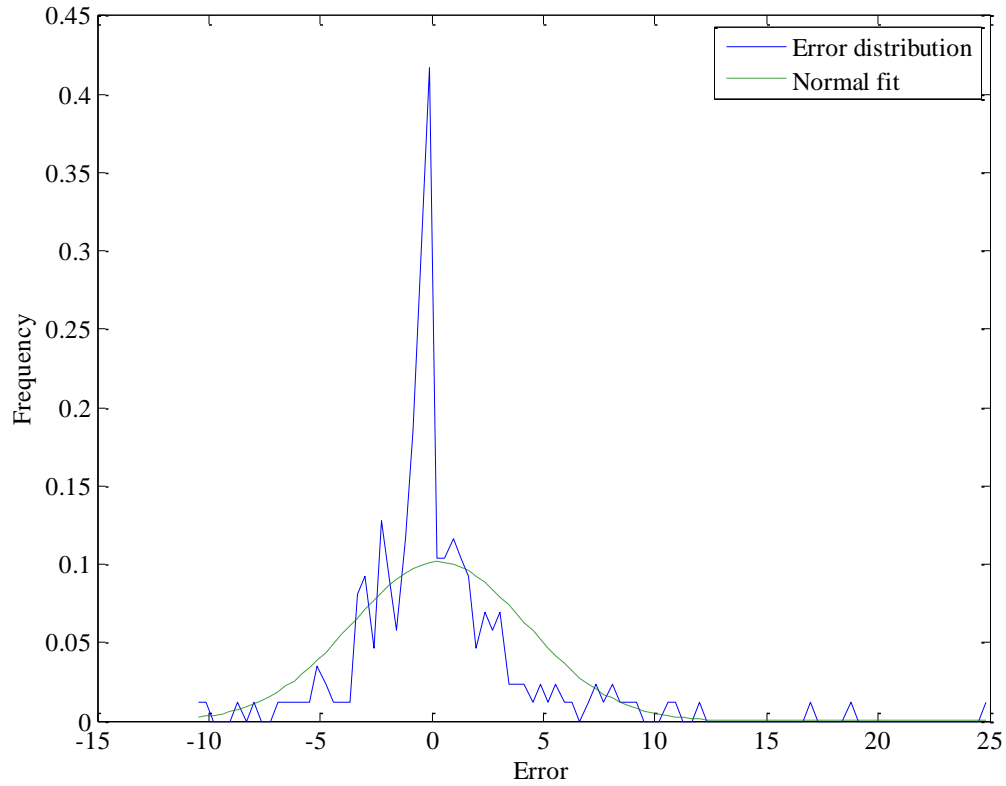


Figure 8-7: Gaussian fit between error distribution and normal distribution.

The cross-correlation of the residual error is shown in Figure 8-8. There is no significant correlation between the samples of the residual. Figure 8-9 shows a comparison between the cross-correlation of the residual error and the cross-correlation of a white noise. The comparison shows the similarity of the resulting graphs.

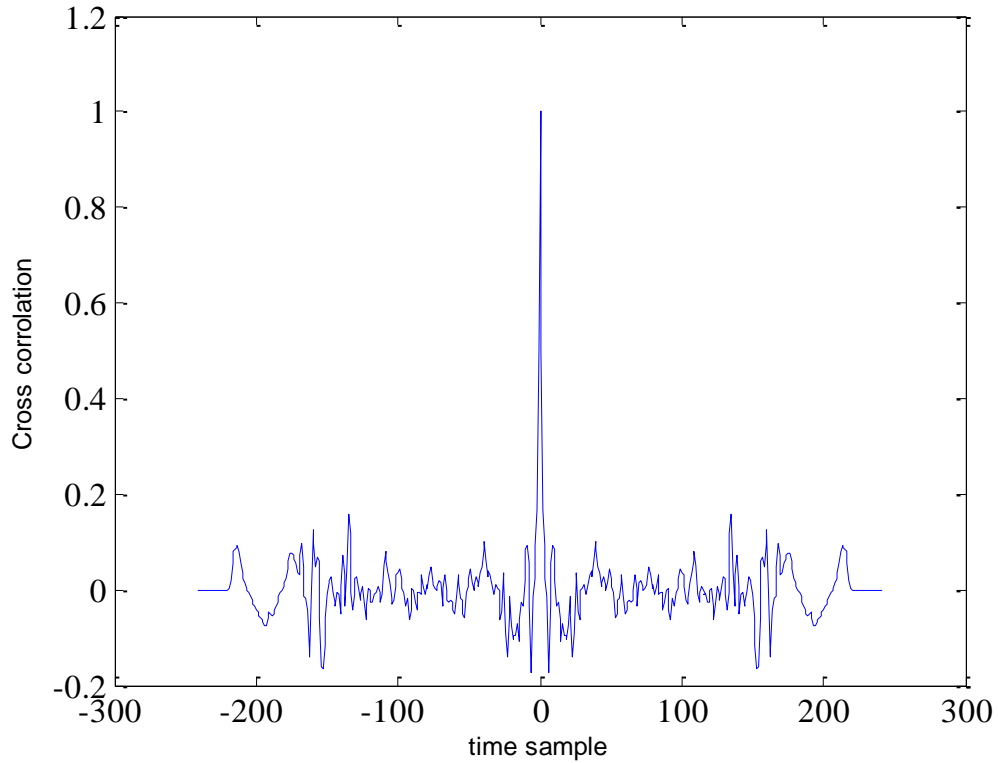


Figure 8-8: Cross-correlation of the residual error.

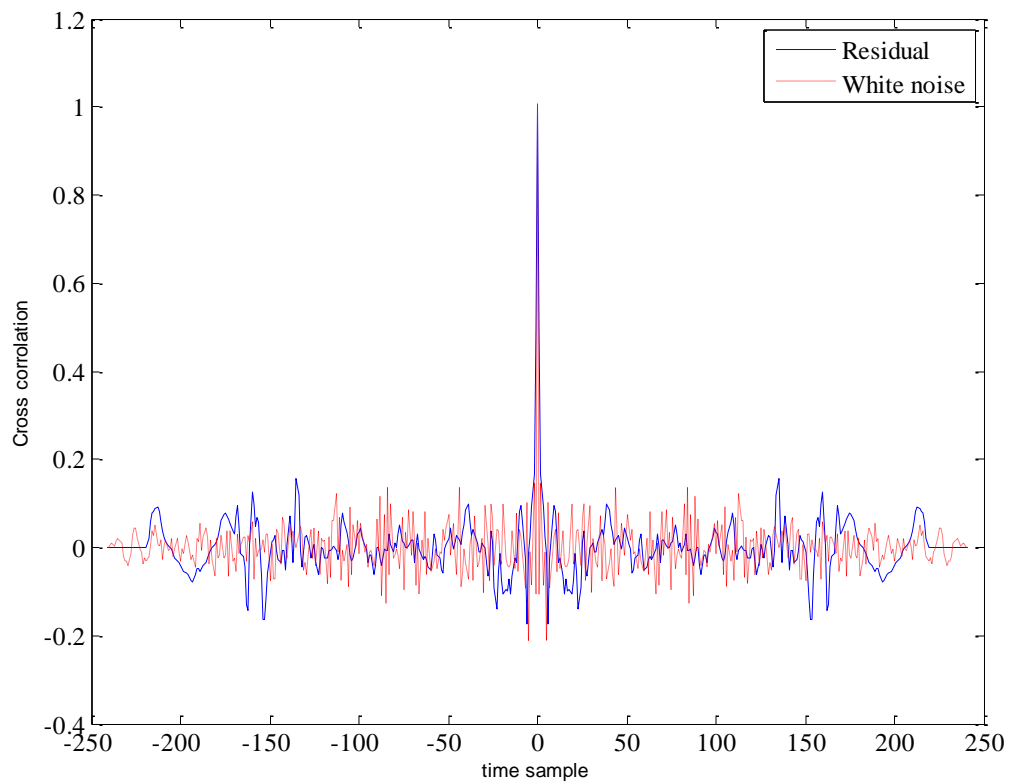


Figure 8-9: Comparison between cross-correlation of the residual and white Gaussian noise.

### 8.1.2 Ischemic ECG

Figure 8-11 shows the results of the inverse problem applied to the ischemic beat shown in Figure 8-10. These graphs show the cardiac region electrical activity at the SA and AV nodes, the bundle branches, the Purkinje fibers, and left and right ventricle. These results are used by the ECM to solve the forward problem and generate an ischemic beat, as seen in Figure 8-12. The upper six graphs represent the cardiac region electrical activity arriving at the positive and negative electrodes. The bottom graph shows the ECM-generated ECG. Figure 8-13 shows a comparison between the actual and the ECM-generated ECG. The error between the two signals is shown in Figure 8-14. It can be seen that the error between the actual and the ECM-generated ECGs is due to additional external noise. Moreover, this error is negligible compared to the signal since it is less than 5% [46].

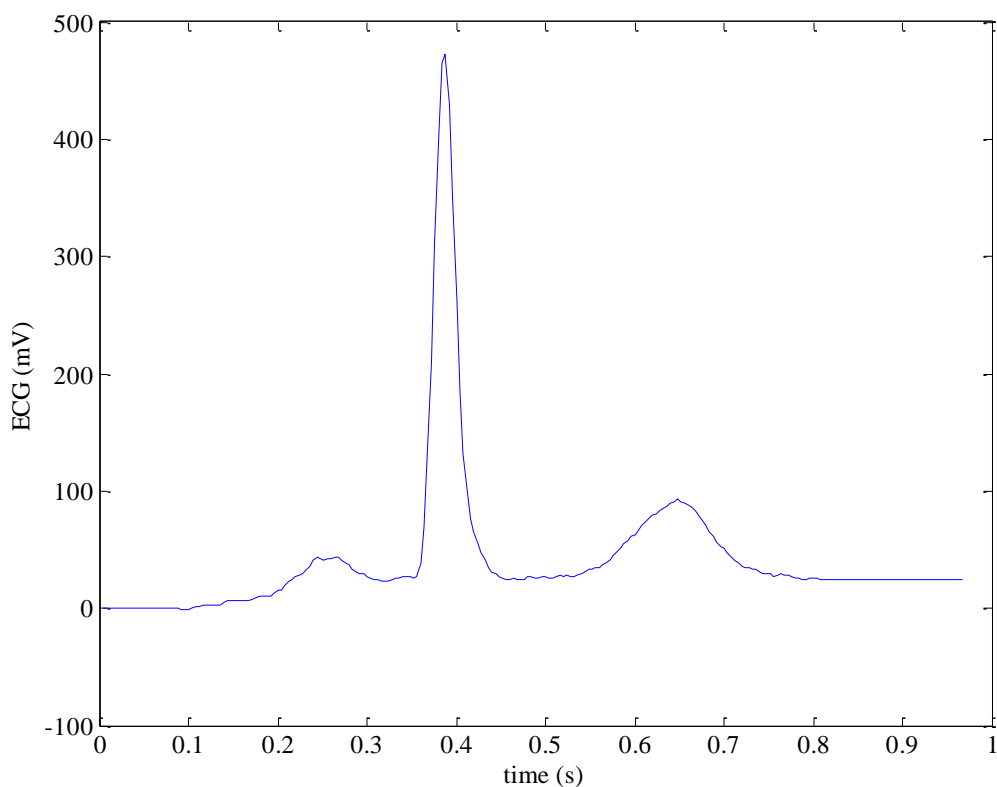


Figure 8-10: Actual ischemic ECG.

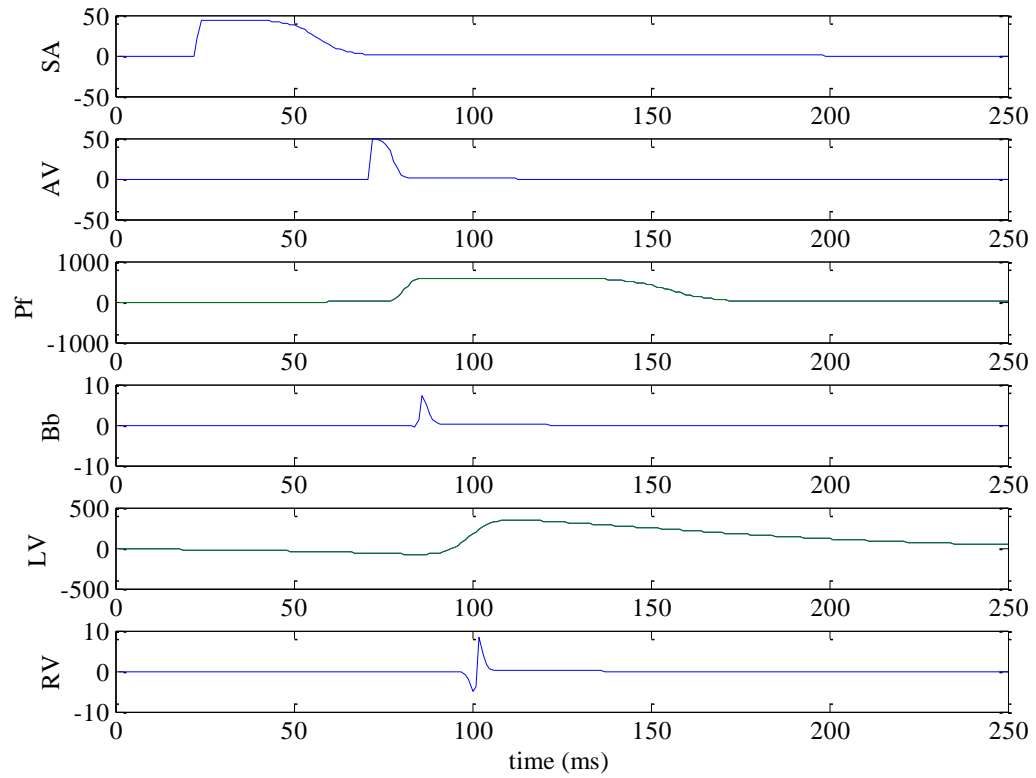


Figure 8-11: Inverse problem solution for an ischemic ECG.

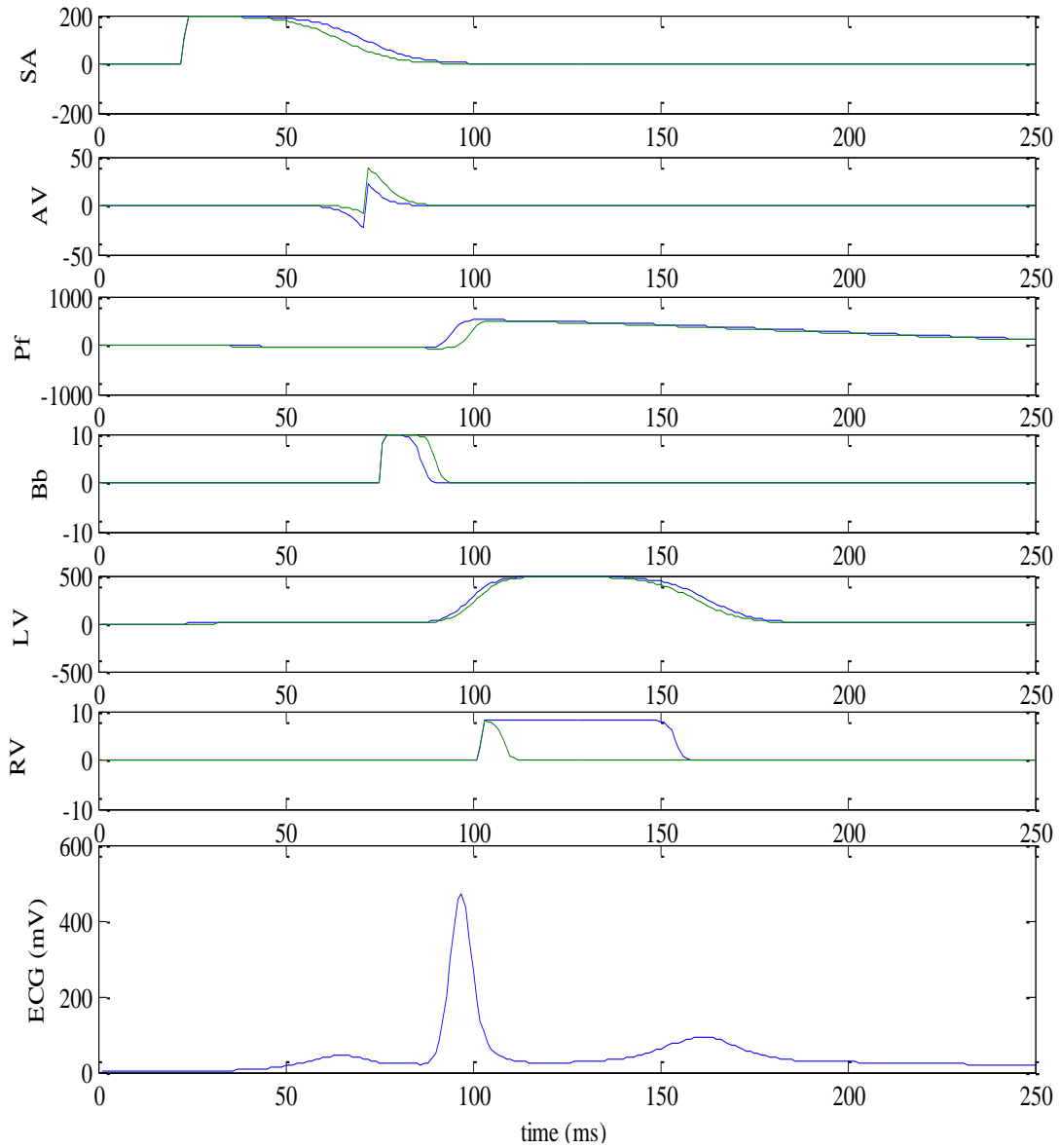


Figure 8-12: ECM-generated ischemic beat, forward problem solution.

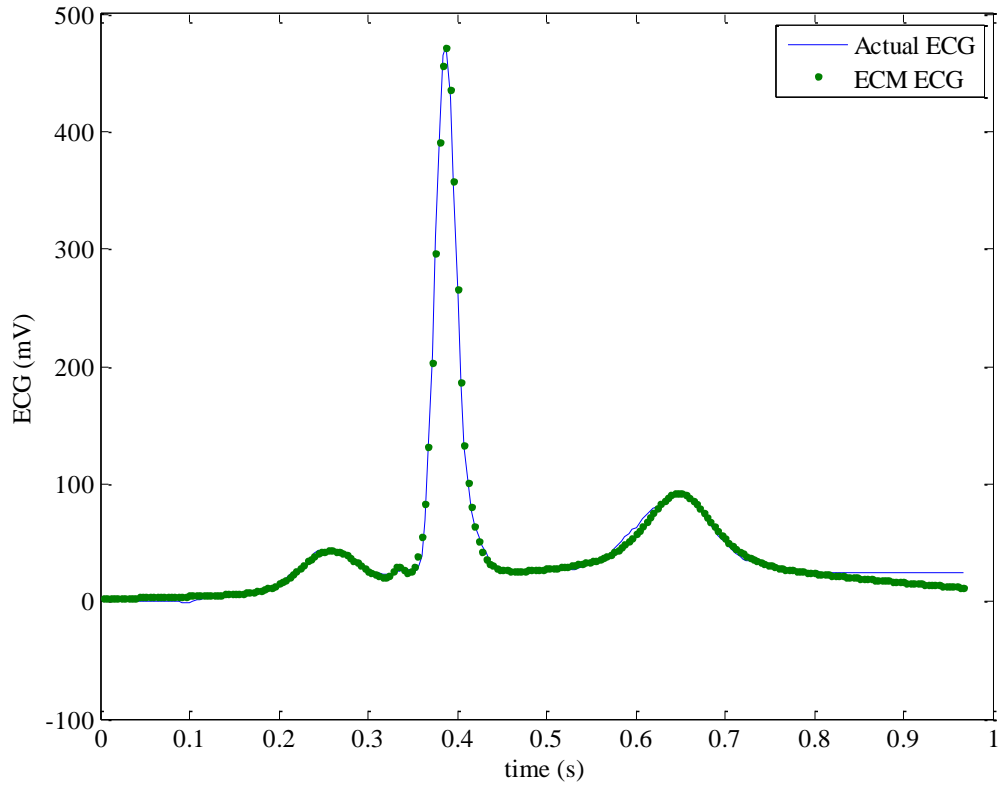


Figure 8-13: Comparison between ECM-generated and actual ECG.

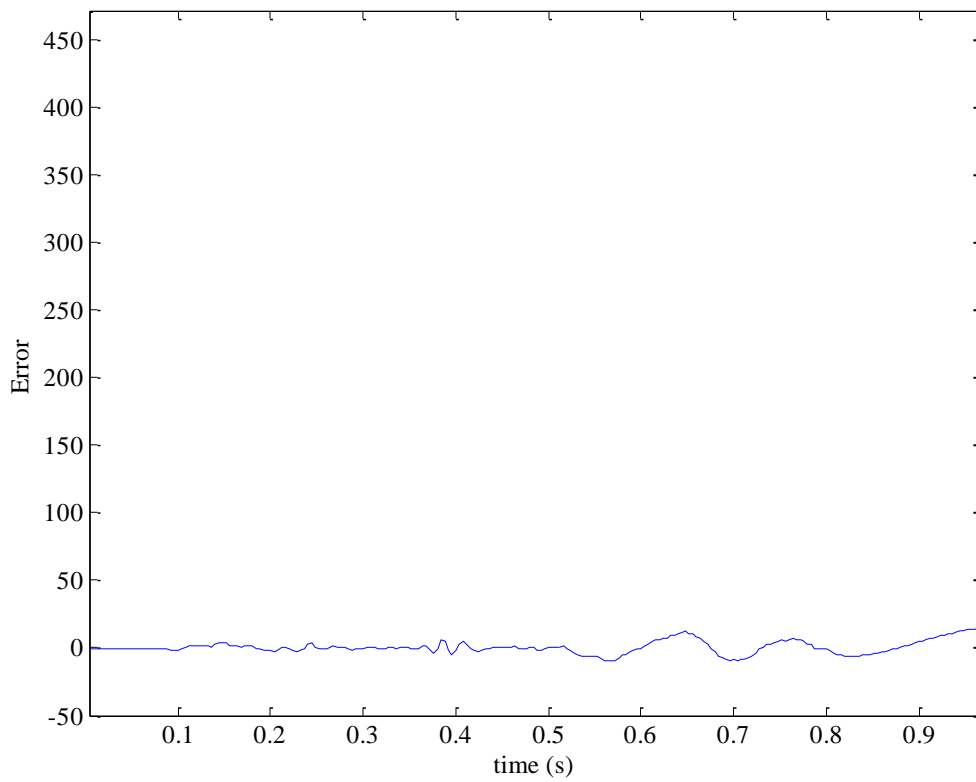


Figure 8-14: Actual error between ECM-generated and actual ECG.

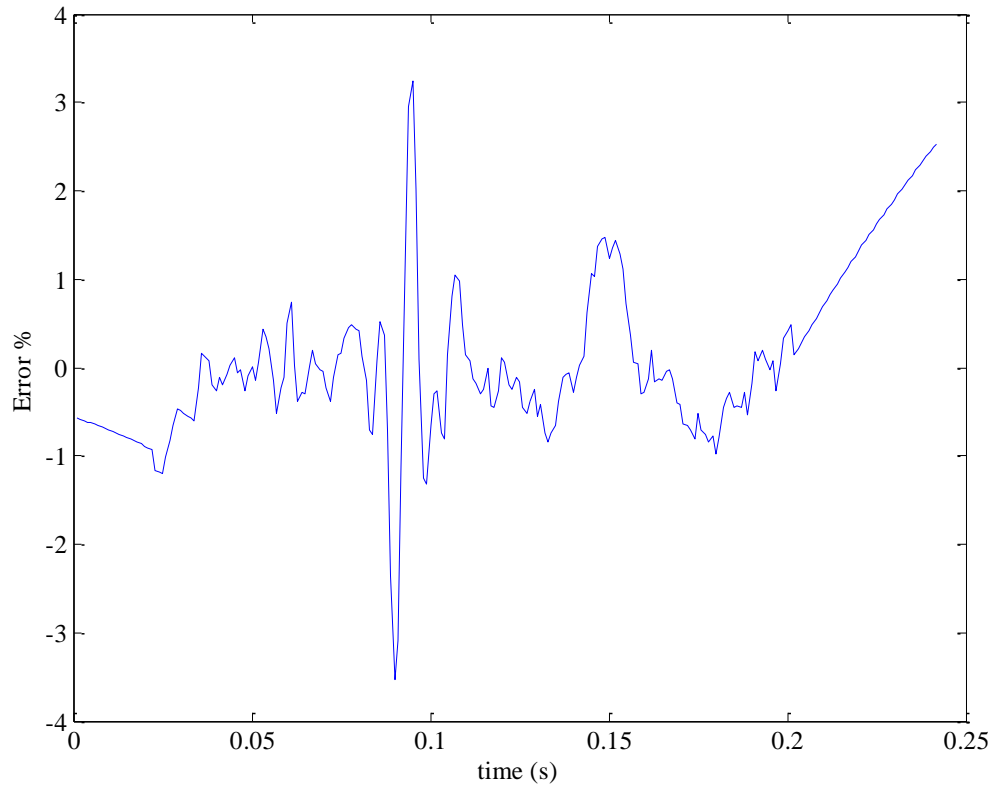


Figure 8-15: Percentage error between the ECM-generated and actual ECG

Similar to the healthy case, Figure 8-16 shows Gaussian function fit to the distribution of the error shown in Figure 8-14. It can be seen that the resulting error between the original signal and ECM-generated ECG is close to a normal distribution. Although the Kolmogorov-Smirnov goodness of fit test resulted in rejecting the null hypothesis, the normal fit had the lowest root mean squared error and highest  $p$  value compared to uniform, Laplace, and Rayleigh distributions. The rejection of the null hypothesis can be attributed to the high frequency noise affecting ECGs at 50Hz-60Hz. Additionally, the cross-correlation of the residual error is calculated and compared to that of a white Gaussian noise signal, shown in Figure 8-17 and Figure 8-18, respectively.

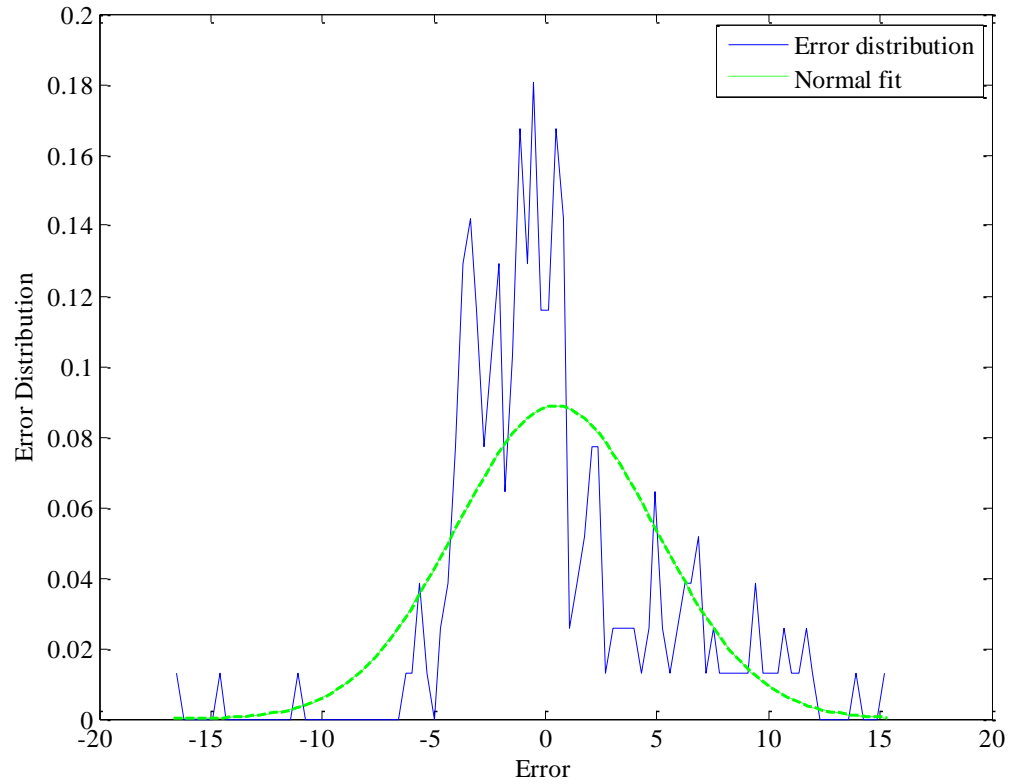


Figure 8-16: Gaussian fit between error distribution and normal distribution

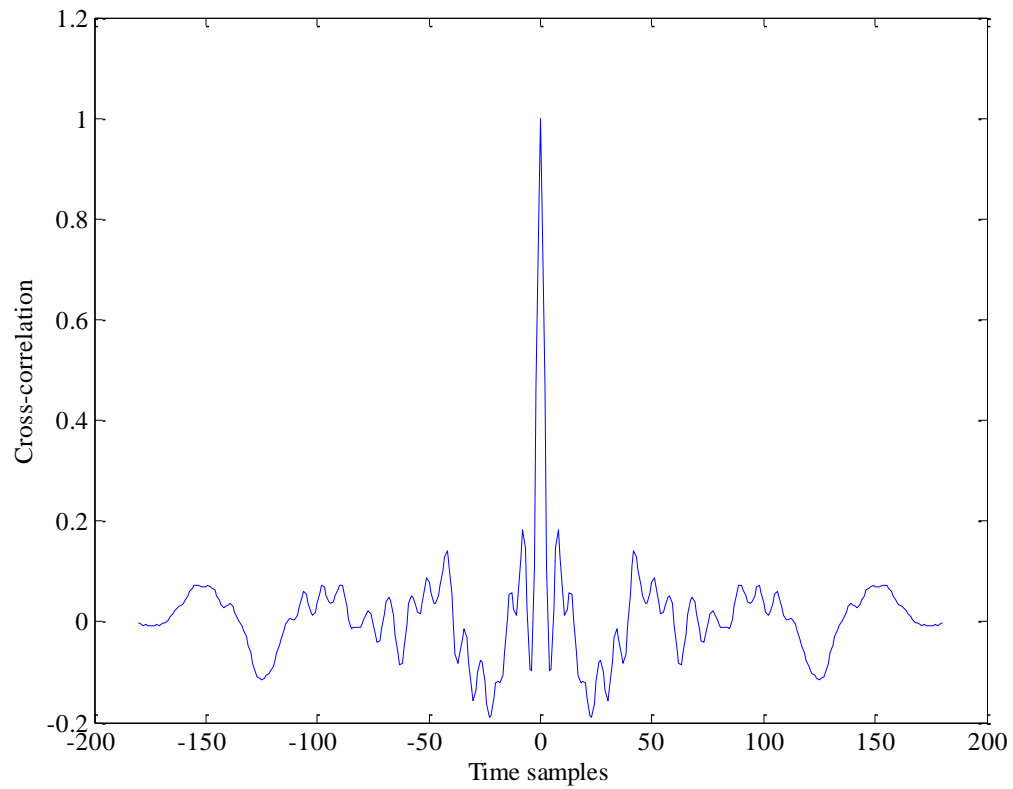


Figure 8-17: Cross-correlation of the residual error.

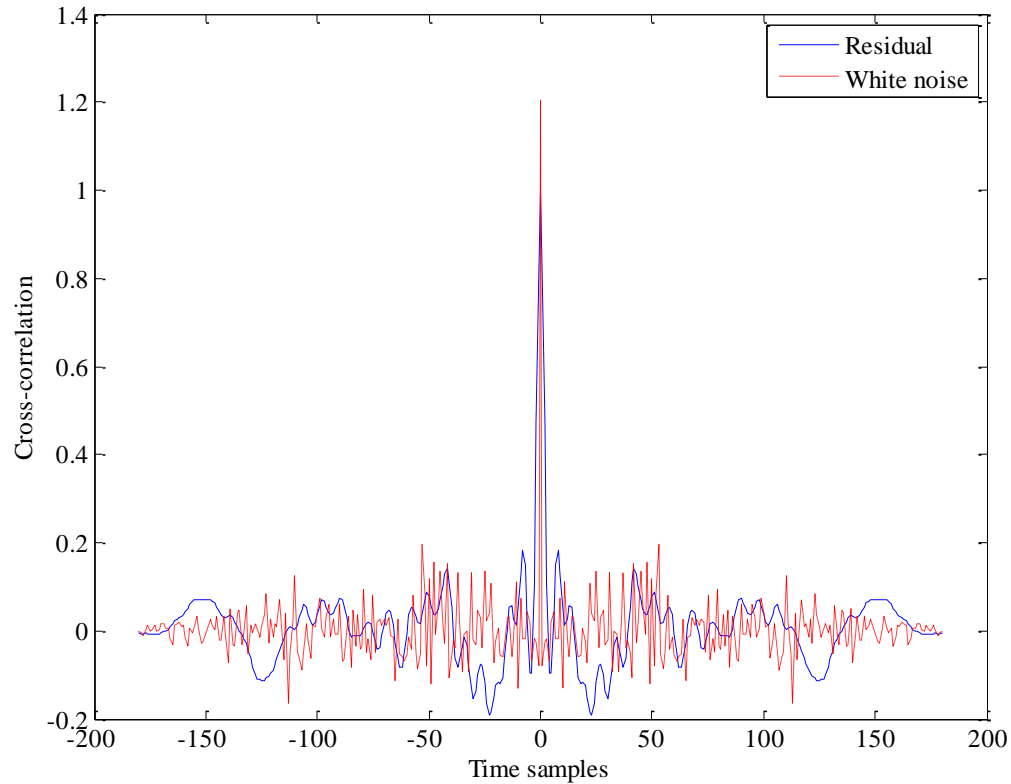


Figure 8-18: Comparison between cross-correlation of the residual and white noise.

### 8.1.3 Infarcted ECG

Figure 8-20 shows the results of the inverse problem solution described in chapter 6 applied to the infarcted ECG shown in Figure 8-19. These graphs show the cardiac region electrical activity at the SA and AV nodes, the bundle branches, the Purkinje fibers, and left and right ventricle. These results are used by the ECM to generate an estimate of an actual infarcted ECG signal. Figure 8-21 shows the forward problem solution. The upper six graphs represent the cardiac region electrical activity arriving at the positive and negative electrodes. The bottom graph shows the ECM-generated ECG. Figure 8-22 shows a comparison between the actual and the ECM-generated ECG. The error between the two signals is shown in Figure 8-23.

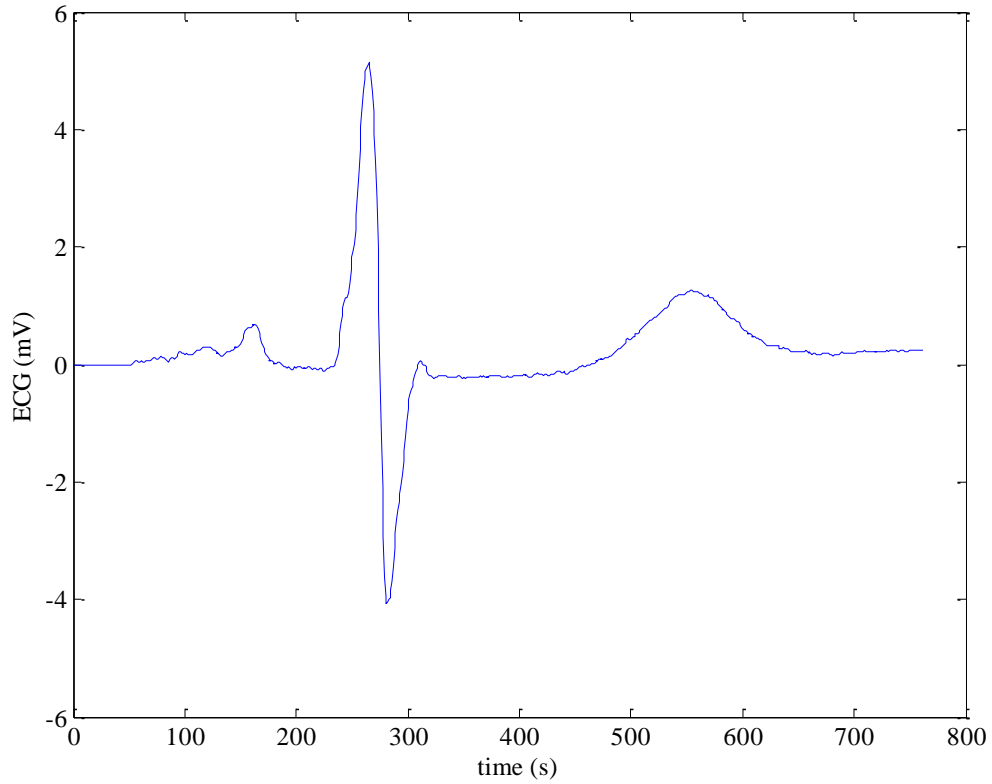


Figure 8-19: Actual infarcted ECG.

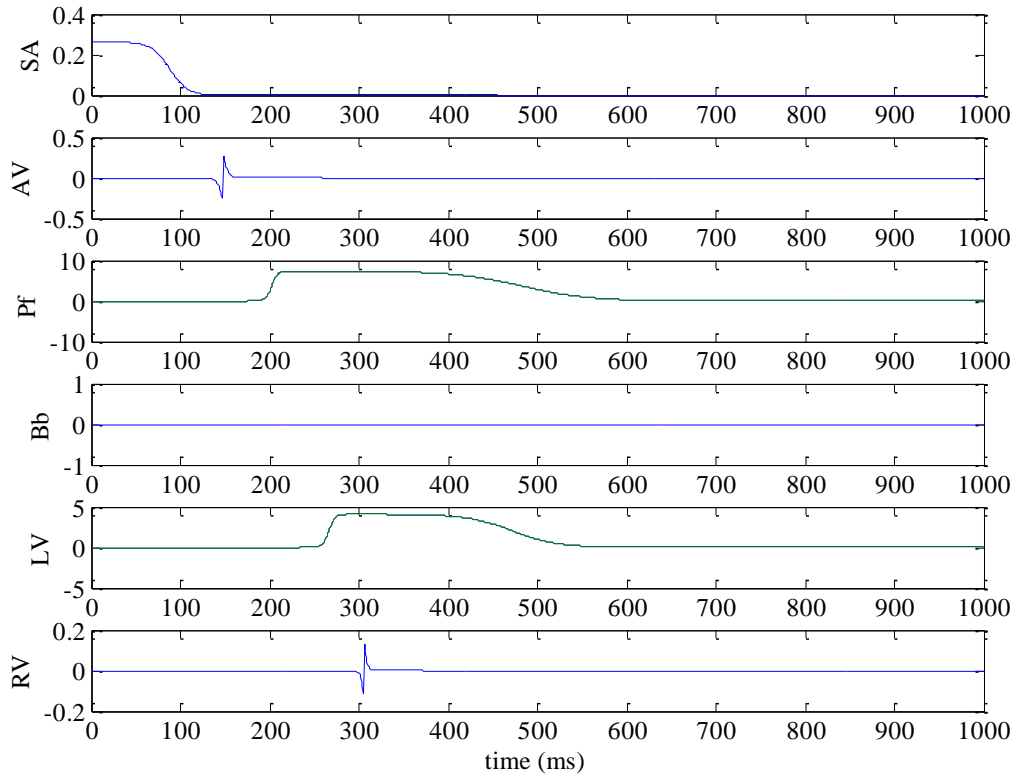


Figure 8-20: Inverse problem solution for an infarcted ECG.

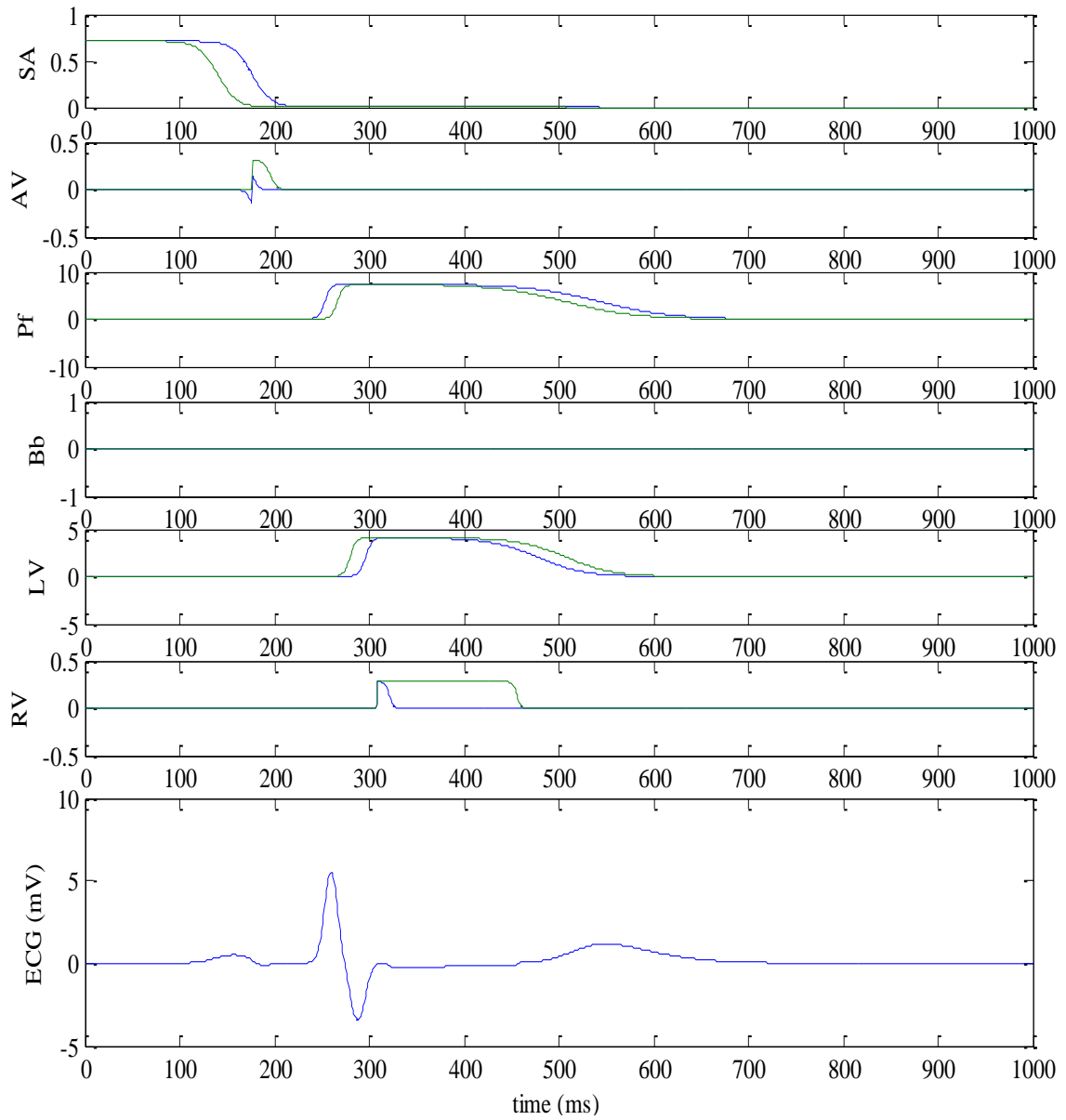


Figure 8-21: ECM-generated infarcted beat, forward problem solution.

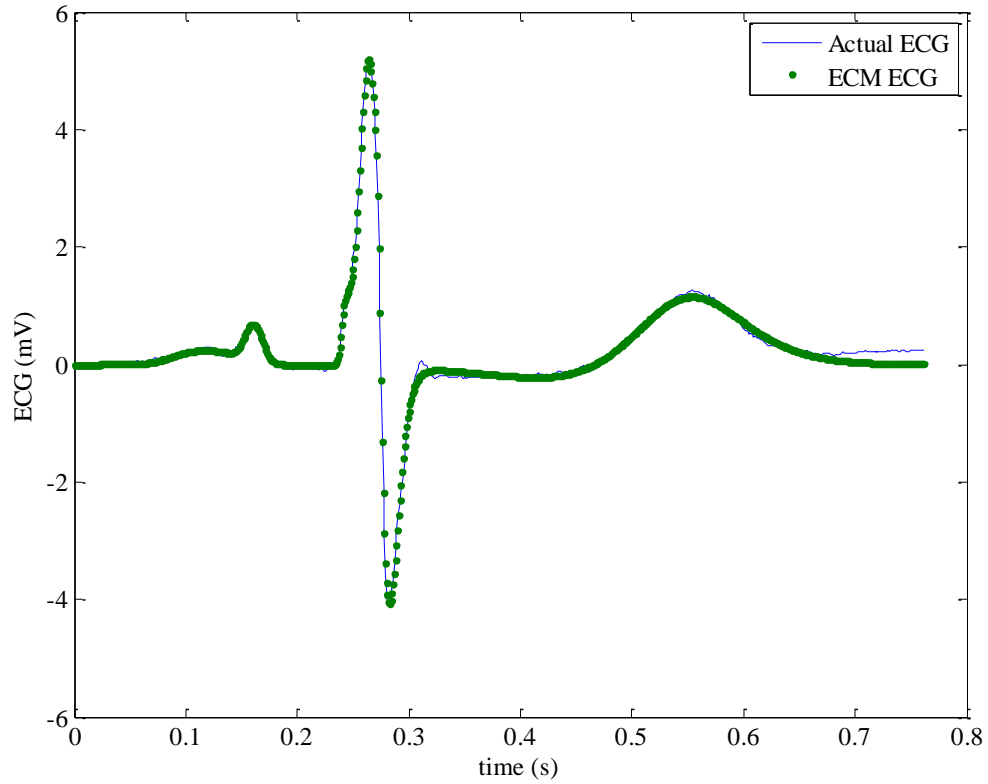


Figure 8-22: Comparison between ECM-generated and actual ECG.

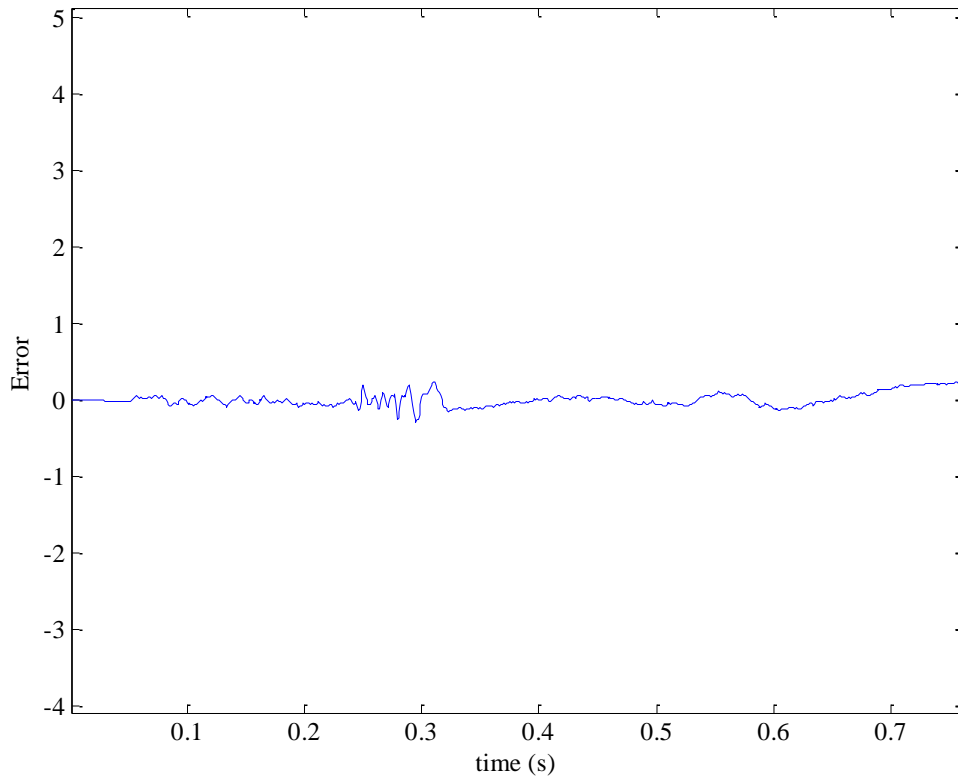


Figure 8-23: Actual error between ECM-generated and actual ECG.

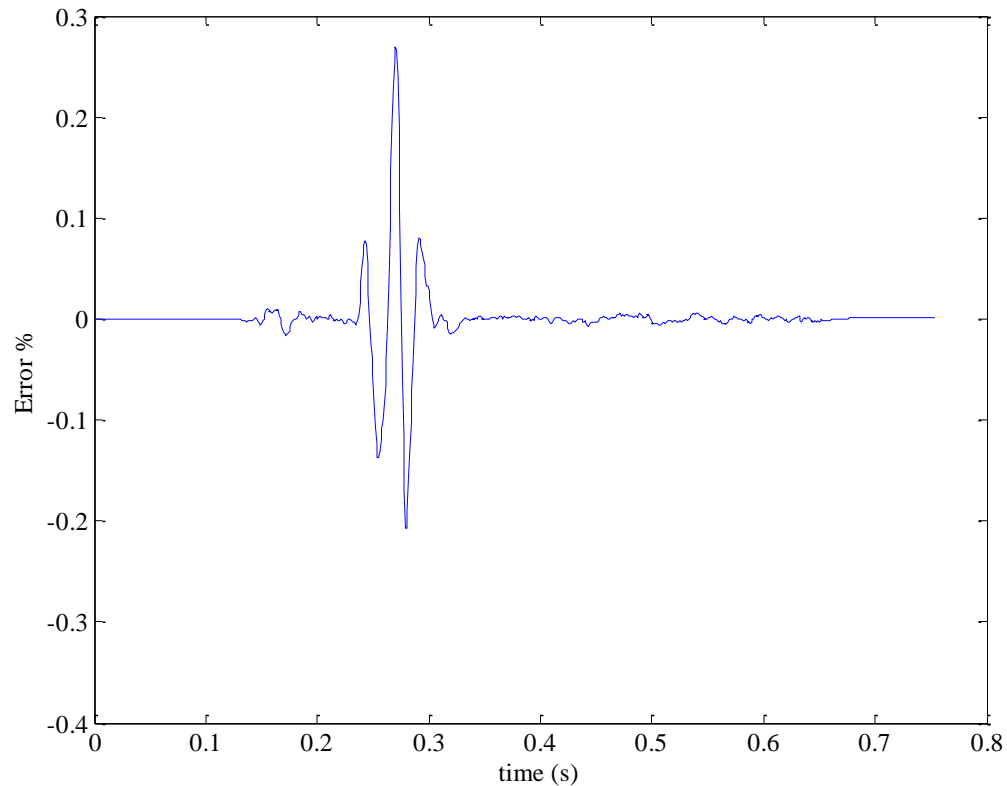


Figure 8-24: Percentage error between ECM-generated and actual ECG.

The distribution of the error fitted with a normal density function is shown in Figure 8-25. It can be seen that the resulting error between the original signal and ECM-generated ECG is close to a normal distribution. Although, the Kolmogorov-Smirnov goodness of fit test resulted in rejecting the null hypothesis, the normal fit had the lowest root mean squared error and highest  $p$  value compared to uniform, Laplace, and Rayleigh distributions. Figure 8-26 shows the cross-correlation of the residual shown in Figure 8-23. The resulting cross-correlation shows that there is a correlation in the residual, which can be attributed to the high frequency noise caused by electric interference during the ECG measurement. Figure 8-27 shows a comparison between the cross-correlation of the residual signal and the cross-correlation of a white noise signal.

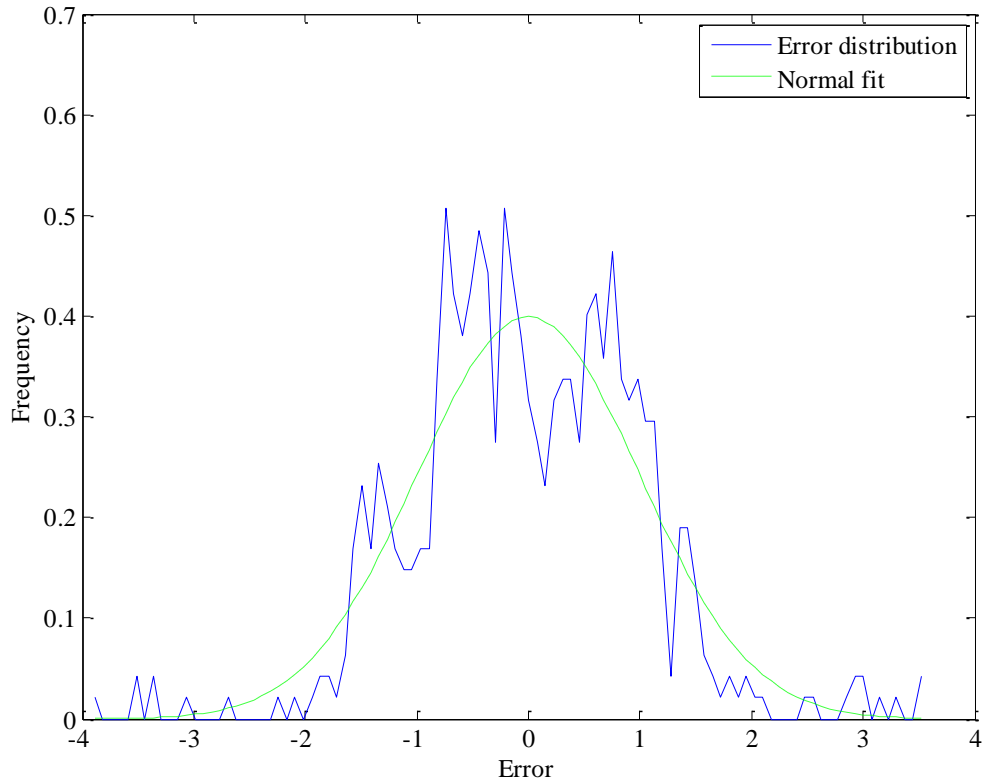


Figure 8-25: Gaussian fit between error distribution and normal distribution.

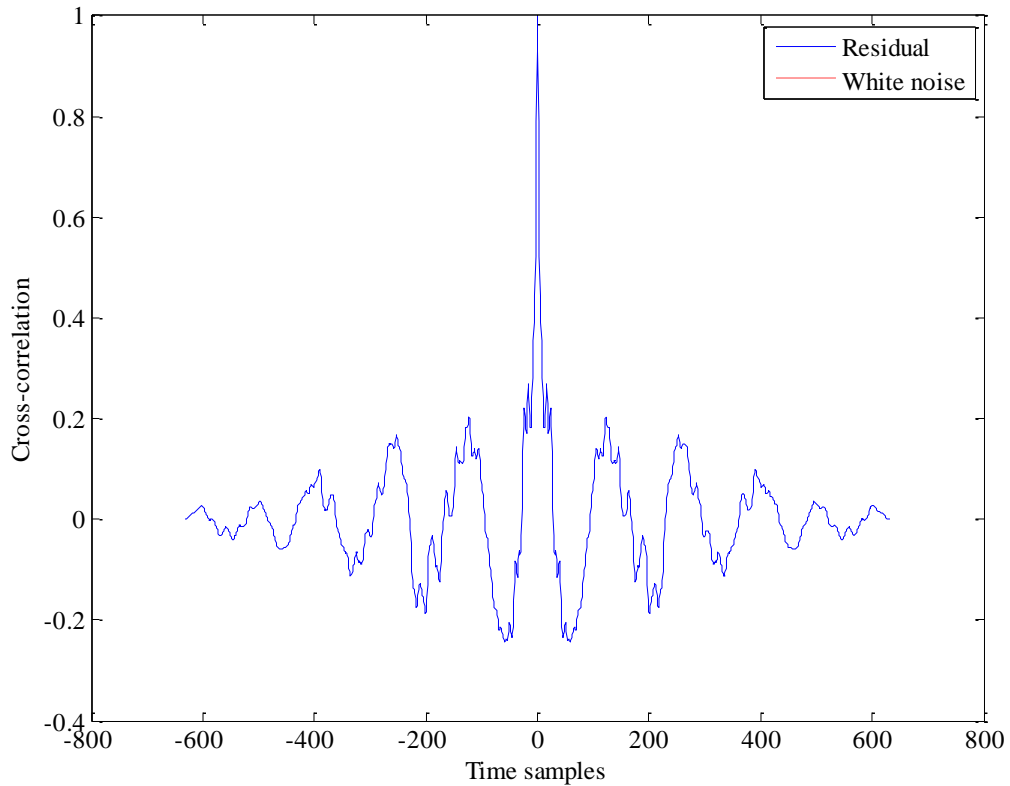


Figure 8-26: Cross-correlation of the residual error.

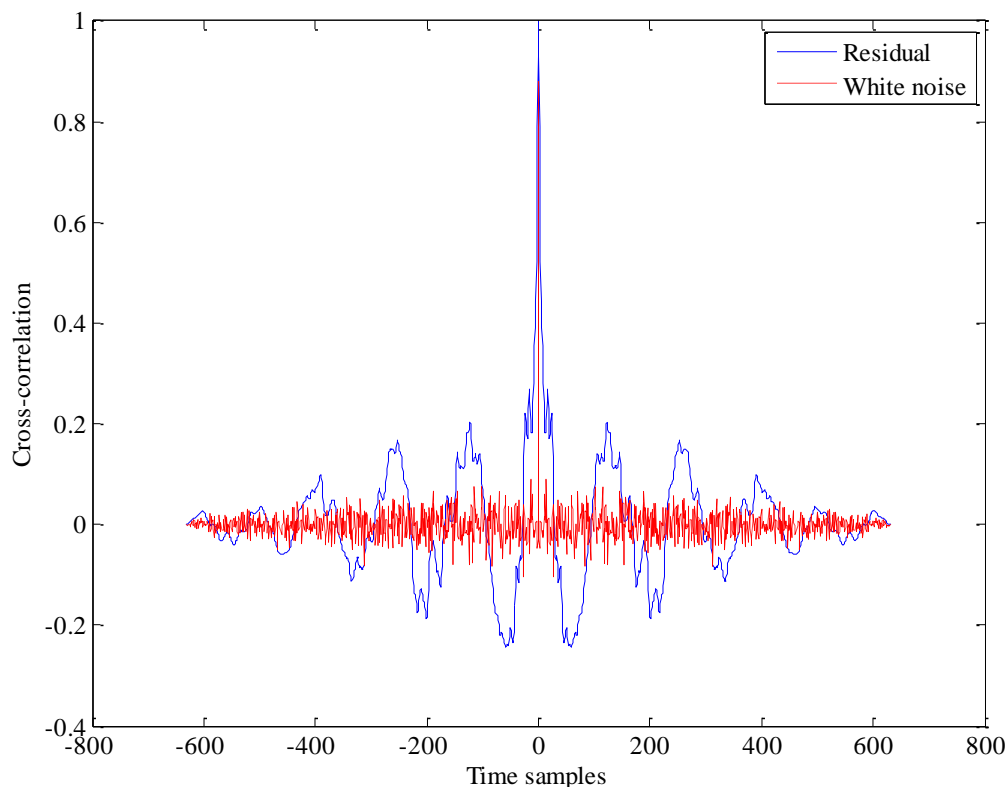


Figure 8-27: Comparison between cross-correlation of the residual and white noise.

## 8.2 Results Analysis

The model has been applied to over 100,000 beats with a misfit percentage of 2-3%. The reasons for this misfit are caused by the automatic beat detector results and the baseline wandering at the beginning of the beat. When a beat has a perturbed sequence of ECG features is passed to the model from the automatic beat detector, the beat would require preprocessing prior to solving the inverse problem. Figure 8-28 shows an ECG with a T wave, P wave, QRS complex, T wave and P wave. This type of beat contradicts the model setup, where the ECG beat contains a P wave followed by a QRS complex and a T wave. If the extra P wave and T wave are zero padded, shown in Figure 8-29. The model fits the resulting ECG as shown in Figure 8-30. The resulting error between the actual and the ECM-generated signal is shown in Figure 8-31. The error still exists at the

QRS complex, and this can be attributed to noise or to the spike in the cellular activity, which was not accounted for by the difference of two sigmoid.

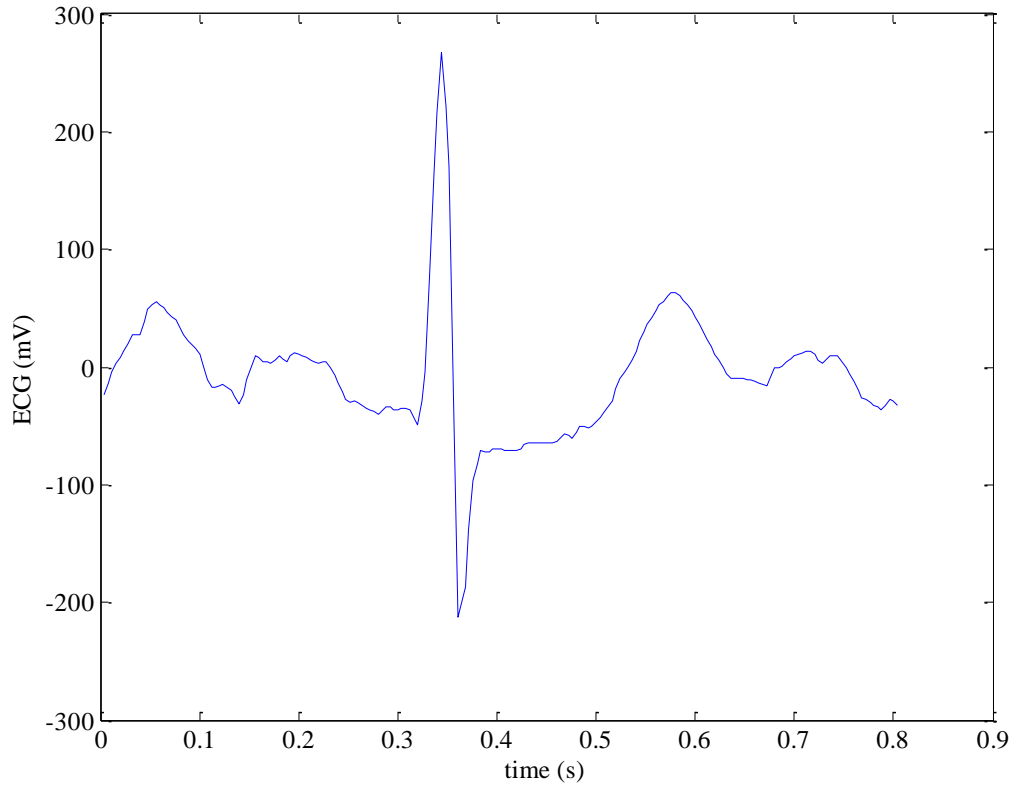


Figure 8-28: Perturbed sequence of ECG features signal measured at lead II.

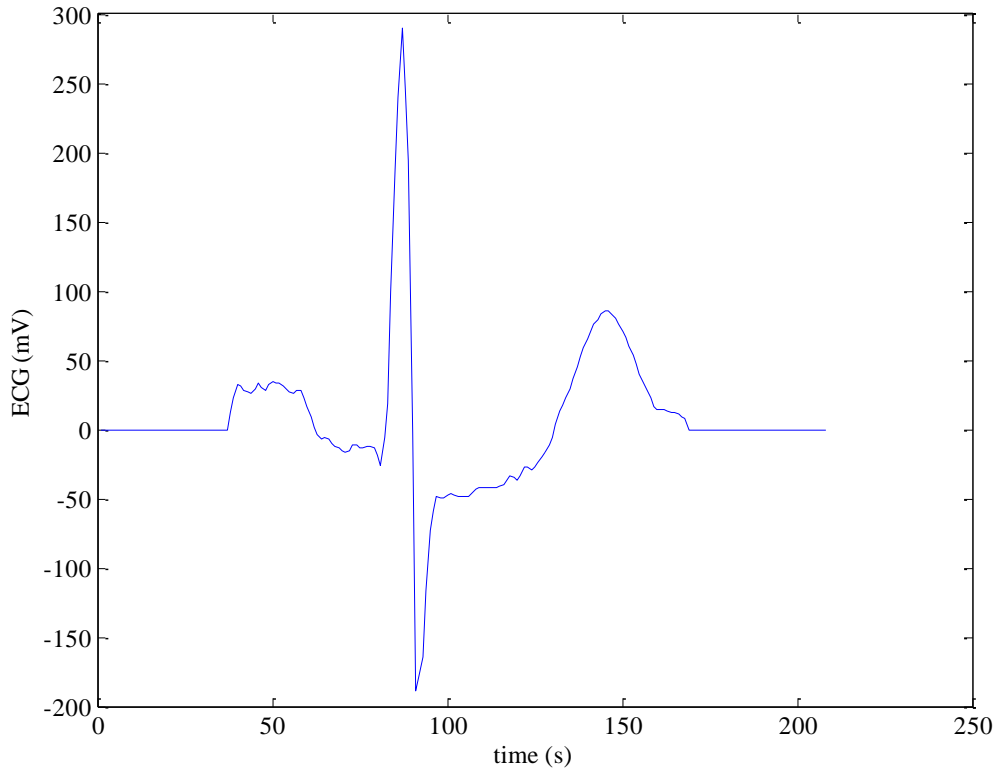


Figure 8-29: Zero patted ECG signal measured at lead II.

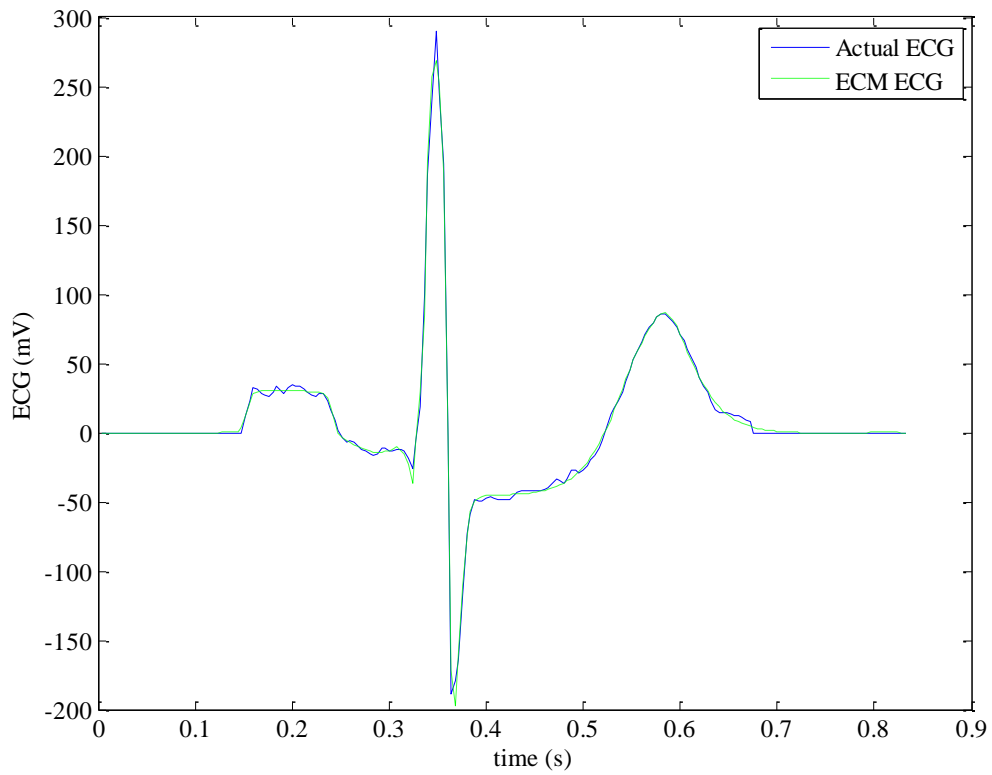


Figure 8-30: Comparison between ECG-generated and actual ECG.

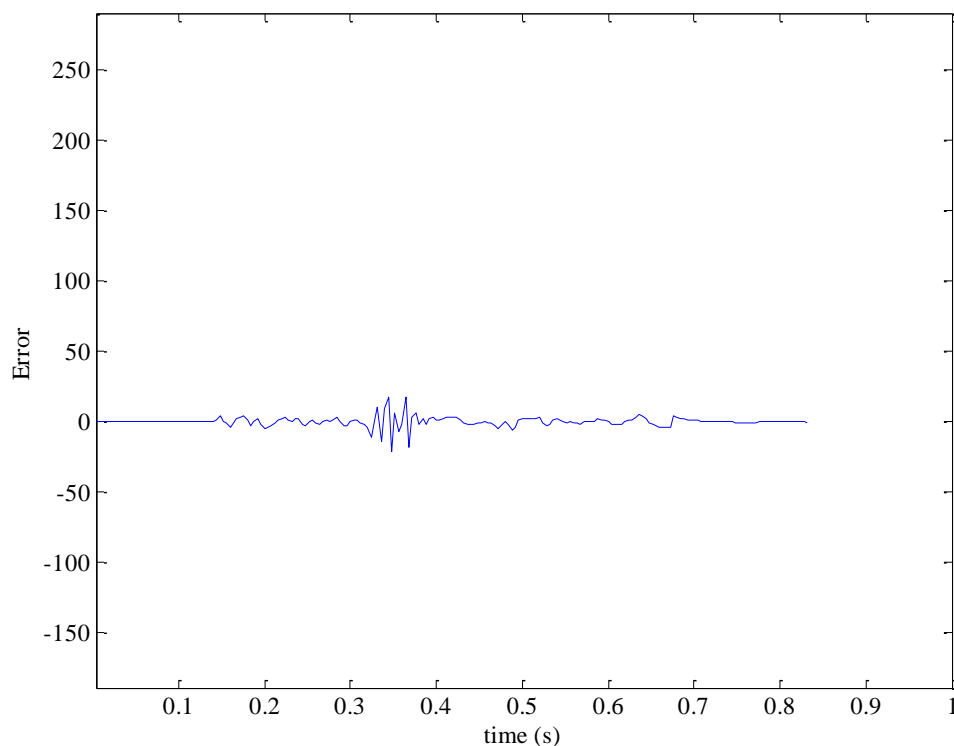


Figure 8-31: Error between ECG-generated and actual ECG

In addition to the perturbation in the ECG features, the location of the zero padding affects the model fit. For example, the model fit in Figure 8-12 and Figure 8-14 can be improved by selecting the beginning of the P wave as the end of the zero padded segment. The results shown in Figure 8-12 and Figure 8-14 are based on using the same time sample for the beginning and end of the zero padding. Figure 8-32 and Figure 8-33 show a comparison between the actual ECG shown in Figure 8-12 and the resulting error. The error in Figure 8-33 is lower than that of Figure 8-14. This is due to the baseline wandering in the segment prior to the P wave, which was accounted for in the record and not on a beat to beat basis.

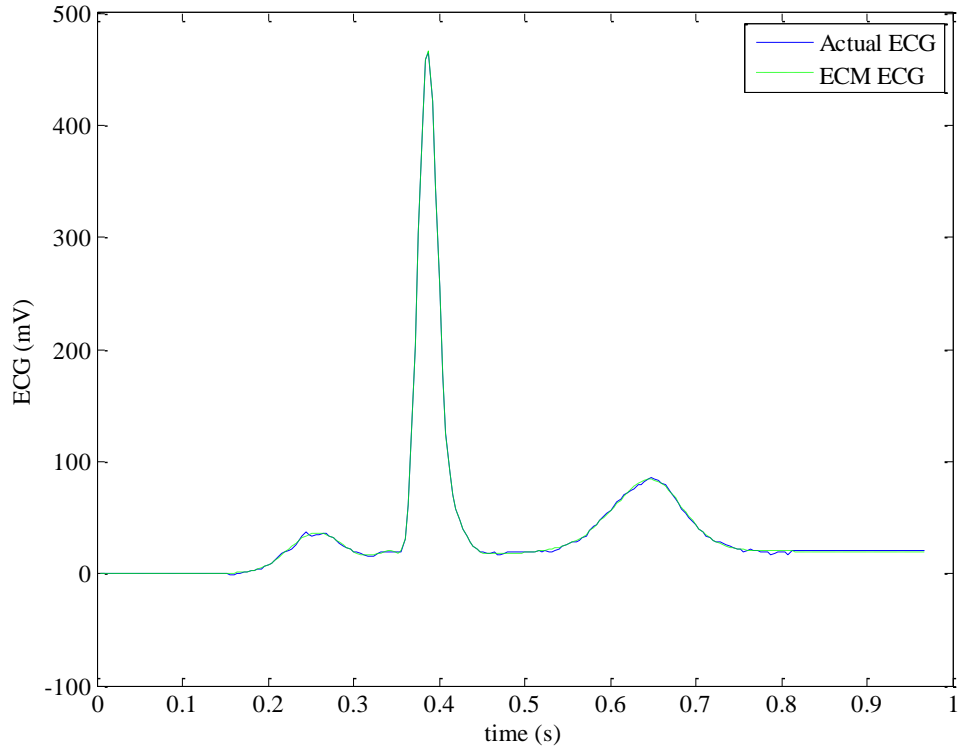


Figure 8-32: Comparison between ECM-generated and actual ECG.

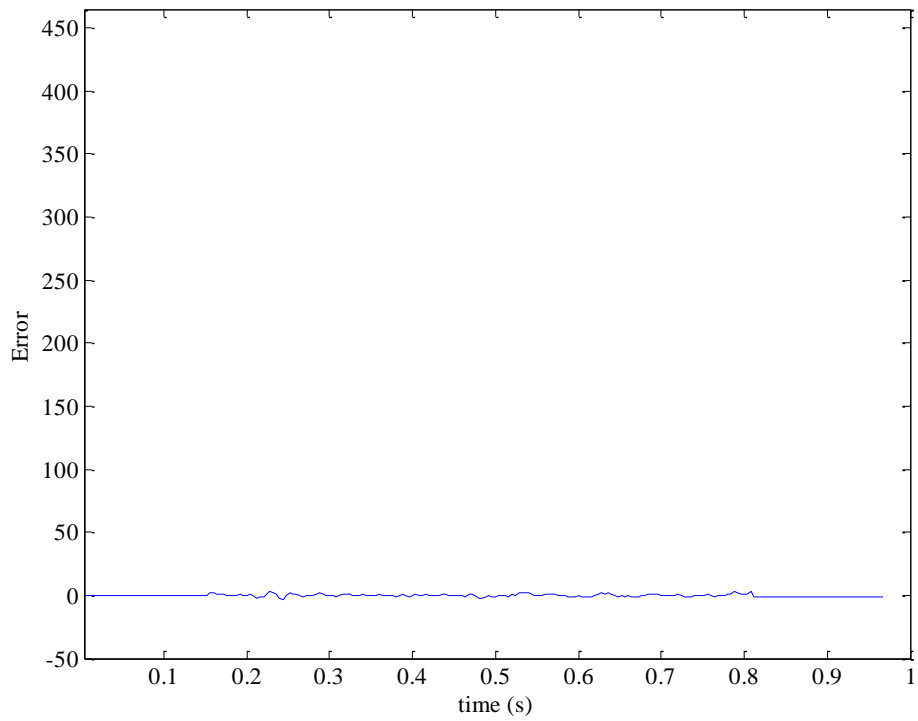


Figure 8-33: Error between Actual and ECM-generated ECG.

### ***8.3 Simulated Electrocardiogram Experiment***

Now that the ECM forward and inverse problems solutions have been applied to actual electrocardiograms, this section presents an analysis of the stability of the forward and inverse problem solutions under different noise conditions. This analysis is used to verify the stability of the inverse and forward problem solutions. The stability of the inverse and forward problems solution is defined as the variation of the solution as the ECG is affected by noise. The stability study is performed by solving the forward and inverse problem for a simulated signal with additional white, pink, and brown noise under different levels. The stability analysis is based on the variation of the T wave end measurement. T wave measurement is important in clinical studies especially in the study of certain cardiac disease [47].

The simulated signals are generated from the model developed in [37]. Figure 8-34 shows a sample simulated signal. Additionally, white, brown, and pink noise are added to the signal at an SNR level ranging from -25 to 5 dB measured at the ST segment [48]. The process is repeated for 40 trials, and the T wave end is measured.

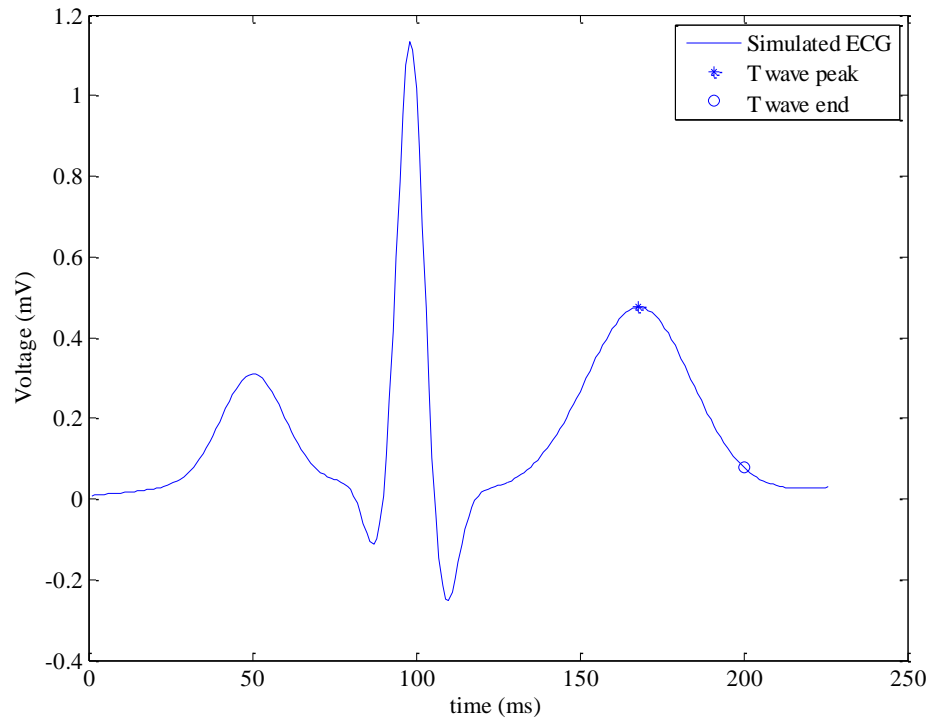


Figure 8-34: The simulated signal used in this experiment.

The variation in the T wave end is used in this work as a quantitative measure of the variation of the forward and inverse solutions because of its clinical importance [47]. The T wave end is obtained using the method that won the Physionet/Computers in Cardiology challenge 2006. The T wave end is located at  $1.85\sigma_T$  from the T peak, where  $\sigma_T$  is the variance of the Gaussian function that fits the T wave. The T wave end is noted at 200 ms as indicated on the graph in Figure 8-34.

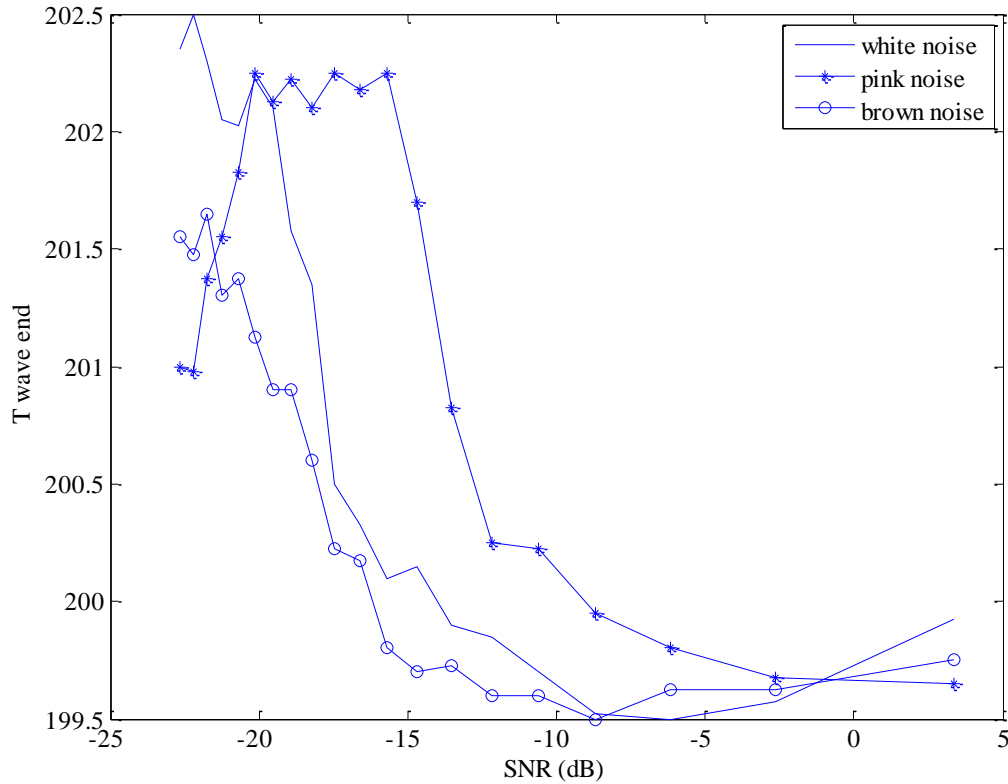


Figure 8-35: T wave end variation.

Figure 8-35 shows the averaged T wave end obtained using the ECM inverse problem solution for 40 runs. Figure 8-35 indicates that the T wave end variation is between 199.5 ms and 202.5 ms for each of the white, brown, and pink noise experiment. Additionally, Table 8.1 shows the mean and standard deviation of the error between the actual and the ECM T wave end. The first column shows the actual error mean and standard deviation between the T wave end determined using the ECM inverse problem solution and the actual T wave end. The second column shows the percentage of the error between the actual T wave end and the ECM T wave end. The mean and standard deviation of the T wave variation is less than 1%, which is negligible in clinical trials [46]. During the Physionet/ Computers in Cardiology 2006 challenge, the average difference between manual annotations of the T wave end variation is 6.67ms [47]

compared to the 2.5 ms of the ECM variation. This shows the stability of the estimated inverse problem solution under different noise conditions. The low error and variation in the T wave shows that the answer to the inverse problem varies with less than 1% under white, pink, or brown noise with noise levels of -25-5 dB.

Table 8.1: Error comparison between original and obtained T wave end.

Noise Type	T wave error	T wave Var. %
White noise	0.87ms $\pm$ 1.14ms	0.44% $\pm$ 0.57%
Pink Noise	1.20ms $\pm$ 0.97ms	0.60% $\pm$ 0.49%
Brown Noise	0.41ms $\pm$ 0.79ms	0.20% $\pm$ 0.4%

Now that the analysis of the ECM for a single lead ECG has been performed, the next section presents the multilead ECG solution.

#### ***8.4 Multilead Electrocardiogram Generation***

This section presents the results of the multilead forward and inverse problem solutions. The ECM multilead solution is applied to an ECG selected at random from the PTB diagnostics database. The leads taken into consideration are the 3 Eindhoven leads I, II, III. Figure 8-36, Figure 8-38, and Figure 8-40 show a comparison between an actual ECG and ECM-generated ECG at leads I, II, and III, respectively. Figure 8-37, Figure 8-39, and Figure 8-41 show the respective errors between the actual and ECM-generated ECG at leads I, II, III. It can be seen that the ECM is able to generate multilead ECGs. Table 8.2 shows the percentage error between the actual ECGs and the ECM-generated ECGs at leads I, II, and III.

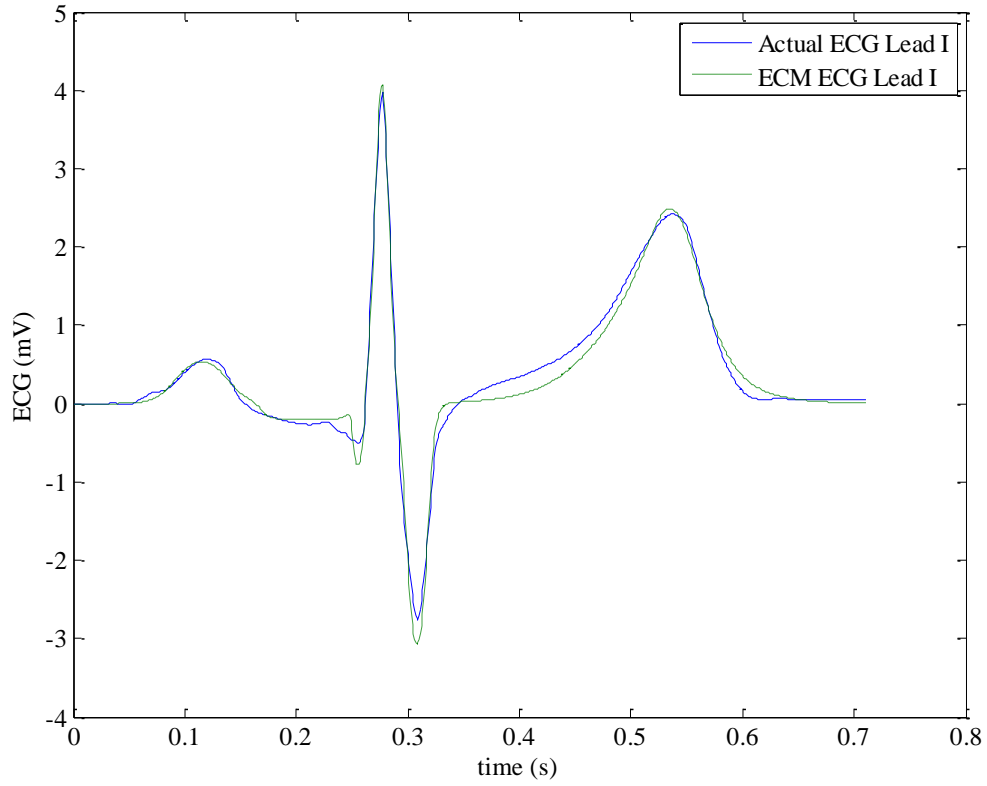


Figure 8-36: Comparison between actual ECG and ECM-ECG at lead I.

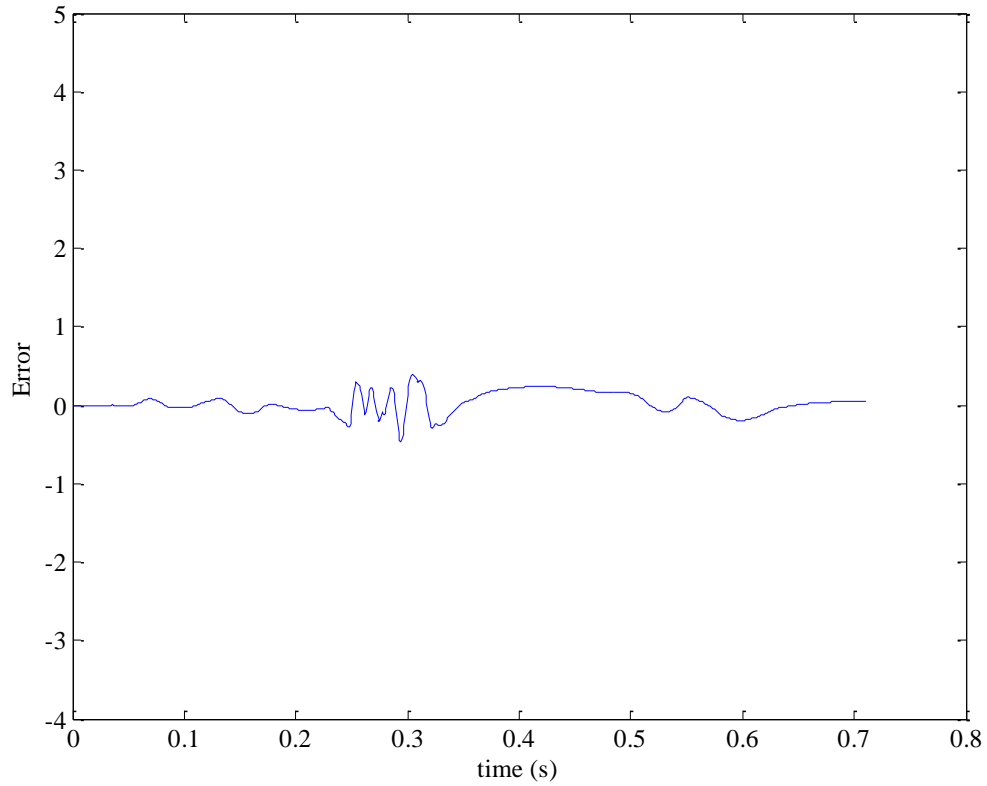


Figure 8-37: Error between actual and ECM-ECG at lead I.

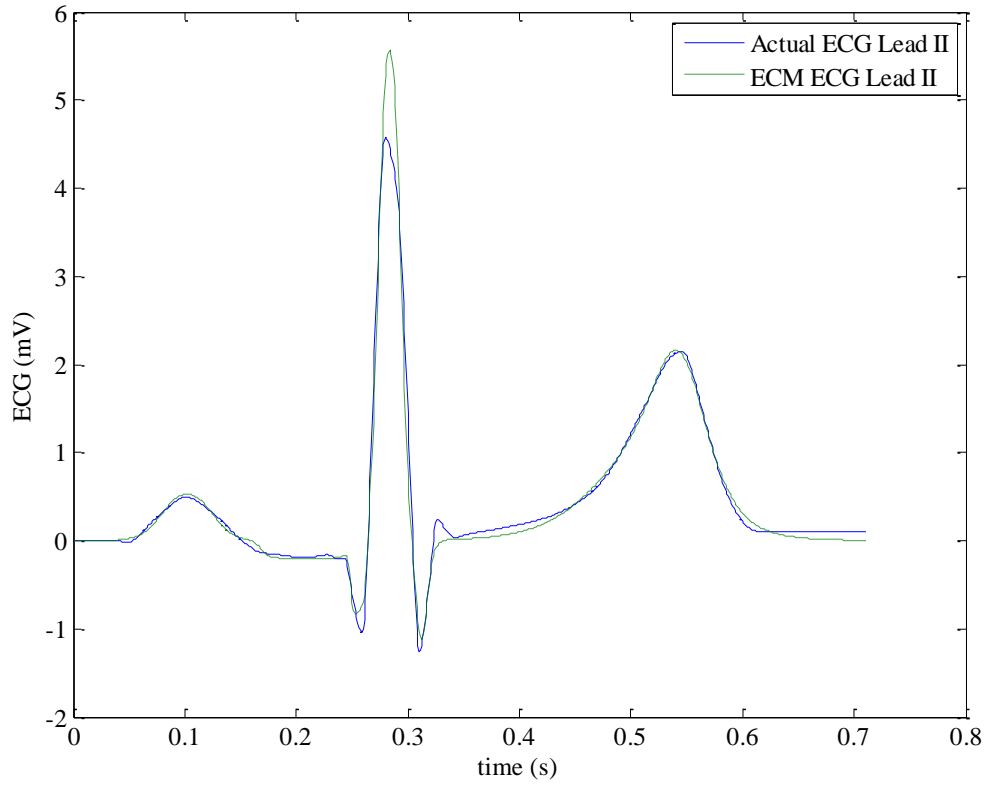


Figure 8-38: Comparison between actual ECG and ECM-ECG at lead II.

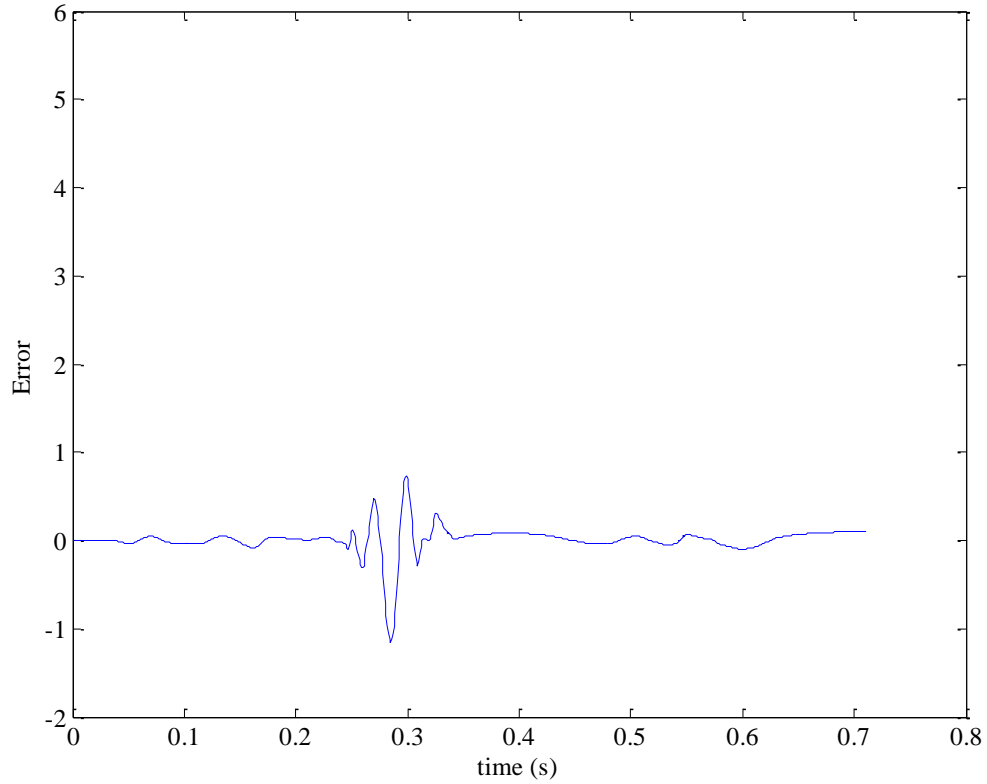


Figure 8-39: Error between actual and ECM-ECG at lead II.

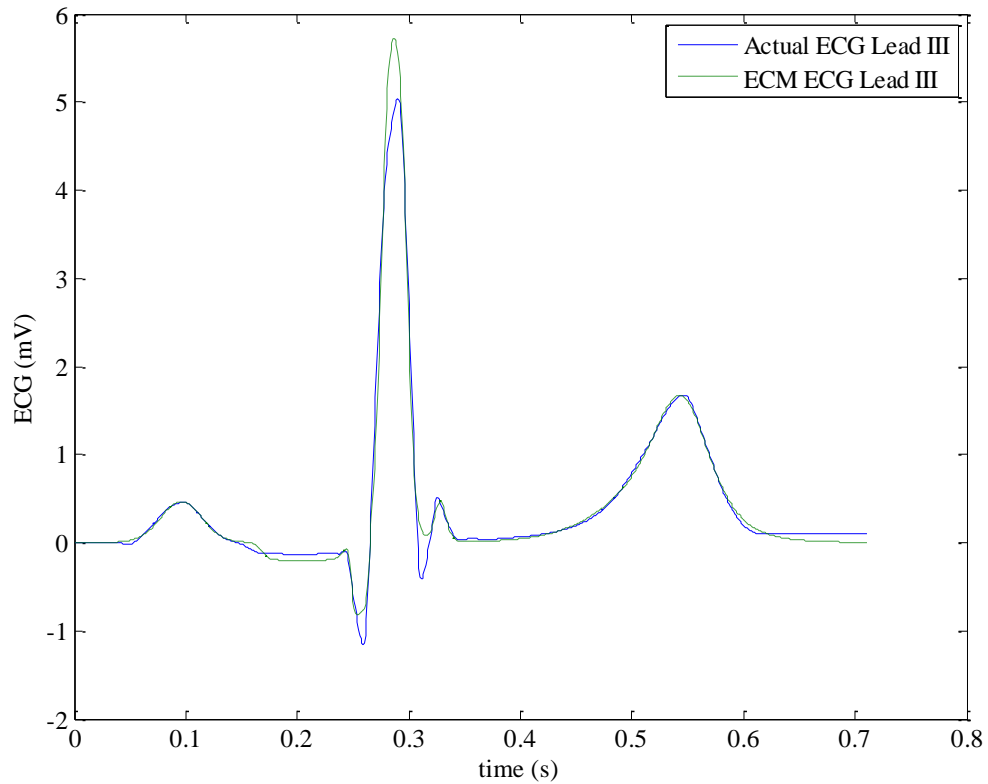


Figure 8-40: Comparison between actual ECG and ECM-ECG at lead III.

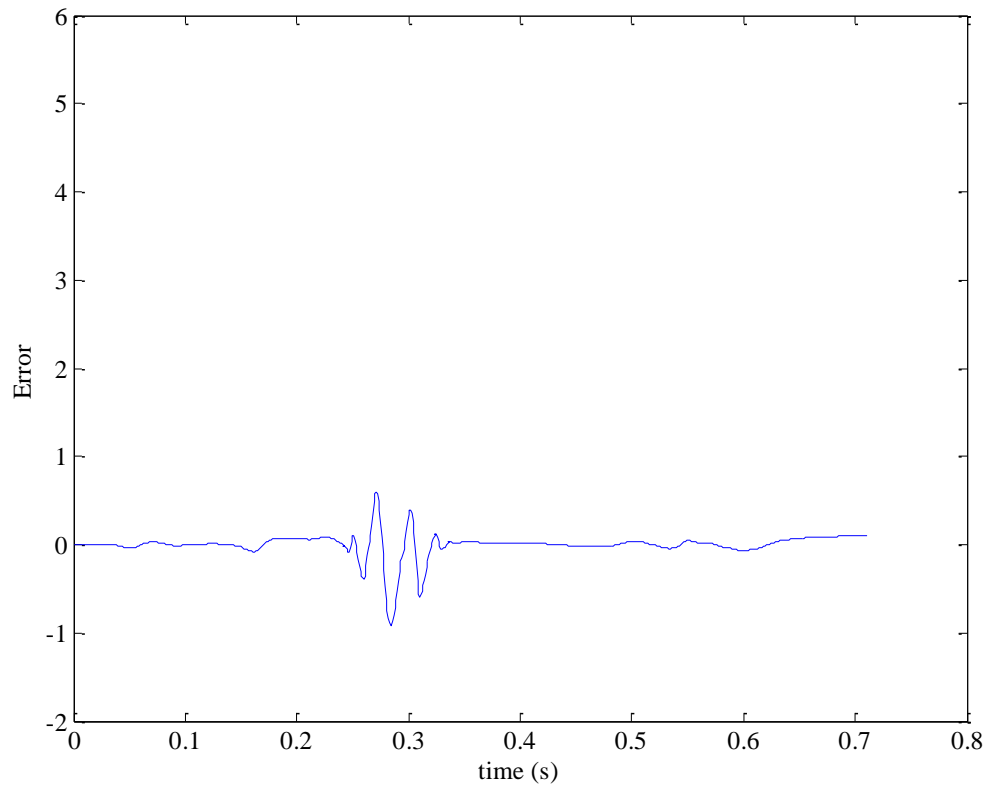


Figure 8-41: Error between actual and ECM-ECG at lead III.

Table 8.2: Percentage error of the comparison of the multilead ECM and actual ECGs

Lead	Lead I	Lead II	Lead III
Error	2.69% $\pm$ 14.27%	0.93% $\pm$ 17.52%	0.24% $\pm$ 15.37%

It can be seen that even with the assumption that the wave propagation of the cardiac region activity is the time delay in the arrival time at the leads, the error is less than 18%. The error is because of the magnitude variation between lead I and leads II and III, which is not accounted for in the presented propagation model. The propagation model is assumed to be a time delay in the arrival time of the electrical activity generated by the cardiac regions at the positive and negative electrodes of the leads. The error between the actual ECGs and the ECM-generated ECGs can be reduced by modifying the propagation model to account for the slopes and magnitude variations of the cardiac region activity arriving at the multiple leads. However, increasing the number of unknowns increases the computational time of the estimation process. The average computation time for a multilead ECG on an Intel Core 2 Duo machine is five minutes, compared to 10 seconds for the single lead case.

### **8.5 Summary and Discussion**

This chapter presents an analysis of the electrophysiological cardiac model. It shows that the model is able to generate accurate single and multi lead electrocardiograms and capture the electrophysiological effect caused by ischemic and infarcted disease. The model parameters are obtained using the solutions for the forward and inverse problems. Additionally, a study regarding the variation of the inverse and forward problem solution is presented. This study takes into consideration white and pink noise, which can occur in real electrocardiogram as electrical interference. Additionally,

the study takes into consideration brown noise, which act in actual ECGs as baseline wandering and electrical interference noise.

The next chapter presents the results of the two clinical diagnostic methods described in chapter 7. The first method is ischemia detection. The second method is infarction localization. These methods use the ECM and the inverse and forward solutions to provide sufficiently fast diagnostic applications.

## Chapter 9 Diagnostic Methods Results

The previous chapter presents the experimental results for the electrophysiological cardiac model (ECM). The analysis of the results shows that the ECM captures the cardiac electrophysiological activity for healthy, ischemic, and infarcted beats. This chapter presents the experimental results for the diagnostic methods presented in chapter 7. These diagnostic methods confirm the hypothesis that the ECM parameters can be used in sufficiently fast clinical diagnostics. The two clinical diagnostic experiments presented in this chapter are the detection of myocardial ischemia and localization of myocardial infarction.

The chapter is divided into four sections. The first section describes the technique used to validate the clinical diagnostic methods. The second section presents the experimental results for the ischemia detection method. The third section presents the results for the infarction localization method. Each experimental method contains an explanation of the experiment procedure, table of results, and discussion and comparison with the current state of the art techniques. The fourth section presents a summary and discussion of the presented results.

### ***9.1 Ten-Fold Cross Validation***

Ten fold cross validation is an accurate method for evaluating classification algorithms [49]. The diagnostic experiments are evaluated using the ten-fold cross validation method. This method is used to ensure the diagnostic experiments are data/patient independent. The ten fold cross validation is described as follows:

1. Divide data into 10 sets of size  $n/10$ , called folds.

2. Train on 9 sets and test on 1 set.
3. Repeat the process 10 times and store the diagnostic results.
4. Combine the results and calculate the overall accuracy.

The folds in this case are selected on a patient by patient basis, where the patients' beats used in the training set are not used in the testing set.

## ***9.2 Ischemic Diagnostic Experiment***

This section presents the results of applying the ischemic diagnostic method to the Long Term ST (LT-ST) database. The LT-ST database contains 20,528 beats, where the number of ischemic beats is 16,794, and the number of healthy beats is 3734. The ten fold cross validation method is used to validate the ischemia detection method.

The approach (ECM-PCA/C4.5) uses the ECM and principle component analysis (PCA) and a C4.5 decision tree classifier to diagnose ischemic beats. The approach is compared to the technique presented in Stamkopoulos et al. [1], described in chapter 3. The Stamkopoulos technique is replicated and applied to the LT-ST database. As mentioned in chapter 7, the beat is detected using the automatic beat detection tool 'WQRS' provided by Physionet [36]. The model parameters are estimated by solving the forward and inverse problems using a nonlinear constrained sum squared error optimization process. The constraints are used to maintain the order of the heart's activation sequences. That is, the atrial activation occurs prior to that of the ventricles and the depolarization event occurs prior to the repolarization. The model parameters are used as features in the classification process to determine whether a beat is ischemic or healthy. A C4.5 decision tree is used in the classification process.

### 9.2.1 Ten-Fold Cross Validation Experiment

As mentioned above, a 10 fold cross validation is performed. The classification method is applied with and without using the PCA components as features. Using the model parameters without the PCA features, the accuracy is 87.83% with sensitivity and specificity of 92.62% and 66.10%, respectively. Using the PCA features without the model parameters leads to an accuracy of 90.11% with sensitivity and specificity of 93.80% and 72.70%. However, when using the PCA features in addition to the model parameters, the accuracy increases to 91.62% with sensitivity of 94.89% and sensitivity of 75.66%. Sensitivity and specificity are defined as the accuracy of detecting the ischemic beat and the accuracy of detecting the non ischemic beat, respectively. The confusion matrices for the approaches are given in Table 9.1, Table 9.2 and Table 9.3 respectively. Confusion matrix is a visualization tool that presents the instances classified as ischemic or healthy in its columns and the actual classification in its rows.

Table 9.1: Confusion matrix for the diagnostic method using ECM without PCA.

	Classified as	
	Ischemic	Healthy
Ischemic	15,608	1,255
Healthy	1,243	2,421

Table 9.2: Confusion matrix for the diagnostic method using PCA.

	Classified as	
	Ischemic	Healthy
Ischemic	15,877	986
Healthy	1,044	2,620

Table 9.3: Confusion matrix for the diagnostic method using ECM with PCA.

	Classified as	
	Ischemic	Healthy
Ischemic	16,035	828
Healthy	892	2,772

It can be seen from Table 9.1 and Table 9.3 that the sensitivity of the ECM-PCA/C4.5 approach increases by 9.5% when using the PCA components in addition to the model parameters as features in the C4.5 decision tree classifier.

As mentioned above, the ECM-PCA/C4.5 approach is compared to the techniques of [1] as applied to the LT-ST database. It can be appreciated from Table 9.4 that the ECM-PCA/C4.5 approach performs better than the previous methods by [1] for the LT-ST database. The confidence intervals for each of the ECM-PCA/C4.5 and Stamkopoulos methods are  $[0.91 \quad 0.92]$  and  $[0.86 \quad 0.87]$ , respectively at a confidence level of  $1 - \alpha = 0.95$ . The comparison in the confidence intervals shows that the lower bound of the ECM-PCA/C4.5's interval is higher than that of Stamkopoulos's method. This comparison shows that the increase in accuracy is statistically significant. Moreover, a student t-test is performed, where the null hypothesis is that two independent samples from the ECM-PCA/C4.5 and the Stamkopoulos results belong to the same distribution with significance level of 5%. The test showed that the null hypothesis can be rejected because the probability  $p = 9.85 \times 10^{-57}$  of accepting the null hypothesis is less than the 5% tolerance. Therefore, the alternative hypothesis is chosen, where the two samples are selected from different distributions. Thus, the ECM-PCA/C4.5 and the Stamkopoulos methods are statistically different.

Table 9.4: Comparison between the ECM-PCA/C4.5 approach and Stamkapoulos method applied to the LT-ST database.

Approach	Accuracy	Sensitivity	Specificity
ECM-PCA/C4.5	91.62%	94.89%	75.66%
Stamkopoulos	86.76%	91.73%	63.86%

### **9.2.2 Summary and Discussion for the Ischemia Detection Experiment**

As a summary, the results for the ECM-PCA/C4.5 applied to the LT-ST database are presented to diagnose ischemic and healthy beats. The approach shows excellent results when diagnosing ischemic and healthy beats. The ECM-PCA/C4.5 diagnostic method uses the ECM parameters obtained from the inverse problem solution. The importance in the ECM model is that it can be related back to the heart's physical and electrical activity. It can be seen that the parameters of the ECM can be used in the detection of ischemic and healthy heart beats, because these parameters capture the information regarding the cardiac regions and their effect on the ECG waves and segments, such as slope, interval duration, magnitude and segment's variation.

The training process for this diagnostic technique is performed offline. The classification/diagnostic process is performed online. The waiting time for this diagnostic method is the inverse problem solution, which as presented in the previous chapter takes 10s. Therefore, this ECM-PCA/C4.5 method is a sufficiently fast diagnostic method.

### **9.3 *Infarction Localization Experiment***

This section presents the results for the ECM-PCA/C4.5 infarction localization method, described in chapter 7. The ECM-PCA/C4.5 approach is applied to the PTB diagnostic database. Table 9.5 shows the location of the infarcts, number of infarcted records, and the class number chosen for each location. The localization method is evaluated using the ten-fold cross validation method presented in section 9.2.1.

Table 9.5: The available infarction locations with the respective number of records.

Infarction Location	Number of Records	Class
anterior, inferior, septal	11	1
anterior, inferior	9	2
anterior, inferior, lateral	5	3
anterior, septal	68	4
anterior, lateral	50	5
anterior, lateral, septal	5	6
anterior	47	7
inferior, septal	4	8
inferior, lateral	51	9
inferior, septal, lateral	24	10
inferior	86	11
septal	4	12
lateral	3	13
Total	367	

The results of applying the localization method to the infarcted records from the PTB database as shown in Table 9.9. Similar to the ischemia detection experiment, the localization approach is applied using either the ECM parameters, the PCA of the signal, and the combination of both as features in the classification process. Table 9.6, Table 9.7, and Table 9.8 show the confusion matrices for the ECM-Localizer, PCA-Localizer, and ECM/PCA-Localizer, respectively.

Since the classes are not mutually exclusive, the accuracy is measured as the percentage of identifying each of the locations. The accuracy is measured as the number of correct locations divided by the maximum between the number actual and predicted locations. For example, if anterior and inferior are predicted in class 1, the accuracy is 66.67% in class 1. As shown in Table 9.9, the accuracy for the ECM-PCA-Localizer shows improvement from the ECM-Localizer and the PCA-Localizer by 6% and 1.6%, respectively.

Table 9.6: Confusion matrix of the ECM-Localizer method.

Predicted:	C1	C2	C3	C4	C5	C6	C7	C8	C9	C10	C11	C12	C13
C1	0	1	0	2	1	1	2	0	2	1	1	0	0
C2	1	1	0	3	1	0	0	0	1	1	1	0	0
C3	0	0	0	0	1	0	0	0	1	0	3	0	0
C4	2	6	0	16	18	4	7	1	3	2	8	1	0
C5	0	5	0	9	14	2	9	1	4	1	5	0	0
C6	0	1	0	0	1	0	1	0	1	0	1	0	0
C7	2	0	0	11	6	0	16	0	1	2	8	0	1
C8	0	0	0	1	1	0	0	0	0	1	1	0	0
C9	6	1	1	3	5	0	3	0	14	4	12	2	0
C10	0	1	1	2	3	0	3	1	5	4	4	0	0
C11	3	3	1	13	8	2	7	2	11	8	25	1	1
C12	0	0	0	1	0	0	0	0	0	0	0	2	1
C13	0	0	0	0	0	0	0	0	0	0	3	0	0

Table 9.7: Confusion matrix of the PCA-Localizer method.

Predicted:	C1	C2	C3	C4	C5	C6	C7	C8	C9	C10	C11	C12	C13
C1	5	0	1	0	1	2	0	0	2	0	0	0	0
C2	0	1	0	3	2	1	1	0	0	0	0	1	0
C3	0	0	0	2	2	0	0	0	1	0	0	0	0
C4	1	3	2	28	12	1	5	0	3	3	10	0	0
C5	1	2	1	10	15	1	6	1	3	2	8	0	0
C6	0	2	0	1	0	1	0	0	1	0	0	0	0
C7	0	0	0	13	9	0	17	1	2	0	5	0	0
C8	1	0	0	0	1	0	0	0	1	0	1	0	0
C9	2	1	2	1	4	0	1	1	17	5	17	0	0
C10	2	0	1	1	1	0	3	0	3	5	8	0	0
C11	1	0	1	10	0	2	4	3	15	8	39	1	1
C12	0	0	0	1	0	1	1	0	0	0	1	0	0
C13	0	0	1	0	1	0	0	0	1	0	0	0	0

Table 9.8: Confusion matrix of the ECM/PCA-Localizer method.

Predicted:	C1	C2	C3	C4	C5	C6	C7	C8	C9	C10	C11	C12	C13
C1	4	1	0	2	1	0	1	0	0	2	0	0	0
C2	0	1	0	1	2	1	1	0	1	2	0	0	0
C3	0	1	1	1	1	0	0	0	0	0	1	0	0
C4	2	0	0	21	11	2	12	1	5	2	11	1	0
C5	0	1	3	12	14	2	9	1	0	1	7	0	0
C6	0	1	1	1	1	0	1	0	0	0	0	0	0
C7	4	1	0	5	11	0	16	0	3	2	5	0	0
C8	0	0	0	2	0	0	1	0	0	0	1	0	0
C9	0	1	0	2	3	0	6	1	20	3	15	0	0
C10	1	1	0	3	2	1	0	1	2	3	10	0	0
C11	0	0	1	7	7	1	6	1	13	7	39	2	1
C12	0	0	1	0	0	0	1	0	1	0	1	0	0
C13	0	0	1	0	0	0	0	0	0	0	2	0	0

Table 9.9: Application of the diagnostic methods for the 13 classes.

Approach	Accuracy
ECM-Localizer	62.50%
PCA-Localizer	66.93%
ECM-PCA-Localizer	68.57%

The ECM-PCA-Localizer is compared to the current best infarction localization technique by Mneimneh et al. [2], winner of the Physionet/Computers in Cardiology Challenge 2007 [22]. The approach uses reconstructed phase space (RPS) embedding and Gaussian mixture models (GMM) to determine the infarct locations. The RPS-GMM approach is described in Appendix B. It can be appreciated from Table 9.10 that the ECM-PCA-Localizer performs better than the RPS/GMM approach. A student t-test is performed, where the null hypothesis is that two independent samples from the ECM-PCA/C4.5 and the RPS/GMM results belong to the same distribution with significance level of 5%. The test showed that the null hypothesis can be rejected because the probability  $p = 0.0057$  of accepting the null hypothesis is less than the 5% tolerance. Therefore, the alternative hypothesis is chosen, where the two samples are selected from

different distributions. Thus, the ECM-PCA/C4.5 and the RPS/GMM methods are statistically different.

Table 9.10: Comparison between the ECM-PCA/C4.5 and RPS/GMM method.

Approach	Accuracy
ECM-PCA-Localizer	68.57%
RPS/GMM	58.74%

### 9.3.1 Summary and Discussion for the Infarction Localization Experiment

The results of the infarction localization applied to records in the PTB diagnostic database are presented in the previous section. The ECM-PCA-Localizer showed good results in localizing multiple infarction locations. These results show the importance of the cardiac model, ECM, and that it can be related back to the heart's electrical activity.

It is noted that, the PTB diagnostic database provides annotations to the infarction location of the record and the leads showing infarction changes. Therefore, the accuracy of the transformation between the annotated infarction location and the leads shown infarctions depend on the accuracy of the Selvester criteria [45]. Therefore, the accuracy can be enhanced if a larger, well annotated dataset is available.

Similar to the ischemia detection method, the training process for the infarction localization diagnostic technique is performed offline. The classification/diagnostic process is performed online. The computational time for this diagnostic method is the inverse problem solution, which as presented in the previous chapter takes 10s. Therefore, this ECM-PCA-Localizer method is a sufficiently fast diagnostic method.

## 9.4 Summary and Discussion

This chapter presents the results of two diagnostic applications for the electrophysiological cardiac model (ECM). The diagnostic methods are myocardial

ischemia detection and myocardial infarction localization. These methods use the ECM parameters, the solutions for the inverse and forward problems, principle component analysis of the signal, and a decision tree classifier. The results shown above provide evidence that the ECM parameters capture the properties of the cardiac region electrical activity and can be used in sufficiently fast clinical diagnostics.

To analyze the parameters of the model in the ischemia detection case, the decision tree is pruned and the parameters with the discrepancy between ischemic and healthy beats are observed. The parameters  $c_2$  and  $\delta_2^+$  of the *RV* region, resulted in the selection of myocardial ischemia by a ratio of 12474 ischemic records to 914 healthy records. The summation of  $c_2$  and  $\delta_2^+$  indicate the duration of the ST segment. Moreover,  $c_2$  and  $a_2$  resulted in selecting the healthy case with a ratio of 1021.0 to 223.0. These results agree with Pardee that the ST segment can be used as an indicator for myocardial ischemia.

Similar to the ischemic case, the decision tree that identifies that detects if Lead I indicates signs of infarction is pruned and analyzed. The parameter that indicated a significant discrepancy between showing signs of infarction and healthy is the  $a_2$  and  $k$  of the *Pf* region that is used to generate the Q wave in the forward problem solution. The discrimination ratio between infarcted and healthy is 260 to 107 beats. This agrees with Selvester's criteria that the change in the slope and magnitude of the Q wave is one of the indicators of myocardial infarction.

## Chapter 10 Conclusion

A novel approach for modeling the heart that addresses both the cardiac electrophysiology at the body surface (forward problem) and the electrical activity in key cardiac regions (inverse problem) has been presented in this dissertation. The electrophysiological cardiac model (ECM) divides the heart into six important electrical regions: sinoatrial (SA) node, atrioventricular (AV) node, bundle branches (Bb), Purkinje fibers (Pf), right ventricle (RV), and left ventricle (LV). A difference of two sigmoid functions is used to represent the electrical activity of each region. The sequence of activations of the cardiac regions, based on the cardiac electrophysiology, is used to develop a direct solution for the forward problem and to solve the inverse problem.

The advantages of the ECM over the finite element modeling methods are the lower level of modeling complexity that allows the development of a direct solution independent of geometrical modeling for the forward and inverse problems. Additionally, the ECM captures the time and pace of activation and conduction of the cardiac regions play important roles in clinical diagnostics, such as myocardial infarction localization and myocardial ischemia detection.

As clinical applications to the ECM, two diagnostic methods based on the heart model are presented. The first allows for sufficiently fast localization of myocardial infarction. The second provides a mechanism for identifying an ischemic heart. These diagnostic methods use the forward and inverse problem solutions, the principle component analysis of the electrocardiogram, and a C4.5 decision tree to diagnose automatically, noninvasively, and accurately these two serious heart conditions. The accuracies for the ischemia detection and infarction localization methods outperform

existing automatic approaches. The average run time for the diagnostic methods is 10 seconds per lead.

The importance of the ischemia detection method can be used in the early screening of an ischemic heart that helps in the prevention of myocardial infarction. Additionally, importance of the rapid and accurate infarction localization method may help physicians quickly treat the blockage at the indicated region with the appropriate drug or procedure [4].

Finally, the experiments in chapter 8 and chapter 9 prove the ability of the ECM to capture information related to the cardiac electrical activity that indicates healthy, ischemic, and infarcted hearts. Therefore, the ECM provides a novel framework for modeling the electrical activity of the heart.

### ***10.1 Future Recommendations***

Three possibilities for extending this work are suggested in this section. The first deals with extending the ECM. The second is related to the solutions of the inverse problems. The third is related to the diagnostic methods that use the ECM.

The first suggestion is to extend the model to account for heart conditions especially when the sequence of activation is disrupted. It would be a possibility to account for arrhythmias, where the cardiac rhythm is abnormal. Generally, arrhythmias occur when cells other than the SA node act as pace makers. This leads to serious malfunction in the mechanical system of the heart. The arrhythmia problem can be solved by using adaptive constraints while solving the inverse problem to account for the different arrhythmias. Additionally, it would be interesting to extend the model to

---

account for multiple beats. This helps in studying the changes of the cardiac activity in time, alternans.

The second suggestion is related to the inverse problem solution. Two interesting topics for future research toward enhancing the current inverse problem solution. The first is enhancing the convergence speed of the optimization method, and the second is extending the inverse problem solution to account for multiple beats. The suggestions related to the inverse problem solution are:

1. It might be possible to develop optimization techniques to solve this specific inverse problem. For example, have a better initial condition can enhance the speed of the optimization. Additionally, the convergence speed of the inverse problem solution might be enhanced by taking advantage of the least squares property.
2. It might be possible to account for multiple beats during the inverse problem solution. The multiple beat inverse problem solution can be inherited from the extension of the model presented in the previous paragraph. This helps in taking advantage of multiple beats to solve the inverse problem.

The third category for future research is the development of diagnostic methods that account for different heart diseases. The beat classification method, presented in this work, can be used as a basis to detect and localize different heart diseases.

## Appendix A Luo-Rudy Model

This appendix describes the Luo-Rudy mode [39]. This model can simulate dynamic changes in ionic concentrations in the cardiac cells. The Luo-Rudy model represents the migration of the ion concentrations through the cell membrane. The general approach is based on a numerical reconstruction of the cell action potential using the following differential equation that describes the rate of change of membrane potential (V):

$$dV/dt = -(1/C_m)(I_i + I_{st}), \quad (\text{A.1})$$

where  $C_m$  is the membrane capacitance,  $I_{st}$  is a stimulus current, and  $I_i$  is the sum of all ionic currents through the membrane. In the Luo-Rudy model,  $I_i$  includes ionic currents through voltage-gated channels and currents carried by other mechanisms (eg,  $I_{NaCa}$  and  $I_{NaK}$ ). Gated channels are based on the Hodgkin-Huxley formulation described in chapter 3. The ionic currents are determined by ionic gates whose gating variables are obtained as a solution to a coupled system of differential equations shown in chapter 3. The model developed here accounts for dynamic changes of ionic concentrations during the action potential. The rate of change of ionic concentrations is given by

$$d[B]/dt = (I_B * A_{cap}) / (V_c * z_B * F), \quad (\text{A.2})$$

where  $[B]$  is the concentration of ion  $B$ ,  $I_B$  is the sum of ionic currents carrying on  $B$ ,  $A_{cap}$  is the capacitive membrane area,  $V_c$  is the volume of the compartment where  $[B]$  is updated,  $z_B$  is the valence of ion  $B$ , and  $F$  is the Faraday constant.

As described in chapter 3, the cumulative ions current is required to solve for the voltage at the cell membrane. The ions used in the Luo-Rudy model are Potassium (K<sup>+</sup>), Sodium (Na<sup>+</sup>), and Calcium (Ca<sup>+</sup>). The cumulative voltage equation becomes

$$dV/d(\text{time}) = -(1.0/C_m) \left( \begin{array}{l} i_{Na} + i_{CaL} + i_K + i_{K1} + i_{Kp} \\ + i_{NaCa} + i_{pCa} + i_{Nab} + i_{Cab} \\ + i_{NaK} + i_{nsCa} + I_{st} \end{array} \right). \quad (\text{A.3})$$

The currents are determined using the equations provided for the Hodgkin and Huxley model in chapter 3.

## **Appendix B      RPS/GMM Approach toward Myocardial Infarction Localization**

This appendix presents the reconstructed phase space (RPS) / Gaussian mixture model (GMM) approach used to localize myocardial infarction. The RPS/GMM approach takes advantage of the representation of the ECG signal through time to classify if an electrocardiogram (ECG) shows changes due to infarcts. The time embedding determined from the ECG signal is used with GMMs and the Selvester criteria [45] to determine the infarcted type/location. The approach is applied on a lead by lead basis. The resulting 12 lead decisions predicted by the algorithm are used with the labeling method provided by [50] to localize the infarcted segments.

The following sections present the RPS/GMM approach and a brief description of the reconstructed phase space and Gaussian mixture model theory.

### **B.1.    RPS/GMM approach**

The RPS/GMM approach uses phase space embedding in order to create a multidimensional representation of the ECG signal that supports differentiation between a lead that indicates an infarction and one that does not. The GMM is used to model the embedded ECG signal from the training data. The GMM then compare the generated model against unknown signals to determine if an infarct is indicated. A block diagram describing the process is presented in Figure B-1. In the RPS/GMM approach, the signals have the same number of samples and the R peaks aligned at the same time sample. The number of samples chosen in the RPS/GMM algorithm is 256 as recommended by [2].

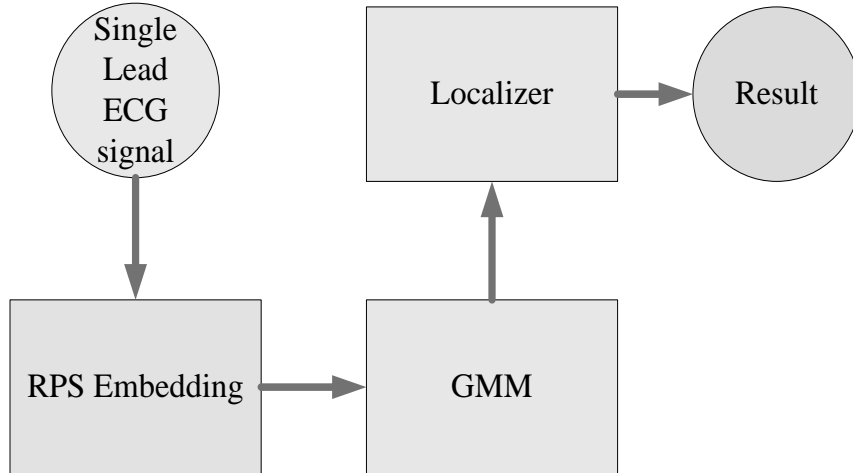


Figure B-1: Block diagram describing the GMM/KLT approach

### B.2. Reconstructed Phase Space

A reconstructed phase space (RPS) is a time delayed embedding of a signal, which may be topologically equivalent to the state space of the system that generated the signal if certain assumptions are met [51]. Previous work has shown that even when these assumptions are not met, RPSs contain important information for classifying a signal [52]. Here these signals are the 12 lead ECGs, and the classes are infarcted or non-infarcted. The definition of each point in an RPS is determined as follows [41]:

$$X_n = \begin{bmatrix} x_{n-(d-1)\tau} & \cdots & x_{n-\tau} & x_n \end{bmatrix}, \quad (\text{B.1})$$

where  $n$  is the dimension of the space,  $t$  is the time delay, and  $d$  is the dimension.

### B.3. Gaussian Mixture Model

GMMs are a set of Gaussian probability density functions used to characterize the distribution of an underlying set of data generated from the RPS. They are widely used in engineering applications, especially speech processing [52]. The equation that defines a GMM is [41]:

$$p(x) = \sum_{m=1}^M w_m p_m(x) = \sum_{m=1}^M w_m N(x, \mu_m, \Sigma_m), \quad (\text{B.2})$$

where  $x$  is the feature vector,  $M$  is the number of mixtures,  $N(x, \mu_m, \Sigma_m)$  is a normal distribution with mean  $\mu_m$  and covariance matrix  $\Sigma_m$ , and  $w_m$  is the mixture weight, with the constraint that the weights sum to unity. The GMM is estimated using Expectation-Maximization (EM). The GMMs are used in a Bayesian maximum likelihood classifier [2]:

$$p(X | c_i) = \prod_{n=1}^N p(x_n | c_i), \quad (\text{B.3})$$

$$\hat{c} = \arg \max_i p(X | c_i), \quad (\text{B.4})$$

where  $x_n$  is the  $n^{\text{th}}$  feature vector,  $X$  is the set of all feature vectors, and  $c_i$  is the  $i^{\text{th}}$  class.

## References

- [1] T. Stamkopoulos, K. Diamantaras, N. Maglaveras, and M. Strintzis, "ECG analysis using nonlinear PCA neural networks for ischemia detection," *IEEE Transactions on Signal Processing*, vol. 46, 1998.
- [2] M. A. Mneimneh and R. J. Povinelli, "RPS/GMM Approach toward the Localization of Myocardial Infarction," in *Computers in Cardiology*. North Carolina, USA, 2007, pp. 185-188.
- [3] World Health Organization, "<http://www.who.int/whr/en/>."
- [4] AHA, "Myocardial Ischemia, Injury and Infarction," 2007.
- [5] AHA, "Heart Disease and Stroke Statistics," 2005.
- [6] F. Dawoud, "Using Inverse Electrocardiography to Image Myocardial Infarction," in *Computers in Cardiology*. NC, USA, 2007.
- [7] D Farina and O Dössel, "Model-Based Approach to the Localization of Infarction," in *Computers in Cardiology*. North Carolina, USA, 2007.
- [8] L. Mertz, *The Circulatory System*. Westport, Conn: Greenwood Press, 2004.
- [9] medicalook, "heart-diseases1," 2007.
- [10] A. J. Pullan, M. L. Buist, and L. K. Cheng, *Mathematically Modeling the Electrical Activity of the Heart from Cell to Body Surface and Back Again*. New Jersey: World Scientific, 2005.
- [11] S. VanRiper and J. VanRiper, *Cardiac Diagnostic Tests: A Guide for Nurses*. Philadelphia: W.B Saunders Company, 1997.
- [12] St. Jude Medical Center, "Conduction system of the heart."
- [13] D. P. Zipes, *Braunwald's Heart Disease : a Textbook of Cardiovascular Medicine*. Philadelphia, Pa: Elsevier Saunders, 2005.
- [14] Y.T.Zhang, "Electrocardiography (ECG):The 12-Lead System," 2007.
- [15] M. W. Zimmerman., "Classification of ECG ST Events as Ischemic or Non-Ischemic Using Reconstructed Phase Spaces." Milwaukee, WI: Marquette University, 2004.
- [16] British Heart Foundation, "How Myocardial Infarction Occurs," in <http://www.patient.co.uk/showdoc/23068792/>, 2006.
- [17] H. Pardee, "An Electrocardiographic Sign of Coronary Artery Obstruction," *Arch Int Med*, vol. 26, pp. 244-257, 1920.
- [18] H. Fozzard and D. DasGupta, "ST-segment potentials and mapping. Theory and experiments," vol. 54, pp. 533-537, 1976.
- [19] M. Janse and A. Kleber, "Electrophysiological changes and ventricular arrhythmias in the early phase of regional myocardial ischemia," *Circulation Research*, vol. 49, pp. 1069-1081, 1981.
- [20] Nucleus Communications Inc, "The Seldinger approach catheterization method ", 2005
- [21] heartfailure.org, "Echocardiogram," in [http://www.heartfailure.org/eng\\_site/hf\\_test\\_ecg.asp](http://www.heartfailure.org/eng_site/hf_test_ecg.asp), 2004.
- [22] G. Moody, "Physionet / Computers in Cardiology 2007," 2007.
- [23] S. M. Pitas I, Grippas S, et al. , "Machine classification of ischemic electrocardiograms," presented at Mediterranean Electrotechnical Conference, 1983.

- 
- [24] TL Shook, V Valvo, M Hubelbank, and et al., "Validation of a New Algorithm for Detection and Quantification of Ischemic ST Segment Changes During Ambulatory Electrocardiography," presented at Computers in Cardiology, 1989.
- [25] F Badilini, M Merri, and J Benhorin, "Beat-to-beat Quantification and Analysis of ST Displacement from Holter ECGs: a New Approach to Ischemia Detection," in *Computers in Cardiology*, 1992, pp. 179-182.
- [26] M. R. Jager F, Moody GB, et al., "Analysis of transient ST segment changes during ambulatory ECG monitoring using the Karhunen-Loève transform," in *Computers in Cardiology*, 1992, pp. 691-694.
- [27] L Senhadji, G Carrault, JJ Bellanger, and et al., "Comparing wavelet transforms for recognizing cardiac patterns.," *IEEE Eng Med Biol.*, vol. 14, pp. 167-173, 1995.
- [28] A. Taddei, G. Constantino, R. Silipo, and et al., "A System for the Detection of Ischemic Episodes in Ambulatory ECG," in *Computers in Cardiology*, 1995, pp. 705-708.
- [29] J Vila, J Presedo, M Delgado, and et al., "SUTIL: Intelligent Ischemia Monitoring System.," *International Journal Medical Informatics*.
- [30] F. D. Papaloukas C, Likas A, et al., "A rule-based technique for the automated detection of ischemic episodes from ECG," in *Europ Med Biol Eng Conf.*, vol. 37, 1999, pp. S728-S729.
- [31] F. D. Papaloukas C, Likas A, et al., "A knowledge-based technique for automated detection of ischemic episodes in long duration electrocardiograms.," *Med Biol Eng Comput.*, vol. 39, pp. 105-112, 2001.
- [32] C Papaloukas, DI Fotiadis, A Likas, and et al., "Use of a Novel Rule-based Expert System in the Detection of Changes in the ST Segment and the T wave in Long Duration ECGs.," *Journal of Electrocardiology*, vol. 35, pp. 27-34, 2002.
- [33] V.-E. Neagoe, I.-F. Iatan, and S. Grunwald, "A Neuro-Fuzzy Approach to Classification of ECG Signals for Ischemic Heart Disease Diagnosis," presented at AMIA Annu Symp Proc, 2003.
- [34] M. R. S. Reddy, L. Edenbrandt, J. Svensson, W. K. Haisty, and O. Pahlm, "Neural network versus electrocardiographer and conventional computer criteria in diagnosing anterior infarct from the ECG," presented at Computers in Cardiology, 1992.
- [35] H. Lu, K. Ong, and P. Chia, "An Automated ECG Classification System Based on a Neuro-Fuzzy System," presented at Computers in Cardiology, 2000.
- [36] A. Goldberger, L. Amaral, L. Glass, J. Hausdorff, P. Ivanov, R. Mark, J. Mietus, G. Moody, C. Peng, and H. Stanley, "PhysioBank, PhysioToolkit, and PhysioNet: Components of a New Research Resource for Complex Physiologic Signals.," *AHA Journal Circulation 101*, vol. 101, pp. e215-e220, 2000.
- [37] G. D. Clifford, "A Novel Framework for Signal Representation and Souch Separation: Applications to Filtering and Segmentation of Biosignals," *Journal of Biological Systems*, vol. 14, pp. 169-183, 2006.
- [38] S. M. Kay, "Efficient Generation of Colored Noise," *Proceedings of the IEEE*, vol. 69, pp. 480-481, 1981.

- 
- [39] C. Luo and Y. Rudy, "A Dynamic Model of the Cardiac Ventricular Action Potential: I. Simulations of Ionic Currents and Concentration Changes," *Circulation Research*, vol. 74, pp. 1071-1096, 1994.
- [40] J. Nocedal and S. J. Wright, *Numerical Optimization*. New York: Springer Science, 2006.
- [41] R. J. Povinelli, "Towards the Prediction of Transient ST Changes," presented at Computers in Cardiology, Lyon, France, 2005.
- [42] R. Quinlan, "Data Mining from an AI Perspective," in *International Conference on Data Engineering*, 1999.
- [43] S. R. Safavian and D. Landgrebe, "A Survey of Decision Tree Classifier Methodology," *IEEE Transactions on Systems, Man, and Cybernetics*, vol. 21, pp. 660-674, 1991.
- [44] E. Frank, M. Hall, G. Holmes, M. Mayo, B. Pfahringer, T. Smith, and I. Witten, "WEKA." The University of Waikato, 2007.
- [45] W. Anderson, N. Wagner, K. Lee, R. White, J. Yuschak, V. Behar, R. Selvester, R. Ideker, and G. Wagner, "Evaluation of a QRS Scoring System for Estimating Myocardial Infarct size. VI. Identification of Screening Criteria for Non-acute Myocardial Infarcts.," *Am J Cardiol*, vol. 61, pp. 729-733, 1988.
- [46] GD Clifford, A Shoeb, PE McSharry, and BA Janz, "Model-based Filtering, Compression and Classification of the ECG," *International Journal of Bioelectromagnetism*, vol. Vol. 7, pp. 158-161, 2005.
- [47] G. Moody, "Physionet / Computers in Cardiology 2006," 2006.
- [48] K. L. Park, M. J. Khil , B. C. Lee, K. S. Jeong, K. J. Lee, and H. R. Yoon, "Design of a wavelet interpolation filter for enhancement of the ST-segment," *Medical and Biological Engineering and Computing*, vol. 39, pp. 355-361, 2001.
- [49] T. M. Mitchell, *Machine Learning*. New York: McGraw-Hill, 1997.
- [50] A. B. d. Luna, G. Wagner, Y. Birnbaum, M. Kjell Nikus, M. Miguel Fiol, A. Gorgels, J. Cinca, P. M. Clemmensen, O. Pahlm, S. Sclarovsky, S. Stern, H. Wellens, and W. Zareba, "A New Terminology for Left Ventricular Walls and Location of Myocardial Infarcts That Present Q Wave Based on the Standard of Cardiac Magnetic Resonance Imaging," *Circulation*, vol. 114, pp. 1755-1760, 2006.
- [51] F. Takens, "Detecting strange attractors in turbulence," presented at Dynamical Systems and Turbulence, Warwick, 1980.
- [52] Kevin M. Indrebo, Richard J. Povinelli, and M. T. Johnson., "Sub-banded Reconstructed Phase Spaces for Speech Recognition," *Speech Communication*, vol. 48, pp. 760-774, 2006.